Materials Advances

ROYAL SOCIETY OF CHEMISTRY

REVIEW

View Article Online
View Journal | View Issue

Cite this: *Mater. Adv.*, 2023, 4, 320

A review on 2D-ZnO nanostructure based biosensors: from materials to devices

M. Sankush Krishna,[a] Sangeeta Singh,*[a] Maria Batool,[bc] Heba Mohamed Fahmy,*[d] Kondaiah Seku,[e] Ahmed Esmail Shalan,[fg] Senentxu Lanceros-Mendez[fh] and Muhammad Nadeem Zafar*[b]

During the COVID'19 outbreak, biosensing devices won increasing relevance, demonstrating their potential in the medical diagnostic field. Hence, the present review reports on the main advances in 2D-ZnO nanostructure-based biosensors. So far, bulk ZnO has shown potential for biosensing, optical, and power electronic applications, mainly based on its wide band gap. In the post graphene era, its 2-D allotropes like ZnO sheets and ZnO nanoribbons have outperformed the bulk ZnO structures for specific applications. ZnO demonstrates various stable and feasible morphologies: nanotubes, nanowires, nanorods, nanosheets, nanoparticles, and nanobelts. As a matrix layer in biosensing applications, ZnO strongly binds to biomolecules due to its high isoelectric point (IEP) and shows a strong sensitivity due to the high surface-to-volume ratio. Further, ZnO nanostructures used as a matrix layer play an important role in inhibiting specific biological interactions and hence improve the sensitivity of sensing devices. Further, bioselective layers are typically immobilized onto ZnO either by direct adsorption or by covalent binding. ZnO based biosensors are categorized into optical, piezoelectric, and electrochemical biosensors, among others, based on their biosensing mechanism. In particular, electrochemical sensors produce signals *via* an electrical pathway for detecting and monitoring the target molecules. Optical sensors produce signals based on luminescence or reflectance, among others. Piezoelectric biosensors produce signals by mass loading of the piezoelectric material. ZnO-based FET biosensors are also reported, showing sensing application by the change in the channel's conductance. Further, recent literature on the detection of COVID-19 using ZnO nanostructures is presented.

Received 31st August 2022,
Accepted 9th November 2022

DOI: 10.1039/d2ma00878e

rsc.li/materials-advances

1. Introduction

The global spread of COVID-19 has been labelled as pandemic by the World Health Organization (WHO). Among the best measures to properly address this issue has been the early diagnosis for the detection of the virus and precautionary measures. The limited availability of testing kits and professional operators made the rapid detection of the COVID-19 virus a challenge. COVID-19 carries a unique RNA sequence, and it can be detected by nucleic acid amplification tests (NAAT) or real-time reverse-transcription polymerase chain reaction (rRT-PCR).[1,2] The second detection approach for the SARS-CoV-2 virus is the Enzyme-Linked Immunosorbent Assay (ELISA) IgG antibody test.[3] The issue with the above methods is the cost of the testing kits and their commercial fabrication.

Further, these methods are time-consuming, and need skilled staff with a possible risk of false positives and false negatives.[4] Hence the fabrication of biosensors with low-cost for the selection of SARS-CoV-2 and other related viruses could prove to be very helpful. Over conventional testing equipment, biosensors are more reliable for COVID-19 detection due to their high specificity and sensitivity at low sample volumes.[5] Advancements in nanotechnology introduced nanostructures in the construction of biosensors. Easy tailoring of nanostructures because of their high surface-to-volume ratio made it suitable to manufacture sensitive biosensors. The urgent need for diagnosis of COVID-19 stressed the development of point-of-care (POC) biosensor devices as they are easy to use, fast,

[a] *Microelectronics & VLSI lab, National Institute of Technology, Patna 800005, India. E-mail: sangeeta.singh@nitp.ac.in*
[b] *Department of Chemistry, University of Gujrat, Gujrat 50700, Pakistan. E-mail: znadeempk@gmail.com, nadeem.zafar@uog.edu.pk*
[c] *Department of Chemistry, University of Management and Technology, Sialkot Campus, Sialkot, 51310, Pakistan*
[d] *Biophysics Department, Faculty of Science, Cairo University, 12613, Egypt. E-mail: hfahmy@sci.cu.edu.eg*
[e] *Engineering Department, Civil Section (Applied Sciences – Chemistry), University of Technology and Applied Sciences, Shinas, Sultanate of Oman*
[f] *BCMaterials, Basque Center for Materials, Applications and Nanostructures, Martina Casiano, UPV/EHU Science Park, Barrio Sarriena s/n, Leioa 48940, Spain*
[g] *Central Metallurgical Research and Development Institute (CMRDI), P. O. Box 87, Helwan, Cairo 11421, Egypt*
[h] *IKERBASQUE, Basque Foundation for Science, 48009 Bilbao, Spain*

cost-effective, portable, and user-friendly.[6,7] POC devices involve spot testing and provide rapid access to the needed information. Thus POC testing is becoming of paramount importance in the biomedical field, particularly when resources are limited. An ideal POC device is generally obtained by designing the biosensors with the ''sample-in-answer-out'' mechanism, some of them being based on the detection of nucleic acids/proteins from respiratory samples/blood samples. To satisfy the increasing need for POC devices, device miniaturization is of paramount importance.[8] Several distinct types of point-of-care (POC) devices have been developed over the past several years, each one based on a different type of portable device used to measure a different type of classical physical parameter. The microfluidic technology allows the development of small and portable systems for POC testing applications. Miniaturized biosensors rely on target identification to determine sensor specificity and enable detection of targets using a portable device or microfluidic platform. An effective tiny biosensor frequently has to be capable of integration, automation, and/or multiplex detection to be used in places where well-trained workers may not be readily available, in addition to the need for high sensitivity and specificity. Miniaturized biosensors for point-of-care use are becoming a commercial reality, and the research and development of portable, integrated, and automated biosensing technologies is a promising new field that could significantly improve the efficiency and quality of care for people living in low-resource areas. They are increasingly required in developing countries where medical facilities are not yet fully available.[9]

Among different nanomaterials for POC and biosensor development, metal oxide nanomaterials such as zinc, magnesium, tin, zirconium, and iron oxides, among others, have grabbed significant attention because of their functional properties, biocompatibility, diverse morphology, and catalytic properties.[10] In particular, ZnO is being used for decades for biosensing applications as a matrix layer that strongly binds the biomolecules due to its high isoelectric point (IEP).

ZnO is being studied a lot for the design of new transducer platforms. This is one of the many nanostructured materials that are being used. Zinc oxide (ZnO) is a good metal–oxide semiconductor that can be used as an intracellular sensor or transducer. ZnO is a fantastic main transducer for generating electrical signals because its dimensions may be tailored to the size of the biological species being detected. Also, ZnO is a good material for designing biosensors because it is non-toxic, doesn't cost much and simpler to synthesize. People have also pointed out that ZnO is biocompatible and that it can have many different shapes that can be easily altered in a controlled manner to increase the surface area. Also, surface properties become more important at the nanoscale, so having varied morphologies and, therefore, varied surface conditions can make its properties change in ways that can be controlled and may be useful for sensing. ZnO has a strong adsorption efficiency with a high IEP of about 9.5.[11] Since antibodies and enzymes have a lower isoelectric point than ZnO and prefer electrostatic interactions, the high IEP aids in immobilising them.

Maria Batool

Maria Batool received her MPhil (Physical Chemistry) degree from Department of Chemistry, University of Agriculture, Faisalabad, Pakistan, in 2018. Currently she is doing her PhD in the research group of Dr. Muhammad Nadeem Zafar in the Department of Chemistry, University of Gujrat, Gujrat, Pakistan. Her research interests include nanocatalysis, nanocomposite synthesis, photocatalysis and electrochemical applications.

Muhammad Nadeem Zafar

Dr. Muhammad Nadeem Zafar attained his PhD degree in Analytical Chemistry from Lund University Sweden in 2011. After that, he started his career as an Assistant Professor in the Department of Chemistry, University of Gujrat, Gujrat, Pakistan and currently working as a Tenured Associate Professor in the Department of Chemistry, University of Gujrat, Gujrat, Pakistan. He was a post-doc fellow at State Key Laboratory of Electroanalytical Chemistry, Changchun Institute of Applied Chemistry, Jilin, China, from 2017 to 2018 under CAS-PIFI. He has been working on various aspects of the use of enzymes in analytical chemistry/bioelectrochemistry and electron transfer between redox enzymes/osmium polymers and electrodes. His research interests are development of enzyme-based biosensors and biofuel cells, synthesis of metal nanoparticles, nanocomposites and metal complexes, pollutant removal through photocatalysis and adsorption, and applications of metal nanoparticles and nanocomposites in energy/water-splitting and biological activities.

Further, its 2-D allotropes, including ZnO sheets and ZnO nanoribbons, outperform bulk ZnO structures for biosensing applications as they provide higher surface-to-volume ratio.[12] The basic process of a biosensor and the state-of-the-art sensing mechanism used are shown in Fig. 1, with the biomolecules being immobilized on ZnO nanostructures which act as a matrix layer. When these biomolecules contact target analytes, they undergo reactions and produce signals which are sent to a transducer and read on a display. The biomolecules could be enzymes, proteins, DNA, and antibodies.

ZnO nanostructures have gained much attention for their application in sensors and actuators.[13–15] ZnO is a semiconductor compound belonging to group II and VI metal oxides. It has a wide bandgap of about 3.37 eV and a large exciton emission energy of about 60 meV. Due to the wide band gap it is widely employed in optical, electrical, and optoelectronics applications.[16] ZnO has a wide variety of nanostructures: zero dimensional nanostructures such as quantum dots,[17] one-dimensional structures like nanorods,[18] nanowires,[19] and nanotubes,[20] and two-dimensional structures like nanodiscs,[21] nanobelts,[22] and nanosheets.[23] ZnO is the preferred candidate to be used as a matrix for biosensing because of its semiconducting properties and variety of morphologies. It can provide an effective channel for transportation of the carriers.

Further, its low cost, non-toxicity, ease of fabrication, and biocompatibility are key factors for selecting this material. 2D-ZnO, with its large surface-to-volume ratio, increases the active surface area of the sensor for biosensing.[24] Certain enzymes are immobilized on biosensors for binding of specific target analytes like glucose oxidase (GOx) for glucose sensors[25] and cholesterol oxidase (ChOx) for cholesterol sensors.[26] The surface properties of the matrix layer influence enzyme immobilization.[11] Nanoporous structures provide higher enzyme loading due to their high surface area.[27,28] The enzyme can be directly immobilized through adsorption techniques or through cross-linking polymers.[29] Different types of biosensors are gaining attention based on the sensing mechanism, with ZnO nanostructures being strong candidates for designing biosensors and POC devices requiring low sample volumes and low operation power.[30]

The present work provides a comprehensive review of ZnO-based biosensors with different types of sensing mechanisms. Immobilization criteria of biomolecules, both based on direct adsorption and through cross-linking agents, are discussed together with biosensor applications of different ZnO nanostructures. The different types of ZnO based biosensors are presented and discussed based on the detection method. Finally, ZnO-based biosensors for COVID-19 detection are presented.

2. Synthesis methods of ZnO nanostructures

Various approaches have been implemented for nanostructure synthesis which can be categorized into top-down and bottom-up methods.[31] In the top-down approach, the process starts with the bulk material, and it is broken/exfoliated to nanosized structures, whereas in the bottom-up approach, the process starts at the atomic level, with the aggregation of atomic level components to produce the nanostructures. The main methods

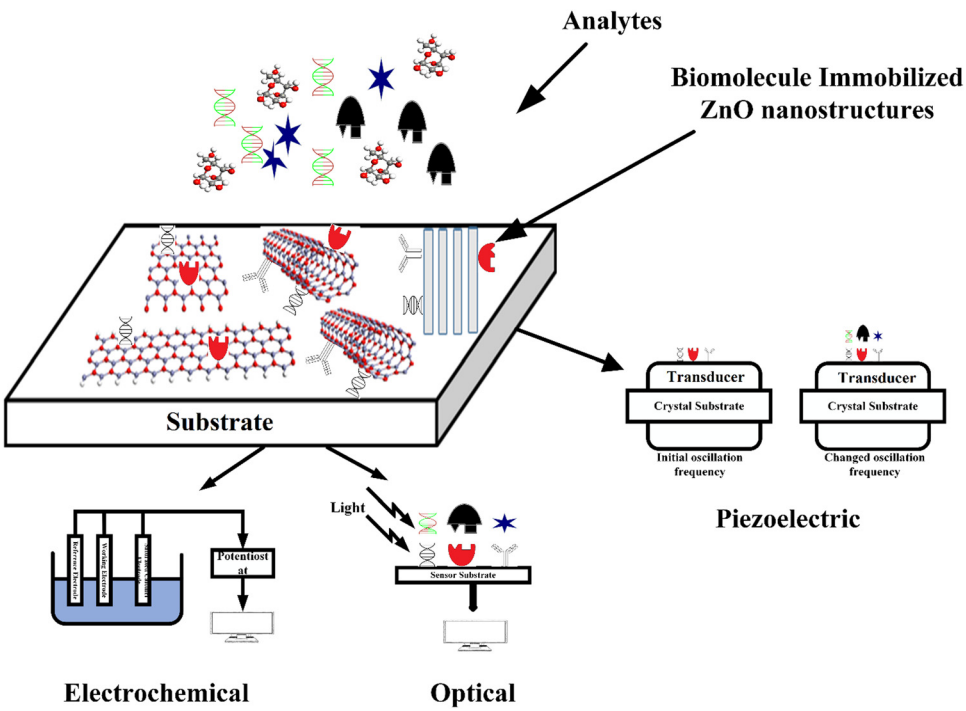

Fig. 1 State-of-the-art biosensing mechanism and the concept of biosensing.

used to develop ZnO nanostructures are presented in the following.

2.1. Pulsed laser deposition

In the pulsed laser deposition (PLD) method, the nanostructures are deposited by focusing a high-energy laser on the bulk crystal. Upon focusing the high-energy laser, the target ablates and deposits as the substrate's nanostructures are placed at a small distance away from the target. Kawakami *et al.*[32] synthesized a 99% pure target of ZnO nanorods with sapphire as the substrate. Nanorods are produced at a substrate temperature of 400–700 °C and 1–10 torr oxygen pressure. The deposition time allows control of the length of rods, and 6 μm long rods with 300 nm diameter are produced after 30 minute deposition. Bae *et al.*[33] synthesized nanocones at 580 °C temperature, 90–100 mJ per pulse energy, and 10 mTorr O_2 atmosphere on a substrate. The PLD method ensures the stoichiometry and good quality of the nanostructures but demonstrates a limited area of nanostructure deposition.

2.2. Sputtering

Sputtering enables flexibility in the growth of nanostructures over a wide area of substrates. In sputtering, Zn/ZnO is the target material and is bombarded with energetic ions like Ar. The collision causes the removal of target atoms that condense on the substrate. In the radio frequency (RF) magnetron sputtering process, a large magnetic field is developed at the target, allowing confinement of the plasma near the substrate. Liu *et al.*[34] synthesized nanotubes by RF reactive sputtering with 99.99% pure Zn as the target material and PVP (polyvinyl pyrrolidone) fibers as the substrate. The tubes were deposited for 20 min with 7×10^{-4} Pa pressure followed by annealing at 600 °C. Chiou *et al.*[35] synthesized nanowires on Cu/Ti/Si wafers at 0.05 torr pressure. Nanowires presented a diameter of around 45 nm with 5 min deposition and 55 nm with 30 min deposition. Nanorods with preferential growth in the (002) direction have been deposited by Venkatesh *et al.*[36] with Ar sputtering at 0.01 mbar pressure and at a substrate temperature of 650 °C with 60 min deposition. Sputtering allows large area deposition, but the quality of the films is compromised relative to PLD.

2.3. Chemical vapor deposition

Chemical vapor deposition (CVD) allow the synthesis of solid nanostructures in a gaseous phase. The chemical reactants/precursors are first vaporized and then deposited as solid structures on a substrate. There are different types of CVD processes like atmospheric CVD, metal–organic CVD (MOCVD), and plasma enhanced CVD (PECVD). Wu *et al.*[37] synthesized ZnO nanorods with Zn acetylacetonate vaporized in a tube furnace at 30–140 °C with N_2/O_2 as carrier gases. Nanorods are deposited with (002) orientation at a substrate temperature of 500 °C with 60–80 nm diameter. Bae *et al.*[38] synthesized sulfur-doped nanowires with Au as the catalyst. The sulfur powder is placed at the beginning of the tube, whereas the Zn powder is placed at the center. Structures grown by MOCVD present good crystallinity with weak deep-level emissions. Kim *et al.*[39] synthesized nanowires with N_2O gas flow rate at 1250 μmol min^{-1} and diethyl zinc (DEZ) as the precursor. Wu *et al.*[40] reported nanotubes with DEZ and O_2. The nanotubes were oriented along the (001) direction with 50–150 nm diameter and a few micrometers of length. Further, Liu *et al.*[41] synthesized nanorods with the PECVD process. DEZ and O_2 as precursors were placed in a bubbler at −26 °C and conveyed to reaction chambers with He gas. Oxygen gas was separately introduced, and microwave plasma at 3–20 mTorr was maintained in the chamber. Later, the substrates were heated to 700 °C, and the nucleation process by pulsing DEZ vapor into the chamber was carried out.

Though CVD has the advantage of good quality nanostructures and high deposition rates, it still has a few drawbacks. The precursors used in CVD could be costly and toxic, especially the ones used in MOCVD. Moreover, by-products of the process are hazardous, and high temperature is needed for deposition, limiting substrate availability.[42]

2.4. Sol–gel

Compared to physical vapor deposition techniques, sol–gel is a low-cost and large area deposition technique, also compatible with high deposition rates,[43] while maintaining excellent control of the morphologies of the nanostructures. Sol–gel methods mainly involve three steps. Firstly, preparation of the sol from starting materials. Secondly, deposition of the sol onto the substrate with a suitable deposition method and then a final heat treatment of the xerogel film. Ahn *et al.*[44] synthesized ZnO nanorods with the sol prepared from $Zn(NO_3)_2{\cdot}6H_2O$ and hexamethylenetetramine (HMTA) in equal proportion. The temperature should be around 95 °C, and crystallite ZnO nanorods with hexagonal wurtzite structures are deposited on the SiO_2/Si substrate. The diameter of the nanorods can be varied by varying the concentration of the starting materials. For the nanotubes and nanowires grown by Wu *et al.*,[45] an aqueous solution of Zn nitrate hexahydrate dissolved in deionized water with urea was used for sol preparation. Under the same growth conditions, nanowires were obtained after 24 hours of deposition and nanotubes after 48 h. Several precursors are used, such as Zn nitrates, chlorides, alkoxides, and Zn acetate dihydrate. Alkoxides are not preferred due to their insolubility in alcohols, inorganic salts like nitrates lead to difficulty in removing the anionic species in the final product,[46] whereas using acetate dihydrate produces volatile by-products. A brief review of the sol–gel process is provided by Lamia Znaidi *et al.*[47]

2.5. Spray pyrolysis

Spray pyrolysis is a powerful tool to obtain high-quality ZnO nanostructures at a low cost. The morphology and stoichiometry can be controlled effectively by properly determining the growth conditions and the ratio of starting materials. The spray pyrolysis method involves preparation of the solution containing the precursor, followed by the generation of mist from it and then transfer into the furnace tube by passing conveyer gas. Finally, some materials are deposited on the substrate, and others are vaporized. The deposition temperature must be

selected such that all other materials except the desired ones are volatile. Htay *et al.*[48] prepared ZnO nanowire structures on glass substrates with zinc acetate and deionized water as starting solutions. The pH is adjusted with ammonium acetate. The structures were deposited at 250–400 °C temperature. Karber *et al.*[49] synthesized nanorods using $ZnCl_2$ as a precursor with soda-lime glass and indium-coated tin oxide (ITO) glass substrates. The structures grown at 550 °C are found to have good optical quality. However, spray pyrolysis still demonstrates a low yield.

2.6. Molecular beam epitaxy

In molecular beam epitaxy (MBE), the crystals are grown by the interactions of the beam of atoms or molecules with the substrate, with sublimation of source materials producing the beam of molecules. Tien *et al.*[50] synthesized ZnO nanorods using metallic Zn, and O_3/O_2 plasma as precursors. Ag islands were developed on SiO_2 and SiNx in the range of 8–30 and 10–65 nm respectively. The base pressure was 5×10^{-8} mbar, and O_3/O_2 pressure varied from 5×10^{-6} to 5×10^{-4} mbar. ZnO nanorods were developed selectively on Ag islands at 600 °C. Heo *et al.*[51] reported nanowires on a Ag coated Al_2O_3 substrate with 30–150 nm diameter and 14 μm length. Feng *et al.*[52] synthesized nanotubes with a plasma-assisted MBE process, with Si being used as the substrate material. MBE is particularly suitable for synthesizing nanostructures with good quality, but it is a slow process and not preferred for large-scale production.

2.7. Electrochemical deposition

In this process, the nanostructures are deposited onto the substrate surface by simple electrolysis of the solution containing the desired material and its complexes. Precise control of the dimensions is possible in this method, and it is low cost and simple, operates at low temperatures, and large area deposition is possible. Hames *et al.*[53] synthesized nanorods by using three-electrode systems. The structures are deposited on both ITO and ZnO-coated ITO substrates. By using a glass/SnO_2:F working electrode, a saturated calomel electrode (SCE) as a reference electrode, and a Pt wire counter electrode, Elias *et al.*[54] were able to calibrate their measurements. The electrolyte was 5 mM KCl and 0.1 M $ZnCl_2$ solution. In the first step, the working electrode is coated with a ZnO buffer layer, and then nanorods are deposited on it. The diameter of the rods can be varied by varying the $ZnCl_2$ concentration. Tang *et al.*[55] synthesized nanotubes with a similar setup.

2.8. Thermal evaporation

In the thermal evaporation process, the source material is heated at a higher temperature, and the evaporated material gets deposited on the substrate. Umar *et al.*[56] synthesized ZnO nanorods with ZnO powder as the source and Ni coated Si as the substrate. N_2 and O_2 gases were pumped at 5–15 and 10–30 sccm, respectively, and the deposition time was 30–120 minutes. 4–5 μm long ZnO nanorods with typical diameters of 300–350 nm were grown at 500–550 °C temperature. Bae *et al.*[57] synthesized nanowires with temperature in the range of 800–1000 °C at 500 sccm of Ar gas. Ga was doped by placing Ga powder along with ZnO powder. Tin (Sn) and indium (In) can be doped similarly by placing Sn and In powders along with ZnO powder. Nanotubes with an outer radius of 200 nm and (001) preferential growth were synthesized at 475 °C by Zhang *et al.*[58] Here Zn powder was the source material and Si wafer was the substrate. Argon was pumped into the tube furnace, and O_2 and O_3 acted as the source of oxidation for Zn to form ZnO. Thermal evaporation does not use any catalyst, which avoids unintentional contaminants. However, high temperature limits the available substrates for the synthesis of ZnO nanostructures.

2.9. Hydrothermal method

The hydrothermal method is often preferred over other methods as it provides nanostructures with controlled morphology and composition. ZnO nanostructures can be deposited at low temperatures, and the method is simple and catalyst-free. Since it is catalyst-free, the purity of the nanostructures can be high. In the hydrothermal process, zinc nitrate hexahydrate is used as a precursor with other materials like hexamethylene tetramine (HMTA). Ammonium compounds can be used to synthesize nanostructures. Wang *et al.*[59] synthesized ZnO nanowires. 1 M $(NH_4)_2CO_3$ and 0.04% PEG dissolved in distilled water with Zn nitrate were used as precursors. Zinc nitrate was gradually dropped into the solution. The solution was spin-coated on a substrate, and the process was carried out at 200 °C for 10 h. Tam *et al.*[60] synthesized ZnO nanorods. Zinc nitrate hexahydrate and HMTA were used as starting materials and polyethylene was added to enhance the aspect ratio. The obtained rods were annealed at 200 °C, 400 °C, and 600 °C, and the deposited structures showed (001) crystallographic orientation. Wei *et al.*[61] synthesized ZnO nanotubes with $ZnCl_2$ and ammonia as starting materials. Nanotubes produced at 95 °C presented 500 nm diameter and 3 μm length. A brief review of the hydrothermal method for the growth of different nanostructures is given by Djurisic *et al.*,[62] as the growing conditions have a considerable influence on the morphology of the nanostructures. Since the hydrothermal method is a wet chemical approach, the high aspect ratios of the synthesized structures cannot be expected, and the crystallinity of the structure is not high. The crystallinity can be improved by using the ZnO seed layer and annealing techniques. The prepared structures present many defects, leading to poor UV emission and enhancement in deep-level emission (DLE), thereby indicating poor optical quality.

All the methods specified above have their advantages and drawbacks. A particular method is typically selected based on the structure to be deposited and the field of application. Table 1 summarizes representative examples for the various methods to synthesize ZnO nanostructures along with their structural dimensions and starting materials.

3. Biomolecule immobilization on ZnO nanostructures

Conventional ZnO is a safe and non-toxic substance, and it is essential to have details of the toxicity of ZnO nanostructures

Table 1 Representative examples of specifications for synthesizing ZnO-based nanostructures by different methods

Method	Starting materials	Substrates	Structure	Dimensions and orientation	Ref.
PLD	99.99% pure Zn and O_2	Sapphire	Nanorods	D = 300 nm, L = 6 μm, O: [0006]	63
	Zn disc and O_2	Silicon	Nanocones	L = 1 μm, D = 100–200 nm, O: [0002]	64
	ZnO bulk	Ag	Monolayer	Two mono-layer thick	65
Sputtering	99.99% Zn, O_2	Si	Nanotubes	R (outer) = 200 nm	66
	ZnO, O_2	Cu/Ti/Si	Nanowires	D = 45–55 nm, O: [0 0 2]	67
	Pure Zn	n-Type Si	Nanorods	D = 125 nm, L = 675 nm	36
CVD	Zn acetyl-acetonate hydrate	Fused silica or Si	Nanorods	D = 60–80 nm, O: [0002], [0004]	37
	DEZ, NO_2	Si/SiO_2	Nanowires	D = 20–60 nm, L = 5–15 μm	39
	DEZ, O_2	Sapphire	Nanotubes	D = 50–150 nm, L = few μm, O: [001]	40
Sol–gel	Zn acetate hexahydrate, methenamine	SiO_2/Si	Nanorods	D = 170 nm	44
	Zn acetate hexahydrate, methenamine, DI water, urea	PAA templates	Nanowires	D = 70 nm	45
	Zn acetate hexahydrate, methenamine, DI water, urea	PAA templates	Nanotubes	D = 50–80 nm	45
Spray pyrolysis	$ZnCl_2$	SLG	Nanorods	D = 0.1–0.2 μm, L = 0.7–0.8 μm, O: [002]	49
	Zn acetate, DI water	ITO glass or SLG	Nanowires	O: [0001], [1010], [1120]	68
MBE	Metal Zn, O_3/O_2 plasma	SiO_2	Nanorods	D = 20–150 nm, L = 5–15 μm	50
	Metal Zn, O_3/O_2 plasma	SiO_2	Nanowires	D = 30–150 nm, L = 14 μm	51
	ZnO thin layer on a substrate, atomic O_2 by EIT	Si	Nanotubes	D = 10–90 nm; O: [0002]	52
ED	KCl, $ZnCl_2$	ITO	Nanorods	D = 250–300 nm, L = few μm	53
	KCl, $ZnCl_2$	Conducting glass/SnO_2:F	Nanowires	D = 25–80 nm, L = 0.5–1.8 μm, O: [0001]	69
	KCl, $ZnCl_2$	Conducting glass/SnO_2:F	Nanotubes	D = 60–200 nm, O: [0001]	55
Thermal evaporation	ZnO powder	Ni coated Si	Nanorods	D = 300–500 nm; L = 4 μm	70
	ZnO powder	Si	Nanowires	D = 80 nm; L = 10 μm, O: [0001]	57
	ZnO powder	Si	Nanotubes	D = 200 nm; O: [0001]	58
Hydrothermal	$(NH_4)_2CO_3$, PEG		Nanowires	D = 50–80 nm; L = 6 μm	59
	HMTA Zn nitrate hexahydrate	Si	Nanorods	O: [0001], D: 55–70 nm, L: 800 nm	60
	Ammonia and Zn chloride	Cu plate	Nanotubes	D = 500 nm; L = 3 μm, T: 50 nm, O: [0002]	61
	HMTA Zn nitrate hexahydrate, sodium citrate	—	Monolayer	O: [0001]	71

for their application in biosensing. More complexity has been added by the current trend toward smaller sizes. Nanomaterials have greater surface area and reactivity than their bulk counterparts, which can allow them to translocate across cell membranes, bind molecular species effectively, and catalyse chemical processes with greater ease.[72] For example, ZnO tetrapods (ZnO-T) have been put to use in a number of biological contexts because they are biocompatible, nontoxic, and harmless to normal cells.[73] The synthesis of nano-ZnO was described by Bhall *et al.*[74] using a surfactant-polyol assembly as a caging agent to keep the ZnO crystallite size down to nano-regime proportions. The surfactant-polyol-assembly acts as the agent for improving the biocompatibility of ZnO structures.

Applications in living organisms require the nanomaterial of interest to be biocompatible and to have less harmful by-products from its production process. Mouse positron emission tomography utilising ZnO NWs as an optical agent is described by Hong *et al.*[75] To increase bio-compatibility and decrease cellular toxicity, the NW conjugate was peptide-functionalized (NW-PEG-DOTA). In HeLa and L-929 cell lines, Li *et al.*[76] used MTT tests (3-(4,5-dimethylthiazol-2-yl)-2,5-diphenyltetrazolium bromide) to demonstrate ZnO NWs' good biocompatibility at concentrations below 100 mg mL^{-1}.

3.1. Criteria for biomolecule immobilization

A biosensor (Fig. 1) is an analytical device that contains a sensitive layer to detect a specific analyte coupled with a transducer which generates a quantifiable signal in proportionate to the analyte concentration.[77] Biosensors generally contain a sensitive layer that interacts with a specific target analyte and produces a signal due to proton exchange, heat or light emission, absorption or reflectance, the release of gases or ions, or any other kind of mechanism. The objective of a transducer is to transform the signal produced to a quantifiable signal that can be monitored.[78] A good biosensor should fulfill various factors such as stability under normal storage conditions and the ability to retain the response for longer days. The sensor must be highly selective and provide results with high reproducibility, sensitivity, and accuracy over a wide linear range of concentrations. The lower detection limit (LOD) must be as low as possible and the shelf-life as high as possible.

The main key factor for the development of biosensing devices is the immobilization of the biomolecule onto the transducer sensing area. The immobilization techniques must be such that the biomolecule should be strongly attached to the transducer sensing area and specific to detecting required materials or substances.[77,79] The immobilization of the

biomolecule must follow a few necessary criteria such as less loss of bioactivity after attachment to the sensor surface area, must be adhered to the sensor surface for a long term with high stability and durability, and must be active to only certain selected substances.[77] Other factors include resistance to pH variations, temperature, and chemical compositions. Also, unnecessary interferents should not influence the sensor activity. Various methods for immobilizing biomolecules include physical/chemical adsorption, covalent binding, and cross-linking between molecules.[80] The formation of a stable bioselective layer is an important task. For this process, ZnO is the best due to its high IEP at a pH of 9.5 as it attracts substances with low IEPs such as proteins or DNA, among others. The structural properties of ZnO play an important role in the immobilization of the bioselective layer. Two main methodologies of biomolecule immobilization are direct adsorption and covalent binding.

3.1.1. Direct adsorption of biomolecules. Direct adsorption of biomolecules is an easier process compared to covalent binding methods. Sasidharan *et al.*[81] reported bovine serum albumin (BSA) adsorption onto zinc oxide nanoparticles. BSA molecules show negatively charged functional groups above the IEP, forming attractive coulombic interaction between BSA and ZnO nanoparticles. The adsorption of BSA onto ZnO nanoparticles is favoured by electrostatic interactions. The BSA presence also stabilizes the size of ZnO nanoparticles effectively. The interaction of proteins with ZnO nanoparticles has been reported by Silva *et al.*[82] ZnO nanoparticles coated with BSA present neutral to slightly negative zeta potential values. Lactate dehydrogenase (LDH) interaction with ZnO nanoparticles is governed by physisorption. A negative correlation between LDH and ZnO nanoparticles indicates that the increase in ZnO concentration increases the sedimentation rate, thus reducing the surface area available for adsorption. An advantage of direct adsorption is that it is a simple process and can be performed under mild conditions. Moreover, a few proteins show better binding to a specific plane. Xie *et al.*[83] reported the plane-specific binding behavior of immunoglobin proteins. As per the results, the whole IgG protein showed binding towards the (1010) plane compared to other planes. A larger surface area enables higher enzyme loading.[84] A uric acid sensor based on ZnO nanosheets has been designed by immobilizing uricase by physical adsorption. ZnO nanosheets increased the surface area, resulting in more enzyme immobilisation and enhanced electron transport between the electrode and antibody. BSA interaction with ZnO nanorods has been reported by Klaumunzer *et al.*[85] High-resolution transmission electron microscopy (HRTEM) images indicate the amorphous shell of the BSA layer on ZnO nanorods. The photoluminescence (PL) spectra show that BSA conjugated ZnO nanorods quench visible emission, indicating the strong interaction of surface states of ZnO with amino acids of BSA. Also, the Stokes shift indicates strong electronic coupling between BSA and ZnO nanorods. Also, Bhogale *et al.*[86] reported interaction between ZnO nanoparticles and BSA using fluorescence spectroscopy. The bare BSA has intense fluorescence, which decreases after adding ZnO nanoparticles due to the formation of the complex by the interaction between ZnO and BSA. The negative free energy indicates that the reaction is spontaneous, and further negative entropy and enthalpy values indicate that the van der Waals interaction or hydrogen bonding is responsible for the binding of BSA to ZnO nanostructures. The role of nanostructure type in the binding of the biomolecule has been reported by Wang *et al.*[87] Different nanostructures of ZnO for protein adsorption are presented. BSA and fibrinogen are studied in ZnO nanorods, nanosheets, nanoparticles, and nanobeams. BSA attains equilibrium faster as compared to fibrinogen and also adsorbs easily over the surface. For multi-protein adsorption, the adsorbed amount falls as the first protein occupies the adsorption sites and causes a decrease in the adsorption sites for the second protein. The direct adsorption process of biomolecule immobilization occurs either through van der Waals forces, ionic binding, or hydrophobic forces. This method's benefits lie in its simplicity and amenability to moderate settings. However, biomolecules have some reversibility, and the binding forces are quite weak.

3.1.2. Immobilization through covalent binding. An alternative method for bioselective layer formation is the covalent binding of the biomolecule. For covalent binding of the ZnO nanostructure and biomolecule, cross-linking elements provide selective surface sites for the biorecognition element.[80]

Silanization through aminopropyl-triethoxysilane (APTES) and mercaptopropyl trimethoxysilane (MPTMS) has been reported. Sanguino *et al.*[88] reported ZnO nanorods for interdigitated immunosensors. Sulfo-MBS, which comprises *N*-hydroxysuccinimide (NHS) ester and maleimide groups, cross-links antibodies to amino acid side chains containing amine and sulfhydryl groups. Protein detection using ZnO nanostructures immobilized with immunoglobin has been reported by Sang *et al.*[89] The substrate was immersed in 2% (v/v) 3-APTES in deionized water. Later, after washing, the substrate was immersed in disuccinimidyl suberate (DSS) and in dimethyl sulfoxide (DMSO). Two cross-linking polymers for ZnO biosensors are reported by Munje *et al.*[90] Dithiobis succinimidyl-propionate (DSP) is a homobifunctional molecule that contains *N*-hydroxysuccinimide (NHS). The NHS esters are responsible for the formation of stable bonds in proteins when reacting with amines. Thiol groups form stable bonds with positive zinc ions and preferentially bind to Zn terminated surfaces. APTES silanizes by forming bonds with hydroxyl groups attached to the oxygen atoms of ZnO surfaces. The substrates are first sonicated in APTES solution with 2% ethanol and then dip-coated in solution. Baking the substrates in an atmosphere devoid of oxygen helps prevent silanization of APTES, which can be caused by exposure to ambient oxygen. Improved performance is obtained by thiol–ZnO interaction using DSP. ZnO nanoparticles for detection of troponin I are reported by Tan *et al.*[91] The ZnO surface is immobilized with an anti-cTnI monoclonal antibody (MAb). APTES with deionized water is dropped onto the ZnO surface. APTES binds with the ZnO surface by forming bonds with hydroxyl groups on oxygen atoms. Later, bifunctional linker glutaraldehyde in deionized water is dropped on the ZnO transducer. Similarly, surface functionalization of ZnO-FET biosensors for cardiac troponin I detection has been reported by Fathil *et al.*[92]

Biomolecule immobilization with DSP molecules and DMSO has been also reported by Jacobs *et al.*[93] Nanostructures of ZnO produced under oxygen-free conditions manifested as nanotextured films with columnar growth. Anti-troponin-T is immobilized onto the surface by first immobilizing the cross-linker molecule. DSP dissolved in DMSO is first dropped onto the surface, followed by anti-troponin T dissolved in phosphate-buffered solution (PBS). The superblock is then inserted to ensure that no DSP molecule has available *N*-hydroxysuccinimide sites. ZnO samples grown without the presence of oxygen displayed enhanced performance compared to samples grown with oxygen. ZnO samples grown without oxygen have mostly Zn terminated surfaces, and thiols bind to the positive Zn ions with higher coverage leading to a higher electrical biosensor response.

Self-assembled monolayers (SAMs) can be effective for surface functionalization due to the formation of a stable sensing surface area. Zhang *et al.*[94] reported surface functionalization of ZnO self-assembled monolayers. Synthesized ZnO nanowires and wafers were submerged in 3-PPA. The SAMs on their surfaces were formed using either an aqueous solution or a 10-phosphonodecanoic acid (10-PDA) methanol solution. ZnO wafers containing SAMs were first put into NHS and 1-ethyl-3-[3-dimethylaminopropyl] carbodiimide hydrochloride (EDC) solution in 2-(*N*-morpholine)-ethane sulfonic acid (MES). Submerging the modified wafers in an IgG solution in MES buffer was the next step. Atomic force microscopy (AFM) images indicated island-like structures for 10-PDA molecule functionalized ZnO. Biomolecule immobilization with phosphoric cross-linking molecules has been reported by Dembereldorj *et al.*[95] 16-Phosphonohexadecanoic acid (16-PHDA) assembled ZnO nanoparticle solution was mixed with the mixture of BSA (or transferrin (Tf)) and EDC. Using 16-PHDA, the proteins were stabilised. Due to the presence of the phosphonic acid group, 16-PHDA was predicted to adsorb onto the ZnO surfaces. By means of an EDC coupling process, the carboxylic groups of 16-PHDA on ZnO's surface reacted with the amino groups of the proteins. Functional groups of enzymes or proteins lead to covalent binding to a solid surface. The advantage of covalent binding is that the biomolecules are strongly immobilized onto the surface and are less likely to detach. This method provides minimal loss of biological activity. Moreover, the availability of several functional groups for covalent immobilisation makes it possible to avoid the active site of the binding process.

4. Classification of biosensors

The basic working principle of biosensors is shown in Fig. 2. ZnO biosensors can be classified based on the transduction method and the bioreceptor.[96] In the case of bioreceptors, ZnO biosensors are classified depending on the type of sensing molecule used. The sensing molecule could be an enzyme, antibody, DNA, and protein.

Enzymes are used to detect specific molecules, which upon interaction with analytes, produce a product that can be detected by one of the transduction methods. Enzymatic biosensors are affected by factors like pH and temperature. A specific antigen binds to the antibody in a highly specific way for antibody-based sensors, making them essential for immunosensors. DNA-based

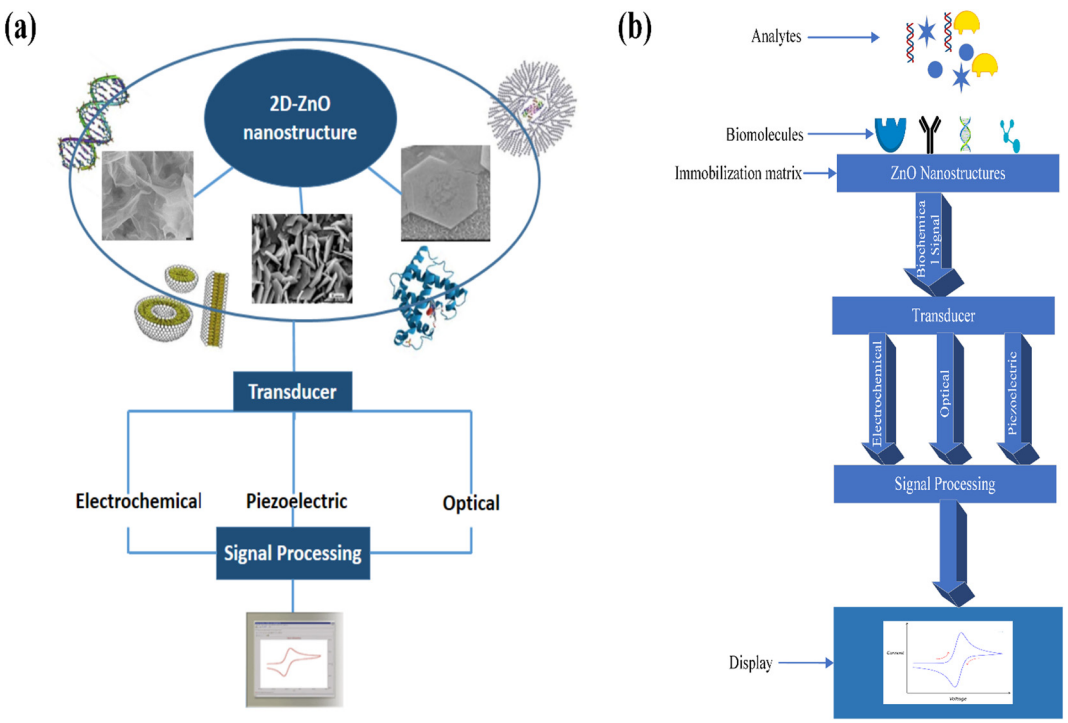

Fig. 2 Schematic representation of the working principle of representative biosensors.

biosensors use complementary nucleotides as the recognition element. For known sequences of DNA, a complementary sequence called a DNA probe is synthesized, labeled, and hybridized to detect the target biomolecule. In detecting proteins, selecting a required protein by neglecting a wide range of other proteins depends on the biocomponent, which serves as a molecular recognition tool in binding the required protein. The specific protein detection requires sensing areas immobilized with antibodies or aptamers that are connected to transduction systems.

ZnO based biosensors are typically categorized into electrochemical, optical, and piezoelectric biosensors based on the transduction method.[97] In electrochemical biosensors,[98] the biomolecule and the target analyte react to produce or consume carriers that produce an electrical signal. Three different methods are used in electrochemical transduction: potentiometry, voltammetry, and amperometry. Amperometry is widely used for biosensor transduction mechanisms. In this method, the sensor is placed at a fixed potential which acts as a driving force for carriers, and the target analyte is added in steps. A change in current occurs with the change in the target analyte concentration, which allows monitoring the amount of the target analyte. The potential is swept between two values between the two electrodes for cyclic voltammetry methods, and the current is plotted against the potential.

The reduction and oxidation peaks appear in the plotting cycle based on the reduction and oxidation reactions. The current response per concentration and area of electrode gives the sensitivity of the biosensor. In the potentiometric method, the charge accumulated at the surface of the electrode causes a change in the potential of the working electrode with respect to the reference electrode. The current produced is plotted against the logarithmic concentration of the analyte to monitor the amount of the target analyte. The slope of the plotted curve provides the sensitivity. In impedimetric biosensors, the production of carriers changes the resistance of the solution, and this measurable parameter is used for the detection and monitoring of the target analyte. Because the relationship between potential and analyte concentration in potentiometric biosensors is logarithmic, the sensors are less sensitive.

Surface plasmon resonance biosensors are used in optical biosensors to detect changes in the refractive index caused by the interaction of analytes with bioreceptors.[99] Variation in density is quantified by observing the angle at which reflected light shifts. The interaction of analytes with adsorbed receptors on the transducer's surface area causes a change in the Raman signal, which is measured by surface enhanced Raman spectroscopy (SERS). This occurs because carriers are transferred between ZnO and the electrodes. For the photoluminescence (PL) technique, the change in the PL spectra is observed before and after adsorption of the bioreceptor and after the interaction with the target analyte. The change in the PL band allows the detection of the target analyte.

The third category of the biosensor transduction method is the piezoelectric method.[100] Piezoelectric biosensors use a piezoelectric material that oscillates at a specific frequency upon giving an electrical signal of a specific voltage, and the frequency of oscillation changes when the mass of the crystal changes or the electric signal changes. The change in the mass on the surface of piezoelectric material upon binding with biomolecules changes the oscillation frequency. A quartz crystal is placed between two electrodes in a quartz crystal microbalance (QCM) device, with the crystal's oscillation frequency being affected by a change in mass. FETs are also explored for biosensor applications. The ZnO nanostructures are used as the channel, and when the target molecules interact with the biorecognition element, the conductance of the channel changes. The change in the channel's conductance is used as the measuring parameter for detecting target molecules. Further detailed information can be obtained from the reviews reported.[101–103] The detailed classification of biosensors based on bioreceptors and transduction methods is shown in Fig. 3.

4.1. Dimension based classification for ZnO biosensing applications

4.1.1 2D-ZnO nanostructures. Typically, 2D materials have a high surface to volume ratio with a large surface area, and their unique electronic structures and atomically thin layers are very enticing because of the exceptional material features they offer that are not possible to produce with conventional bulk structures.[104] ZnO nanoflake based linker-free electrochemical biosensors have been reported by Alam *et al.*[105] for the detection of L-lactate from the sweat. The ZnO nanoflakes grown on gold-coated flexible polyethylene terephthalate (PET) substrates are immobilized with lactate oxidase for higher sensitivity. The sensor showed a wide linear range from 10 pM to 20 mM with 1.26 nM LOD and a sensitivity of 11.76 μA per decade per cm^2. Further, the sensor showed a recovery of about 85% with relative standard deviation $<4\%$ for real human samples. ZnO/MoS_2 nanocomposites grown on glassy carbon electrodes have been reported as a sensing platform for DNA assay.[106] Furthermore, nanostructured ZnO/MoS_2 showed DNA immobilisation capability due to the strong electrostatic contact between negatively charged DNA and positively charged ZnO. To detect epinephrine, Zhu *et al.*[107] presented flower-like ZnO nanosheets integrated inside a 3D ferrocene-functionalized graphene framework (3D graphene@Fc) (EP). The resulting ZnO/3D graphene@Fc hybrid, which has the shape of a flower, shows improved electrocatalytic activity for the oxidation of EP and its product. As a result, a highly sensitive and selective electrochemical biosensor is described for EP detection, with a linear response of 0.02 to 216 M, a LOD of 0.0093 M, and excellent stability (97.7% capacity retention after scanning for 20 h). Electrochemically reduced graphene oxide/ZnO nanocomposites grown on indium tin oxide electrodes have been reported for the detection of uric acid.[108] The linear response of the sensors was seen throughout a concentration range of 1 mM to 400 mM, and their sensitivity was 150.7 μA cm^{-2} mM^{-1}.

The structure of ZnO nanoflakes is directed towards a nano-honeycomb structure when grown on an Al coated glass capillary.[109] The ZnO nanoflakes can be immobilized with GOx and then coated with Nafion for higher sensitivity. Glucose concentrations can be measured from human adipocytes and

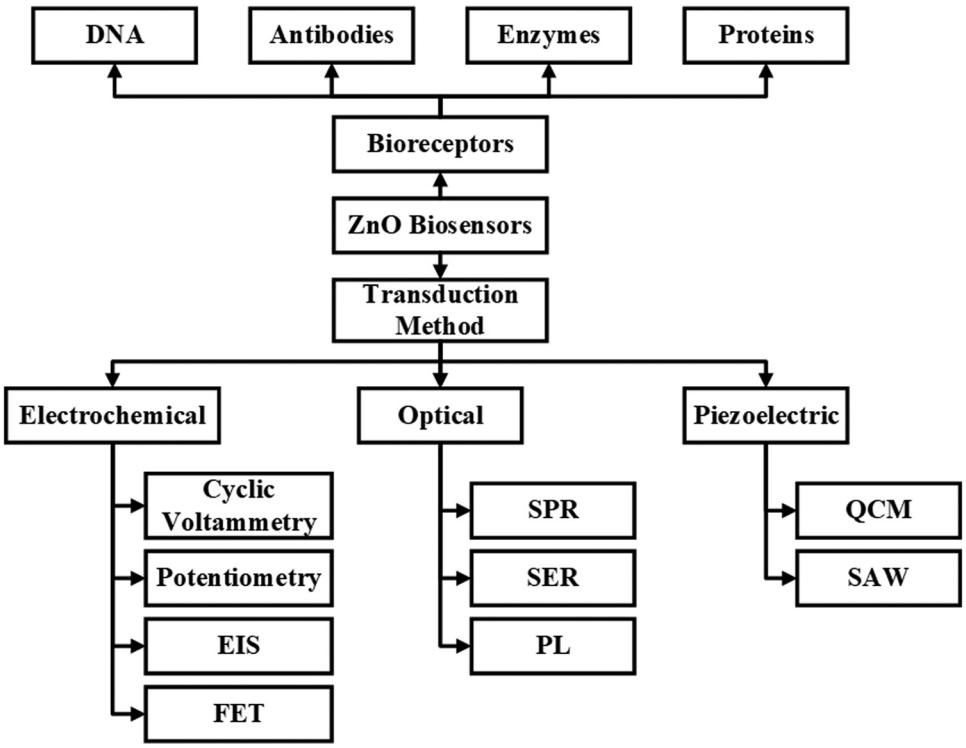

Fig. 3 Classification of different biosensors based on bioreceptors and transduction methods.

frog oocytes. The sensors showed a linear response from 500 nM to 10 mM with a fast response within 4 s. ZnO nanoflakes for uric acid detection are reported by Ali *et al.*[110] The SEM images are depicted in Fig. 4(a). Uricase along with Nafion coating is dropped on ZnO nanoflakes for detection of uric acid. Uric acid is oxidized to allantoin and carbon dioxide in the presence of uricase. Allantoin is converted to allantoinium ions in water, which causes a potential change at the ZnO electrode. The potentiometric results show a wide linear response from 500 nM to 1.5 mM with 66 mV dec^{-1} sensitivity, with the sensors being inert toward ascorbic acid and glucose. Chauhan *et al.*[111] reported the detection of *Helicobacter pylori* using the ZnO tetrapods grown on screen printed electrodes. The designed electrochemical immunosensor showed a good linearity in the range of 0.2 0.2 ng mL^{-1} to 50 ng mL^{-1} with a LOD of 0.2 ng mL^{-1}. Also, ZnO–Ag_2O composite nanoflowers are proposed for the detection of dinitrotoluene in water.[112] The composite ZnO modified Ag electrode showed enhanced sensor performance compared to ZnO or Ag_2O electrodes. The sensor exhibited a sensitivity of 5 μA μM^{-1} cm^{-2} with an LOD of 13 nM in a linear range from 0.4 μM to 40 μM. Psychoyios *et al.*[113] reported biosensors for cholesterol by using ZnO nanowalls immobilized with ChOx. ZnO nanowalls facilitate electron transport between the enzyme and the electrode by providing a high surface area for enzyme loading. The lipid coating not only aids in the preservation of the enzyme's function, but it also improves biocompatibility. The sensor is highly sensitive with 57 mV dec^{-1} sensitivity in a linear concentration range from 1×10^{-6} M to 1×10^{-3} M with a response time of around 5 s. MoS_2 assisted the growth of ZnO nanostructures for biosensing as reported by Yang *et al.*[106] Thus DNA biosensors were fabricated through ZnO nanowalls grown on 2D MoS_2 (Fig. 4(b)).

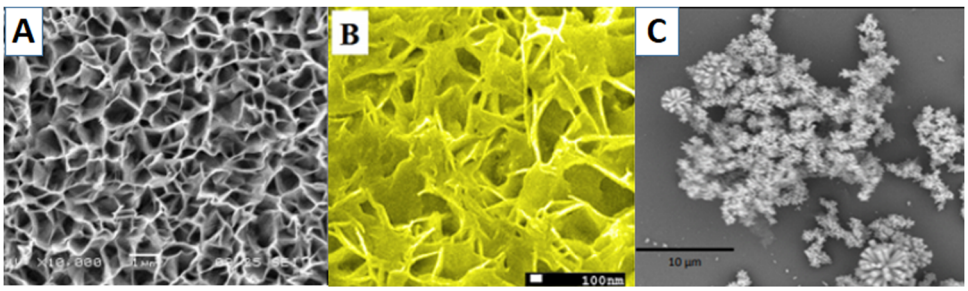

Fig. 4 ZnO 2D nanostructures: (a) as-fabricated ZnO-nanofiber arrays,[110] (b) ZnO/MoS_2 nanowalls[106] and (c) ZnO nanoflowers grown on an activated glass surface.[114]

Promyelocytic leukaemia and retinoic acid receptor alpha (PML/RARA) fusion genes were closely monitored with the sensor. The ZnO nanostructures are vertically aligned on the MoS_2 layer and show higher hybridization efficiencies than individual structures. Porous structures provide a higher surface area for bioreceptor immobilization. Similarly, nanoporous ZnO films for uric acid detection were reported by Mozaffari *et al.*[28] The cavities in the nanoporous films increase the surface area for enzyme loading, thus reducing the diffusion distance for the substrate to access the enzyme. The sensors present good sensitivity with linear detection from 0.83 to 23.24 mM and a LOD of about 0.40 mM.

ZnO nanoflower-based biosensors for amyloid detection have been reported by Akhtar *et al.*[114] ZnO nanoflowers with thioflavin were grown on a silver film-coated glass slide (Fig. 4(c)). This sensor worked by enhancing the fluorescence of thioflavin T bound insulin due to the waveguiding capacity of ZnO nanoflowers, thus acting as a reflecting mirror in a Fabry–Perot resonator. ZnO's rough surface provided a larger surface area for sensor activity, as Saha *et al.*[115] reported. High sputtering pressure introduced Zn interstitial defects, which increased the electrical conductivity and electron transferability. Though 2-D ZnO nanostructures do not have a particularly high surface area, as shown in Fig. 3, their high surface charge density proves to be a good aspect for biosensor applications. Also, the synthesis procedures for 2-D ZnO nanostructures are simpler than for 1-D nanostructures. Owing to their planar structure, they can provide a higher density of bioreceptor immobilization, thereby improving the sensitivity of the biosensor. Furthermore, for a particular structure, the biosensitivity can be more efficient for certain biomolecule targets.

4.1.2. 1D ZnO nanostructures. 1-D ZnO nanostructures provide larger aspect ratios for enzyme immobilization. The performance of ZnO nanorod based GOx biosensors for glucose can be improved by electrodeposition of AuNPs.[116] AuNPs increase the transfer of electrons between the GOx and electrode and also inhibit the recombination of electron–hole pairs. AuNPs increase the sensor sensitivity by 5 times while the LOD is reduced. Other parameters such as stability, linear range, and selectivity are also improved. Riduan *et al.*[117] reported the use of Pt nanodendrites (PtNDs) for the performance enhancement of the glucose biosensor. The ZnO nanorods coated with PtNDs present better performance than the biosensor without the PtND. The sensors showed an increased sensitivity from 15.71 μA mM^{-1} cm^{-2} to 98.34 μA mM^{-1} cm^{-2} with the use of PtNDs. Polydopamine was deposited on ZnO and the ZnO–PDA composite was used for the detection of glucose.[118] Glutaraldehyde was used as the cross-linking polymer to immobilize GOx. The sensor had a good response in the glucose concentration range from 0.0062 to 0.120 mM.

Shukla *et al.*[119] reported that higher aspect ratios support to improve enzyme immobilization (Fig. 5). Also, the charge transfer resistance decreases, which further enhances the electron transferability. Therefore, higher sensitivity is recorded for ZnO structures having a higher aspect ratio with a response time of around 5 s. Lee *et al.*[120] reported that nanorods with higher deposition times have better efficiency for detection of DNA oligonucleotides. To detect streptavidin, Sang *et al.*[121] reported rod nanowires, hexahedral puncheons, and sharp ZnO nanowires. Sharp ZnO nanowires showed a better response as they present a high aspect ratio and higher binding sites on the surface than rod nanowires and hexahedral puncheons. Pradhan *et al.*[122] reported ZnO nanowires for glucose biosensors. GOx immobilized ZnO nanowires on Au-coated polyester exhibited a high sensitivity of 19.5 μA cm^{-2} m^{-2} M^{-1}, with a response time of less than 5 s.

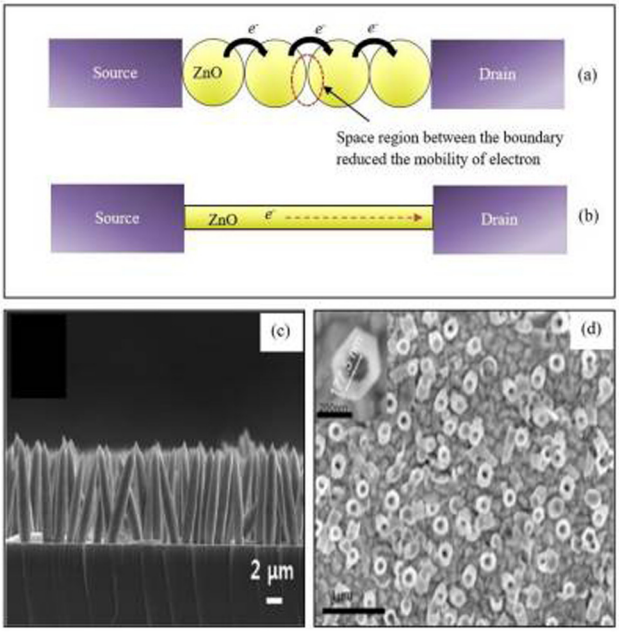

Fig. 5 The schematic diagram of electron flow through ZnO nanostructure bridges between source and drain for (a) nanoparticles and (b) a single lateral nanowire. (c) Cross-sectional image of ZnO nanorods. (d) Top view FESEM image of ZnO nanotubes.[127]

Uric acid biosensors involving ZnO nanorods grown on glassy carbon electrodes have been reported by Zhang *et al.*[123] The surface area of ZnO nanorods facilitates direct electron transfer between uricase and the electrode. The amperometric measurements also showed a linear response for the concentration range 5.0×10^{-6} to 1.0×10^{-3} mol L^{-1} with a LOD of 2.0×10^{-6} mol L^{-1}. Kong *et al.*[124] reported glucose biosensors based on ZnO nanotubes immobilized with GOx. The sensor demonstrated a detection range of 50 μM to 12 mM with a LOD of 1 μM and a sensitivity of 21.7 μA cm^{-2} mM^{-1}. Copper-doped ZnO nanofibers have been implemented for malaria detection by Paul *et al.*[125] The copper-doped ZnO nanofibers functionalized with mercaptopropylphosphonic acid are used for the detection process. Mercaptopropylphosphonic acid enhanced the ability of functional groups for enzyme immobilization. In this system, copper enhanced the electrical conductivity, and the electric field created at the copper–ZnO junction brought the target closer to the mercaptopropylphosphonic acid-treated nanofiber. Ag doping is found to improve biosensor performance, as reported by Zhou *et al.*[126] The ZnO nanorods doped with Ag and immobilized with GOx are used for the detection of glucose.

The Ag doping makes the surface of ZnO nanorods smoother and reduces the contact area of the solid–liquid interface. Also, it allows reduction of the charge transfer resistance and enhancement of the electron transferability of the ZnO nanorods. Moreover, the catalytic activity of GOx is also improved. Due to the above factors, the glucose biosensor performance is enhanced, and the optimum doping of Ag is around 2 mM, with higher Ag doping leading to the formation of Ag_2O, which reduces the performance of the biosensor. The linear range of the sensor is from 1.5×10^{-3} to 6.5 mM, and its sensitivity is 85 μA mM^{-1} cm^{-2} with an LOD of 1.5. μM.

ZnO biosensor performance also depends on the dimensions of the nanostructures. Kim *et al.*[128] reported glucose biosensor performance based on ZnO dimensions. The ZnO nanorods grown on the substrate are classified into three groups based on dimensions. The ZnO nanorods with lower diameters and high aspect ratios are densely packed and found to have the highest sensitivity of 69.8 nA μM^{-1} cm^{-2}. The large surface area of ZnO nanorods has a larger amount of GOx and hence improved performance of the sensor. 1-D nanostructures provide a higher surface area for biomolecule immobilization and also better electrical conductivity. The high aspect ratio of the nanostructures also improves their sensitivity as it allows higher biomolecule immobilization. Densely packed structures can also provide improved results. Small signal strength, difficulties in creating electrical connections, incompatibility with the CMOS process, and the typical nanostructure production procedure, which normally needs high temperature, are all limitations of 1-D ZnO in the context of the CMOS process for biosensors.[129]

4.1.3. ZnO quantum dots. ZnO quantum dots are also called 0-D nanostructures and they provide a higher surface area for biomolecule immobilization. The detection of tetracycline using europium-grafted ZnO quantum dots was reported by Wu *et al.*[130] The internal reference is yellow-emitting ZnO QDs, with the signal reporting unit being Eu^{3+} chelated on the surface of ZnO QDs. The nanoprobe exhibits a LOD of about 4 nM and its fluorescence changes from yellow to red for higher concentrations of tetracycline. Ali *et al.*[131] reported ZnO quantum dots for the detection of uric acid. It has also been reported that uricase immobilised on ZnO quantum dots is used to make the uric acid sensor. In the concentration range from 1 mM to 10 mM, the sensor's linear response was seen at a high sensitivity of 4.0 μA mM^{-1} cm^{-2}. ZnO nanoparticles affect the insulation property of the polyvinyl butyral (PVB) membrane. A glucose biosensor with ZnO nanoparticles in conjugation with GOx has been reported by Ren *et al.*[132] The cyclic voltammetry of bare Pt wire is reduced when coated with the PVB membrane, and the current peaks reappear after GOx with ZnO nanoparticles is introduced. By providing a conductive channel from the enzyme to the electrode and a broad surface area for enzyme immobilisation, ZnO nanoparticles speed up the electron transfer rate and boost the current response. The sensor shows a good selectivity at a pH of 6.8 and a temperature of 35 °C with the photovoltaic effect being found to improve the catalytic activity of GOx and hence enhance the performance. ZnO quantum dots for dopamine detection have been reported by Zhao *et al.*,[133] with the fluorescence being quenched due to the electron transfer between the ZnO quantum dots and oxidized dopamine quinone.

Hybrid ZnO nanostructures with carbon nanotubes (CNTs) are also explored due to the good catalytic activity of CNTs. Hayat *et al.*[134] reported cholesterol biosensors constructed by ZnO nanoparticles incorporated onto carbon nanotubes immobilized with ChOx. The cholesterol reacts with ChOx and produces H_2O_2. The H_2O_2 is then used to oxidize 2,2′-azinobis(3-ethylbenzthiazoline-6-sulfonic acid) (ABTS), thus producing a green-colored product that helps in quantizing the cholesterol content through calorimetric analysis. The nanocomposite structure of ZnO and CNTs catalyzes the oxidation of ABTS. Fidal *et al.*,[135] on the other hand, reported that Al-doped ZnO immobilized with GOx showed a better response in terms of sensitivity, linearity, and LOD compared to the bare ZnO structure immobilized with GOx. GOx bioactivity can be improved by avoiding leakage with poly diallyl dimethylammonium chloride (PDDA) layer coating. Wang *et al.*[136] reported a multi-layer structure of biosensors for glucose detection. The nanocomposite of ZnO nanoparticles and multi-walled carbon nanotubes (ZnO/MWCNTs) immobilized with GOx was reported to be coated with the PDDA layer. The PDDA layer avoids GOx leakage, thereby improving the bioactivity of GOx. The electrocatalytic response towards H_2O_2 indicated that ZnO nanoparticles do not influence the MWCNTs. The sensor had a

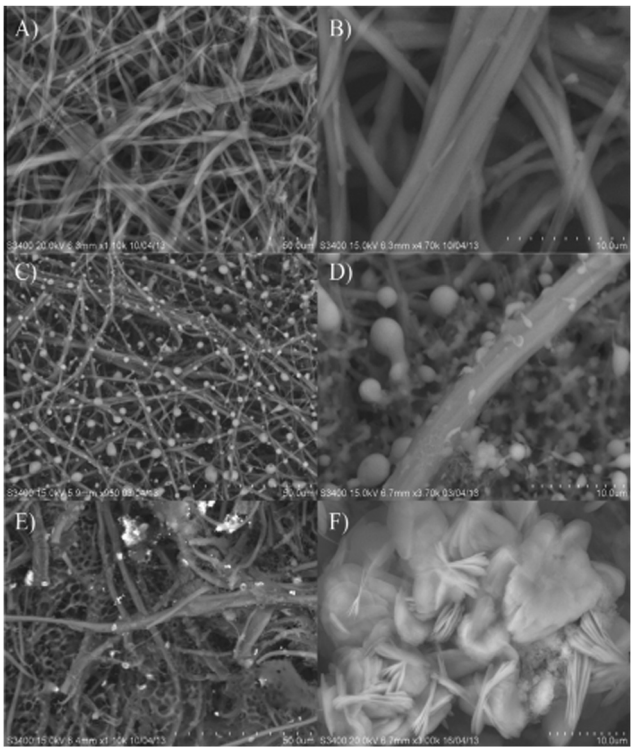

Fig. 6 A scanning electron micrograph of the (A) and (B) eggshell membrane [ESM], (C) and (D) GOx immobilized ESM [GOx/ESM] and (E) and (F) ZnO and GOx immobilized ESM [GOx/ZnONPs-[EMIM][Otf]/ESM].[137]

LOD of 250 nM for 2.0 U of GOx and retained 90% of the initial response after 160 days.

Aini *et al.*[137] reported electrochemical glucose biosensors based on ZnO nanoparticles immobilized with GOx, ionic liquid, and an eggshell membrane onto a glassy carbon electrode (Fig. 6). Methylene blue was used as a redox indicator. The ZnO nanoparticles in the egg shell membrane and ionic liquid increase the surface area of the sensor. The sensor with the ESM showed a better response than the one with a chitosan (CHIT) membrane. The LOD was 10^{-13} M with a linear detection range from 1×10^{-12} to 6 mM. The novel method of ZnO synthesis from leaf extract is reported by Dayakar *et al.*[138] Glucose detection is done by utilising ZnO nanoparticles generated by a bio-mediated approach employing *Ocimum tenuiflorum* leaf extract. The sensor has a linear range of 1 to 8.6 mM, a LOD of 0.043 mM, and a sensitivity of 631.30 μA mM^{-1} cm^{-2}.

Furthermore, a biosensor designed by using doped ZnO nanostructures was presented by Mahmoud *et al.*[139] A non-enzymatic glucose biosensor was designed by using Cu doped ZnO. Cu doping is found to increase the electrochemical properties of the sensor. The nanocomposites with their catalytic features exhibit enhanced activity.[140] ZnO quantum dots are reliable candidates for the design of the biosensor. The major aspect of ZnO quantum dots is the size of the nanoparticles. Reduction in the nanoparticle size increases the surface area for higher enzyme loading, thereby enhancing the biosensor's performance. One of the drawbacks of quantum dots is their degraded mobility with increasing grain boundaries.[141]

4.2. Types of ZnO biosensors

4.2.1. Electrochemical biosensors. Electrochemical biosensors are widely used because of their high sensitivity, wide detection range, reproducibility, and low cost. Innovations in biosensors are intertwined with the fields of architectural engineering and materials science. Therefore, material selection is an integral part of the biosensor design and manufacturing process. Two electrodes serve as the transducer in an electrochemical biosensor, which also includes a layer of biological recognition molecules and a protective layer. The materials, size, and shape of a sensor are heavily influenced by factors including the transducer's operating principle, the characteristics to be detected, and the working environment. Typically, just a working electrode and a stable reference electrode are used in electrode systems for measuring ion concentrations in liquids and dissolved gas partial pressures, although a counter electrode is frequently used in these experiments as well. Furthermore, the method employed to immobilise the sensor's biological recognition components might have a significant impact on biosensor performance. In electrochemical biosensors, the biosignal is generated by means of an electrical response which could be measured by either cyclic voltammetry, potentiometry, amperometry, or electrochemical impedance spectroscopy (EIS). Fig. 7 shows the mechanism of electrochemical biosensors. The electrodes act as transducers which help in producing the signals in the form of electric currents, which in turn allows the detection and monitoring of the amount of the target analyte.[142]

ZnO–rGO nanocomposites have been functionalized with tyrosinase for the detection of dopamine.[143] The sensor's LOD was as low as 8.75 ± 0.64 pM, and its linear range was as large as 0.1–1500 pM. Its sensitivity was 39.56 ± 0.41 μA nM^{-1}, which is rather impressive. The sensor had a response time of 0.34 ± 0.09 s and showed excellent selectivity for DA in a variety of blood serum components. ZnO nanoarchitecture decorated rGO is reported for the non-enzymatic detection of uric acid and glucose.[144] The sensor was sensitive to uric acid in the concentration range from 0.02×10^{-3} to 7.2×10^{-3} mM with a LOD of about 0.012 mM whereas for glucose the concentration range was 0.02×10^{-3}–18×10^{-3} mM with a LOD of 0.008 mM. The biosensor was shown to have a sensitivity of 682.8 mA mM^{-1} cm^{-2} for urea, while for glucose the sensitivity was only 481 mA mM^{-1} cm^{-2}.

Reports of Ag/ZnO with a variety of ZnO nanostructures for non-enzymatic urea detection have been made.[145] By combining a sputter deposition and solution growth technique, ZnO nanorods and nanoflakes with varied crystallographic orientations were produced. The Ag/ZnO nanorods on carbon electrodes are found to exhibit better characteristics than ZnO nanoflakes due to the larger surface area. Another non-enzymatic biosensor based on ZnO nanorods with an Au coating has been described for the detection of glucose. The Au–ZnO nanorods allowed for a high sensitivity of 4416 μA mM^{-1} cm^{-2}, a low LOD of 0.12 μM, and a linear range of up to 15 mM. Baruah *et al.*[146] reported Co and Fe codoped ZnO for glucose sensing. The PL intensity of the

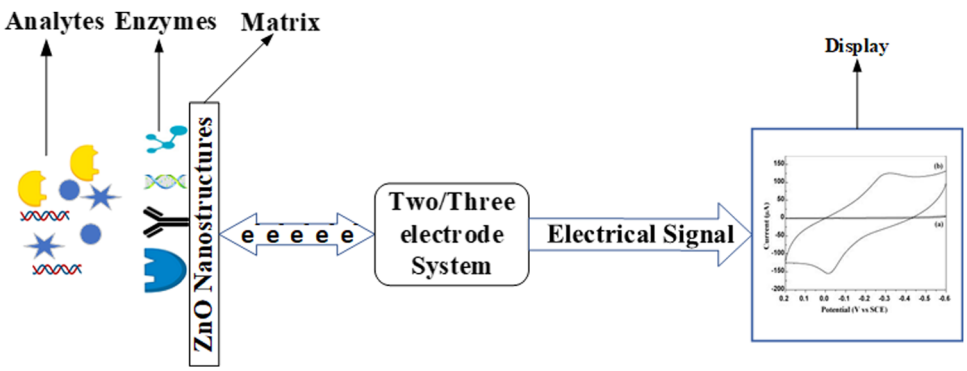

Fig. 7 Schematic representation of the working principle of electrochemical biosensors.

doped ZnO was reduced and it showed better conductivity than the pristine ZnO. The doped ZnO was modified with GOx for the detection of glucose. The sensor presented 2-fold improved sensitivity compared to pristine ZnO of about 32.2 μA mM^{-1} cm^{-2} with a linear range from 0 to 4 mM. Fig. 8 depicts the merits of various ZnO nanostructures with different morphologies.

Israr *et al.*[148] reported the detection of cholesterol by ZnO nanorods. Ag/AgCl was used as a reference electrode, and the ZnO/Ag electrode with dip-coated ChOx served as the working electrode. The variation in the concentration of the cholesterol electrolyte solution causes potential difference between the electrodes, which is due to a change in cholesterol concentration. The reference electrode exhibits constant potential, but the working electrode causes a change in emf due to the reactions between the electrolyte solution and ChOx. Recently Supraja *et al.*[149] reported a CNT embedded ZnO nanofibre-based biosensor. The nanofibre modified the electrode and immobilized it with an antiatrazine antibody for atrazine detection. The sensor showed good electrical conductivity and exhibited a sensitivity of 21.61 kΩ μg^{-1} mL^{-1}. Potentiometric results of the bioelectrode are plotted against the logarithmic concentration of electrolytes.

Ali *et al.*[150] reported the detection of uric acid by using ZnO nanowires immobilized with uricase. The uric acid solution was used as the electrolyte, Ag/AgCl as the reference electrode and the uricase immobilized ZnO nanowire electrode as the working electrode. The potential response against concentration showed a linear response from 1 μM to 1 mM on the log scale. In another work, Israr *et al.*[151] reported the detection of cholesterol by using ZnO nanowall structures immobilized with ChOx. Detection of C-reactive protein (CRP) by using ZnO nanotubes was reported by Ibupoto *et al.*[152] ZnO nanotubes were immobilized with monoclonal anti-c-reactive protein and glutaraldehyde using the physical adsorption method. The sensor showed a linear response for CRP in the concentration range 1×10^{-5} mg L^{-1} to 1×100 mg L^{-1} with a sensitivity of approximately 13.17 mV per decade. The sensor has a lifetime of three days, and hence it can be used as a disposable sensor. The sensor electrode showed good reproducibility with a relative standard deviation of less than 5%. Further, when tested with human blood serum, which contains interferents like glucose, sodium and potassium ions, uric acid, *etc.*, the sensor shows good selectivity.

The same type of biosensor was reported for L-lactic acid detection.[153] The sensor was constructed by using ZnO nanorods immobilized with lactate oxidase along with glutaraldehyde. The potentiometric analysis of the sensor indicated a linear range of detection within the concentration range from 1×10^{-4} to 1×100 mg L^{-1} with 41.33 1.58 mV dec^{-1} sensitivity. The sensor showed good selectivity in the presence of interferents such as glucose, ascorbic acid, galactose, magnesium ions, and calcium ions. The sensor had a stability of about three weeks. ZnO nanoflakes immobilized with GOx were reported for detection of glucose by Fulati *et al.*[154] The potentiometric response showed linear response within the concentration range 500 nM to 10 mM. The sensor had a fast response time of about 4 s. Improved glucose biosensing performance was reported by incorporating graphene nanoplates beneath ZnO nanowires by Rafiee *et al.*[155] The sensor reported a linear range from 0.003 to 30 000 mg dL^{-1} with a response time of 5 s.

ZnO nanorods were used by Ibupoto *et al.*[156] to detect penicillin by an aqueous chemical growth method. Nanorods were immobilized with penicillinase along with *N*-5-azido-2-nitrobenzoyloxysuccinimide as a cross-linking polymer.

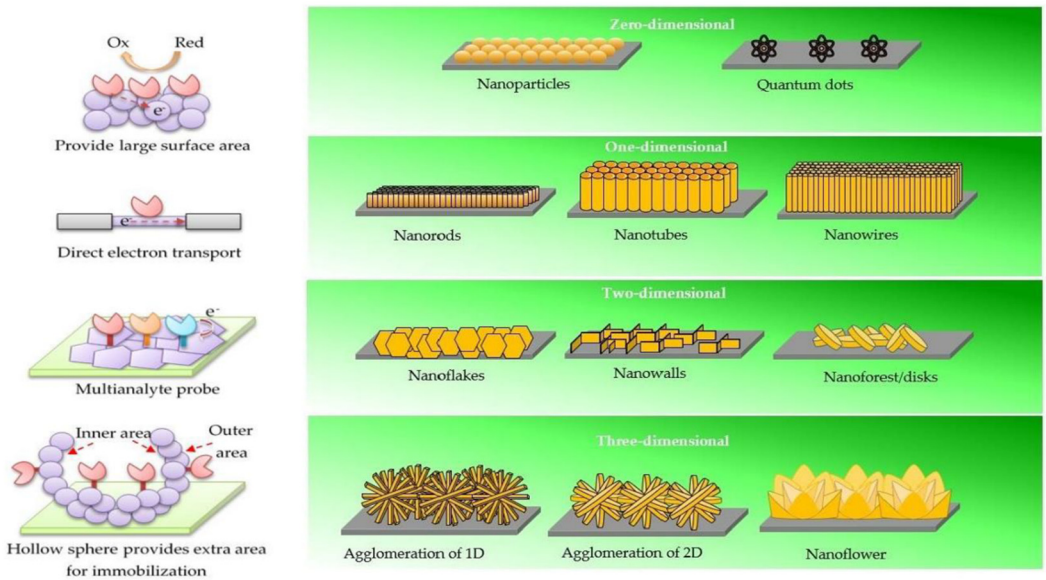

Fig. 8 Size-dependent benefits of ZnO nanostructures. 0-D nanostructures have a higher surface area. Electron transport in 1-D nanostructures is both stable and direct. Two-dimensional nanostructures provide specific planes for the immobilisation process, allowing for the multiplexed detection of analytes. Extra outer and inner surface area of 3-D nanostructures means additional immobilisation sites.[147]

The potentiometric analysis revealed good sensor selectivity with negligible response to sucrose, glucose, ascorbic acid, uric acid, *etc.*, with a good sensitivity of 121 mV dec^{-1}. The sensor had a linear response for concentration ranging from 100 μM to 100 mM with a response time of 5 s. Indirect detection of mercury ions by a glucose biosensor was reported by Chey *et al.*[157] The ZnO nanorods were observed to be immobilized with GOx along with the CHIT membrane and glutaraldehyde. The sensor showed inhibition activity from 0.5×10^{-6} mM to 0.5×10^{-4} mM and from 0.5×10^{-4} mM to 20 mM of mercury ion for 1 mM glucose. The inhibition was further reduced for 10 mM glucose concentration. The sensor showed good selectivity with a response time of 8 s and 90% sensitivity even after three weeks.

Furthermore, Ali *et al.*[158] reported a glucose biosensor based on ZnO nanotubes immobilized with GOx along with Nafion coating. The sensor had a linear response over the concentration range of 0.5×10^{-6} to 12×10^{-3} M with a response time of 4 s and a sensitivity of 69.12 mV dec^{-1}. The sensor was found to be less influenced by interferents like uric acid and ascorbic acid. Later, Khun *et al.*[159] reported the detection of galactose by using a ZnO nanorod-based biosensor, immobilized with galactose oxidase and glutaraldehyde as a cross-linker. Potentiometric analysis of the sensor demonstrated its linear response throughout the concentration range of 10 mM to 200 mM, with a sensitivity of 89.10 ± 1.23 mV dec^{-1} and a reaction time of less than 10 s. The sensor can be used for about four weeks which is its shelf-life. In order to detect the BCR/ABL fusion gene, Xia *et al.*[160] built a new biosensor based on ZnO nanorods/Pt. The linear detection range for this sensor was between 1 pM L^{-1} and 1 nM L^{-1}, and the LOD was 2.75×10^{-13} mol L^{-1}.

In another work, Singh *et al.*[161] reported the detection of cholesterol using nanoporous ZnO immobilized with ChOx. The cyclic voltammetry measurements indicate the oxidation peak at 0.5 V and the current at 0.5 V, which increased further by an increase in cholesterol concentration from 25 to 500 mg dl^{-1}. The sensor had a response time of 15 s. Its oxidation peak at lower cholesterol concentration indicated an enhanced electron transfer rate. DNA based detection of bacterial meningitis was presented by Tak *et al.*[162] using flowerlike ZnO nanostructures. The cyclic voltammetry measurements were performed on a Pt/Si electrode, ZnO/Pt/Si electrode, single-stranded thiolated DNA probe modified ZnO/Pt/Si electrode, and double-stranded DNA probe modified electrode. The redox peaks were high for Pt/Si electrodes, then reduced due to ZnO's semiconducting nature. DNA probe modified electrodes have shown further reduced peaks due to repulsion between the phosphate backbone of DNA and PBS solution containing $[Fe(CN)_6]^{3-/4-}$ but for the double-stranded DNA modified electrode, the redox peaks are barely visible.

An amperometric biosensor for glucose detection was reported by Liu *et al.*[163] The cyclic voltammetry curves for Nafion coated ZnO nanorod film/ITO glass exhibited the typical capacitive squared curves, thus indicating its electrochemical inactivity in the potential window from 0.2 to −0.6 V. The GOx immobilized electrode showed well-defined peaks at −300 and −20 mV. Later, amperometric measurements were carried out by adding glucose aliquots. For each successive glucose injection, the current increases, and the response time is noticed to be less than 5 s. ZnO/Co-based nanoclusters with high specific surface area and better electrocatalytic activity for a glucose biosensor were investigated by Zhao *et al.*[164] The cyclic voltammetry curves indicated a sharp increase in current in the presence of glucose at 0.3 V. The amperometric tests were performed by adding glucose stepwise. The current increased for each addition of glucose, and the steady-state currents were attained within 8 s. The sensor has a LOD of 20 μM and a sensitivity of 13.3 μA mM^{-1} cm^{-2}. MWCNTs and AuNPs were employed to improve biosensor sensitivity, as reported by Wang *et al.*[165] A DNA biosensor was fabricated from carbon nanotubes, ZnO nanowires, and gold nanoparticles (AuNPs). Then a working electrode was designed *via* ZnO nanowires and MWCNTs immobilization with AuNPs. The differential pulse voltammetry (DPV) measurements were performed by dipping the electrode in Tris–HCl solution containing 1.5×10^{-4} M$[Ru(NH_3)_6]^{3+}$. The reduction peak in RuHEX increased for MWCNT/ZnO nanowires, then an increase in the reduction peak was observed for the AuNP electrodeposited electrode. Finally, enzyme immobilization further increased the redox current. The sensor showed a detection range for DNA of 1.0×10^{-13} to 1.0×10^{-7} M with a LOD of 3.5×10^{-14} M. Also, Liu *et al.*[166] reported a DNA biosensor based on ZnO and a modified glassy carbon electrode. Differential pulse voltammetry (DPV) measurements were performed using methylene blue (MB) as an indicator. The ssDNA probe was used to hybridize the target DNA sequences of different concentrations. Linear reduction peak currents were noticed against logarithmic DNA concentration from 3.57×10^{-11} mol L^{-1} to 3.57×10^{-7} mol L^{-1} with a LOD of 1.09×10^{-11} mol L^{-1}.

Dispersing nanoparticles on chitosan (CHIT) helps better immobilization of enzymes due to their biocompatibility and film-forming ability. Khan *et al.*[167] reported a cholesterol biosensor based on a ZnO/CHIT nanocomposite film. The working electrode was designed by immobilizing ChOx on the nano ZnO–CHIT/ITO electrode. The electrochemical impedance spectrum was measured for CHIT/ITO, nano ZnO–CHIT/ITO, and ChOx/nano ZnO–CHIT/ITO electrodes. The charge transfer resistance was measured to be 6.68×10^2, 4.47×10^2, and 9.38×10^2 Ω, respectively, for the three electrodes. The increased resistance of the ChOx immobilized electrode was due to the hindrance of electron transfer by ChOx. Xiang *et al.*[168] reported direct electrochemistry of horseradish peroxidase (HRP) based on a flower-like ZnO/Au/Nafion-based nanocomposite. The HRP immobilized ZnO/GNPs/Nafion glassy carbon electrode showed well-defined peaks in cyclic voltammograms indicating direct electron transfer between protein and respective electrodes. The electrolytic activity of the ZnO/GNPs/Nafion/HRP/glassy carbon electrode showed reduced oxidation currents and increased reduction currents upon the addition of H_2O_2, indicating the reduction of H_2O_2. The resulting biosensor showed a wide linear range of 1.5×10^{-5} to 1.1×10^{-3} M with a low LOD of 9.0×10^{-6}.

It was also discovered that tetragonal pyramid-shaped porous ZnO nanostructures (TPSP–ZnO) could provide better

biosensing abilities due to their large specific surface area and shape. TPSP–ZnO immobilized with GOx was used for glucose detection by Dai *et al.*[169] The GOx immobilized TPSP–ZnO/Nafion electrode showed stable redox peaks in cyclic voltammetry plots. This was due to the electron transfer between the electroactive center of GOx and bioelectrode. The sensor showed the highest redox peaks when the solution was at a pH of 7.0. The interferents were observed to not affect the sensor response except for ascorbic acid, which reduced the peaks by 2.1%. The sensor has a linear response within the concentration range of 0.05 to 8.2 mM with a LOD of 0.01 mM. Similar detection of glucose was reported by using porous ZnO nanostructures by Fatemi *et al.*[170] The sensor has a LOD of 10 μM and a response time of 7 s with 23.4 mA mM^{-1} cm^{-2} sensitivity. The skin template ZnO was found to enhance the direct electron transfer between GOx and electrode. High sensitivity and faster response time were due to the smaller crystallite size and more mesopores. A ZnO/CuO nanocomposite was used for dopamine detection, as reported by Khun *et al.*[171] The cyclic voltammetry results showed a wide linear response over the range of 10^{-3}–8 mM with a sensitivity of 90.9 μA mM^{-1} cm^{-2}. The sensor showed a good response time of about 10 seconds and good selectivity over interferents like ascorbic acid, uric acid, and glucose. Direct electron transfer was reported in a GOx immobilized ZnO nanorods/graphene heterostructure by Zhao *et al.*[172] The ZnO nanorods helped to immobilize GOx as well as reduce the distance between the active redox center of GOx and electrode, thus facilitating the direct electron transfer process. The sensor had a linear response for amperometric calibration of glucose from 0.2 to 1.6 mM. The sensitivity was measured to be around 89.84 μA mM^{-1} cm^{-2}.

Energy-saving, environment-friendly, green, and cost-efficient methods for the synthesis of NPs have emerged in response to rising environmental concerns. For electrochemical detection and removal of 4-nitrophenol, Chakraborty *et al.*[173] reported microwave-assembled Ag_2O–ZnO composite nanocones. A quick, cheap, and energy-efficient biosensor was designed using microwave-assisted Ag_2O–ZnO composite nanocones synthesised using a green aqueous solvent. Electrochemical sensing and photocatalytic degradation of hazardous 4-NP were achieved with these Ag_2O–ZnO composite nanocones. The improved sensor outperformed the pure ZnO modified electrode at neutral pH with an excellent sensitivity of 1.6 μA μM^{-1} cm^{-2} s and a very low LOD of 23 nM, substantially lower than the permissible limit of 0.43 μM in drinkable water. The sensor also selected 4-NP above other possible interferents. Sharma *et al.*[174] reported green ZnO nanoparticle production utilising plant extracts. A systematic strategy was employed to green synthesise zinc oxide nanoparticles (ZnO NPs) utilising *Carica papaya* seed extract. The generated ZnO NPs were integrated with multiwalled carbon nanotubes (MWCNTs) on the GCE to evaluate silymarin sensing. MWCNTs/ZnONPs/GCE had 2-fold stronger electrochemical signals than MWCNTs/GCE and bare GCE. Electrochemical detection employing our methodology and the MWCNTs/ZnO NPs composite could detect 122 mg of silymarin in the 160 mg commercial Milk Thistle pill, indicating a detection efficiency of 76%.

For the sensors based on direct electron transfer, the electrode and the enzyme both work in the redox potential window of the enzyme. This is an advantage as it provides superior selectivity and make them less prone to interferents. The voltammetry analysis provides information about an analyte based on the current obtained by varying the potential. The voltage is measured between two electrons when the potential is swept between two values. The amperometric analysis includes the measurement of current with an increase in the concentration at a fixed potential. Amperometric sensors are found to have better sensitivity as compared to potentiometric sensors. In potentiometric analysis, the accumulation of charge potential is measured at the working electrode in comparison with the reference electrode. The potentiometric analysis would be useful for measuring lower concentrations in small sample volumes.

ZnO's unique properties make it a promising biosensing material. These include a high exciton binding energy (60 meV) and a broad band gap (3.37 eV), as well as improved electron mobility. Owing to its other merits such as biocompatibility, ease of synthesis, and cost-effectiveness, it can be employed in the design of electrochemical biosensors.[147,175]

4.2.2. Optical biosensors. ZnO nanostructures have been used to make very effective biosensors owing to their unique optical characteristics. With a biorecognition sensing element integrated with an optical transducer system, an optical biosensor is a small, portable analytical tool (Fig. 9). The most fundamental function of an optical biosensor is to provide a signal that is directly proportional to the concentration of an analyzable material (analyte). Surface-penetrating light is used to measure changes in luminescence or reflectance before and after a sensitive layer is immobilised and brought into contact with analytes. Variations in the optical signal caused by the target analyte adsorption make it possible to trace the relationship between the analyte concentration and the biosensor signal. Biorecognition elements might be in the form of antibodies, receptors, enzymes, antigens, nucleic acids, entire cells, or tissues

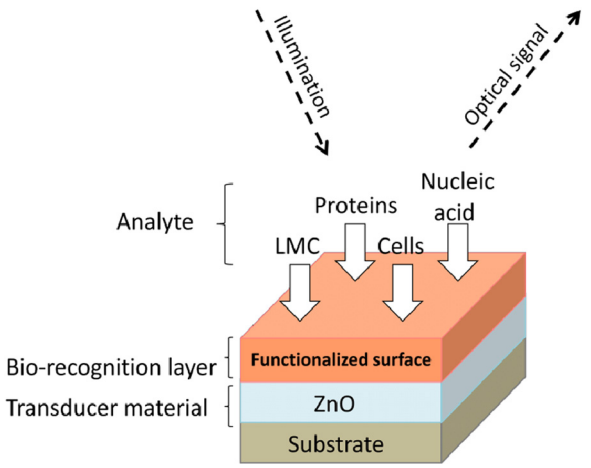

Fig. 9 Optical biosensing mechanism. Reproduced with permission from ref. 178.

that can be used with the optical biosensor. Optical waveguide interferometry, evanescent wave fluorescence, and surface plasmon resonance all use the evanescent field at the biosensor's surface to detect the biorecognition element's reaction with the analyte. Fig. 9 shows the optical biosensor working mechanism. The optical signal produced after the interaction of the analyte with the biorecognition layer help detect the specific target analyte.[176,177]

Galdamez *et al.*[179] studied different orientations of ZnO/Au nanowires for biosensing applications, when functionalized with the thiolated oligonucleotide probe labeled by cyt5. The SERS signal for random-standing nanowires was found to be amplified due to chemical and electromagnetic enhancement. The PL of ZnO nanowires functionalized with DNA revealed surface modifications prior to and after DNA immobilisation, with results favouring the zigzag orientation of ZnO nanowires. ZnO nanorods targeted by MAbs anti-CD5 could be employed to construct a biosensing platform for detecting human leukemic T-cells.[180] T-Lymphoblast cells were found to bind with CD5-targeted ZnO nanorod platforms having great selectivity, and the PL signal was much higher than that of IgG2a-targeted platforms. Human MOLT-4 cells conjugated with anti-CD5 MAbs were detected using the ZnO nanorod platform at concentrations as low as 3–128 cells in a 1.0 mm^2 well. Myndrul *et al.*[181] reported aflatoxin detection using polyacrylonitrile/zinc oxide nanofibers. The nanofibers were then modified with APTES, glutaraldehyde, bovine serum albumin and MAbs (anti-AFB1). The alteration in PL developed by the AFB1/anti-AFB1 complex was investigated. When tested, the sensor's sensitivity range was determined to be between 0.1 and 20 ng mL^{-1}, and its PL rose in proportion to the concentration of the analyte. The LOD was around 39 pg mL^{-1}.

Sodzel *et al.*[182] reported the detection of H_2O_2 and glucose using ZnO nanoparticles based on UV and visible luminescence. Fig. 10 represents the schematic of the ZnO nanoparticles' PL sensitivity for H_2O_2. The ZnO nanoparticles showed two peaks corresponding to near band edge (NBE) emission and dry low emission (DLE) emission. After immobilization of GOx, the structure was tested for the detection of hydrogen peroxide. Reduction in PL spectral peaks was observed after adding H_2O_2 to the solution in the concentration range from 0.05 mM to 100 mM. This PL peak reduction occurred exponentially. The sensitivity of low concentrations of H_2O_2 about 0.05 mM was attributed to the large surface area. The same structure was used to detect glucose concentration in solution as GOx oxidizes glucose and produces H_2O_2, reducing the PL intensity. The detection range of glucose levels was from 10 mM to 130 mM.

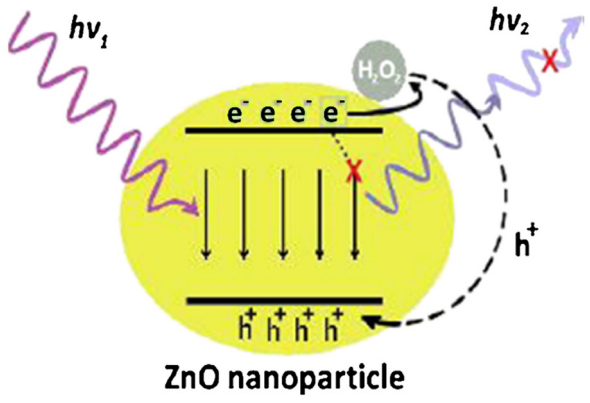

Fig. 10 Mechanism of ZnO nanoparticles' PL sensitivity for H_2O_2.[183]

A ZnO nanorod-based non-enzymatic glucose biosensor was reported by Sarangi *et al.*[184] The PL intensity decreased upon adding glucose, which continued to decrease with increased glucose concentration. The production of H_2O_2 happened due to glucose, being responsible for PL quenching. The sensor had a sensitivity of about 1.4%/mM with a linear concentration range from 0.5 to 30 mM. The sensor was unaffected by interferents like amino acids, uric acid, and BSA, generally present in human blood samples.

Furthermore, Viter *et al.*[185] reported ZnO nanorods for the detection of salmonella. The PL spectrum of ZnO nanorods showed NBE emission at 380 nm and DLE emission at 590 nm. Anti-salmonella antibodies were immobilized to detect salmonella antigens, and the BSA blocking agent was also added for specific binding. The PL intensity increased after immobilization of antibodies, and the BSA coating further increased the PL peak intensity. After interaction with the antigens, the PL intensity was reduced. The optimal response was observed for the concentration range from 10^2 to 10^6 cells per mL. The ZnO nanorods and the antigens interact by hydrophobic and van der Waals bonds. Dengue virus detection was accomplished by using ZnO thin films by Iyer *et al.*[186] ZnO thin films were immobilized with sequence-specific probe strands for the detection of dengue virus DNA. ZnO has strong adsorption efficiency towards negatively charged DNA.

Liu *et al.*[187] reported bi-functional ZnO nanorod arrays. The PL spectra of ZnO nanorods increased with the immobilization of dimercaptosuccinic acid (DMSA) and BSA. BSA immobilization reported a higher increase in the PL spectral intensity. Moreover, upon adding HSA to BSA immobilized ZnO nanorods, a twice increase in PL intensity was observed. Also, Chang *et al.*[188] reported the detection of carbohydrate antigen CA 15-3 by using an Au/ZnO thin film. The proposed structure was found to have better SPR intensity than the Au/Cr structure. The detection of antigen was done by recording the phase intensity. The SPR intensity was observed to increase with an increase in antigen CA 15-3. A linear response was obtained for antigen concentrations from 1 to 40 U mL^{-1} above which quantification was impossible. The phase intensity increased by two-fold for the Au/ZnO thin film compared to Au/Cr, and it increased by three-fold for lower concentrations such as 0.1 and 0.025 U mL^{-1}. The LOD decreased four-fold to 0.025 U mL^{-1}.

Later, Kim *et al.*[189] reported glucose biosensors based on ZnO nanostructures. ZnO nanostructures were reported to be synthesized by using the mercaptoundecanoic acid (MUA) surfactant, which provides water solubility and biocompatibility. GOx was immobilized on ZnO nanocrystals for the detection of glucose. The PL peak intensities were measured by adding

glucose to the ZnO/MUA/ GOx electrode. The PL peak intensity was reduced with an increase in the concentration of glucose from 1.6 to 33.3 mM, covering the general physiological glucose level. The sensor response time was less than 5 s with a LOD of about 0.33 mM. The sensor also showed specificity to cholesterol. A cholesterol biosensor by using ZnO thin films was reported by Kaur *et al.*[190] Three cases of Au/prism, ZnO/Au/prism, and ChOx/ZnO/Au/prism were investigated. The resonance angle for Au/prism was 43.54°, which increased drastically upon adding the ZnO layer due to its dielectric properties.

Upon addition of ChOx the resonance angle again decreased to 45.37° as the cholesterol concentration had increased the resonance angle to higher values. The sensor is characterized by a LOD of 0.12 mM with a detection range from 0.12 to 10.23 mM.

Further, ZnO–Au nanocomposites can be used as active SERS substrates, as reported by Sun *et al.*[191] Simple hydrothermally synthesized ZnO Au nanocomposites (hybrid A) and white light-emitting ZnO–Au nanocomposites were synthesized by treating hybrid A materials with HCL. These substrates showed greater enhancement in their ability and then showed a reduction in Au thickness. The lower thickness of Au showed a weaker SERS signal and *vice versa*. Nevertheless, for very high thickness, the SERS signal was again observed to be weaker.

Malachite green (MG) detection using Ag nanocomposites on ZnO nanodomes was reported by Sivashanmugan *et al.*[192] The Ag nanocomposites on ZnO nanodome hybrid nanosystems were prepared by the coupling of relatively flat and smooth ZnO nanodomes with Ag nanocomposites. A high SERS enhancement factor (EF) was obtained for the Ag/ZnO nanocomposite for sensing the crystal violet molecular probe and MG at low concentrations. The enhanced effect of SERS was attributed to the generation of strong local electromagnetic fields induced by Ag nanoparticles on ZnO nanodomes and intra nanocomposite interactions. More hotspots were anticipated to be produced due to the existence of metal–semiconductor-induced gap states. Glucose detection by using a ZnO modified gold disc was reported by Singh *et al.*[193] Efficient glucose sensing was observed with a LOD for glucose of about 0.01 mM. The sensor showed linear sensitivity for glucose concentrations up to 250 ng mL^{-1}, and the sensitivity saturated beyond 250 ng mL^{-1}. Electromagnetic fields on a gold surface induce electron transfer from Au to ZnO at resonance, thus resulting in good sensitivity. The presence of oxygen defects also enhanced the sensitivity by providing electrons to the active layer.

Later, Tao *et al.*[194] reported the growth of ZnO nanorods on Si wafer and considered them a SERS substrate for detecting rhodamine. With Ag decoration, they were found to form scaffold-like structures. The Raman enhancement factor (EF) was measured for increased Ag deposition. As the Ag deposition time was increased, the EF was also seen to increase by four times. For this, the EF was calculated with different concentrations of rhodamine; for the concentration of 10^{-8} M, an EF of about 10^7 was noticed, which indicated its sensitivity towards a lower rhodamine concentration. For UV irradiated substrates, the detection of rhodamine was weakened, and no Raman signal was observed for substrates irradiated with UV for 2 hours. In another work, Yang *et al.*[195] reported the detection of cancer cells by using ZnO nanorods. The ZnO nanorods were connected with the epidermal growth factor receptor (EGFR) of squamous cell carcinoma (SCC) cells. The ZnO/EGFR antibody probes were tested for SCC, epithelial cancer that arises in multiple organs. The PL spectra displayed a purple light upon UV light excitation, which indicates cancer cells' presence. The cancer cells can also be identified by the peak intensity ratio of UV and green light. Dorfman *et al.*[196] reported protein–protein interactions existence with ZnO nanoscale structures. ZnO nanorods grown on Si wafers were investigated. Neither as-synthesized nor protein G-treated ZnO nanorods showed any fluorescence.

Further, a clear green emission indicated protein–protein interactions when reacting with fluorescein-conjugated anti-bovine IgG (FITC-antiIgG) to detect protein G adsorbed nanorods. Later, ZnO strips of 20 μm width were studied with repeated structures. Two chambers were placed on ZnO, and proteins fibronectin and IgG were introduced into one chamber. Further upon interaction with FTIC anti-IgG, strong fluorescence was observed from the chamber containing the IgG protein, indicating protein interactions. Also, Dorfamn *et al.*[197] reported the detection of DNA molecules by using ZnO nanoscale structures. Two oligonucleotides were designed to correspond to *B. anthracis* (bas) and *Bacillus cereus* (bce). A 6-carboxyfluorescein modified oligonucleotide (basr) complementary to bas was also designed. ZnO nanoplatforms with two DNA strands of bce and basr did not show any fluorescence, while the nanostructure with bas and basr showed fluorescence, indicating the formation of a DNA complex. Optical biosensors detect biomolecules based on fluorescence, photoluminescence, SPR, and SERS techniques. Amongst the methods mentioned above, SERS, SPR, and fluorescence are costly. Though photoluminescence is cost-effective, the sensitivity will be compromised. It is also an easier and more prospective method.

For optical biosensors, the biosensor platform requires specific materials with advanced structural, electrical and optical properties for the effective transformation of biological interaction into physical signals. Metal oxides are quite attractive for biosensor applications as they possess all required physical properties (conductivity, luminescence and absorbance) as well as biocompatibility. Moreover, ZnO is an n-type semiconductor with wide band gap (3.37 eV), high isoelectric point (pH = 9–9.5) and intense room temperature photoluminescence.[177] Owing to their peculiar optical properties, ZnO nanostructures can be potentially deployed for the design of optical biosensors.

4.2.3. Piezoelectric biosensors. Piezoelectric biosensors are based on the integration of piezoelectric materials in the detection system. Fig. 11 shows the piezoelectric biosensors based on nano QCM. The piezoelectric biosensors belong to the group of analytical devices that work on the principle of affinity interaction recording. The theory behind a piezoelectric platform, also known as a piezoelectric crystal, is that the mass attached to its surface causes an alteration in the crystal's oscillations. As a type of mass-based biosensor, piezoelectric

biosensors respond to mechanical stress by generating an electrical signal. The quartz crystal microbalance model is an example of a piezoelectric biosensor. Fig. 4 illustrates the basic QCM operation. There are a wide variety of applications for QCM in the electronics sector. The fundamental mode frequency of these tools is normally between 1 and 20 MHz, and they are utilised as attenuators in modern electronic devices. A quartz crystal, outfitted with metal electrodes, is the primary material utilised in the creation of the QCM sensor. Sensors can detect the presence of a target analyte in the environment owing to a sensitive coating material on the sensor's surface. To transform the measured amount into an electrical signal, a suitable electronic circuit is required. The quartz crystal oscillations change by loading of mass on the surface. A change in frequency occurs due to the interaction with target analytes, thus helping to determine the target analyte.[198]

A self-powered creatinine biosensor was reported by Wang *et al.*[199] The biosensor can detect creatinine concentration based on the piezo-enzymatic reaction of the ZnO nanowires. The detection range of the creatinine biosensor was measured to be around 1×10^{-5}–1×10^{-1} mM and the sensitivity was 0.0229 V mM^{-1}.

Reyes *et al.*[200] reported the detection of DNA oligonucleotide molecules using ZnO nanostructures based on the QCM device. The ZnO nanotips were grown on to the nano QCM sensing area. The sensing area was made superhydrophilic by exposure to UV light, increasing its sensitivity ten-fold compared to the standard QCM and reducing the required sample volume. ZnO nanotips were functionalized for DNA in three steps. Firstly, the sensing area of the QCM was immersed in a linker solution, and then DNA incubation followed by hybridization was carried out. Following the above three step, the ZnO-based QCM exhibited an increase in frequency shift, indicating the uniform distribution of immobilized and hybridized DNA molecules. Later, only QCM was tested for DNA molecules, and no shift in the frequency was observed, thus indicating that ZnO nanotips aid in detecting DNA molecules.

Similar detection of DNA molecules was also reported by Lee *et al.*[201] *via* ZnO nanorods. The QCM with ZnO nanorods was coated with titanium and gold films. The device was then tested for mercaptohexanol solution. Compared to the QCM without ZnO, the QCM with ZnO nanorods coated with gold showed greater frequency shifts. The same phenomenon was observed for the ZnO nanorod QCM over the bare QCM coated with gold for DNA oligonucleotide molecules. Wang *et al.*[202] reported ZnO nanorods coated with QCM to detect CA 15-3 antigens. For strong binding, the QCM sensors coated with ZnO nanorods were immobilized with anti-CA 15-3 using APTES and glutaraldehyde. Time-dependent frequency shifts of ZnO with anti-CA 15-3 are nearly 1 Hz and even less. 10 QCM sensors with ZnO nanorods and anti-CA 15-3 were designed and tested for different concentrations of CA 15-3 from 0.5 to 30 U mL^{-1}. A linear response was noticed within the concentration range 0.5–26 U mL^{-1} with a sensitivity of 25.34 ± 0.67 Hz per scale and a regression coefficient of about 0.99. To check reproducibility, 20 sensors were designed for CA 15-3, showing a reproducibility with a relative standard deviation of 2%.

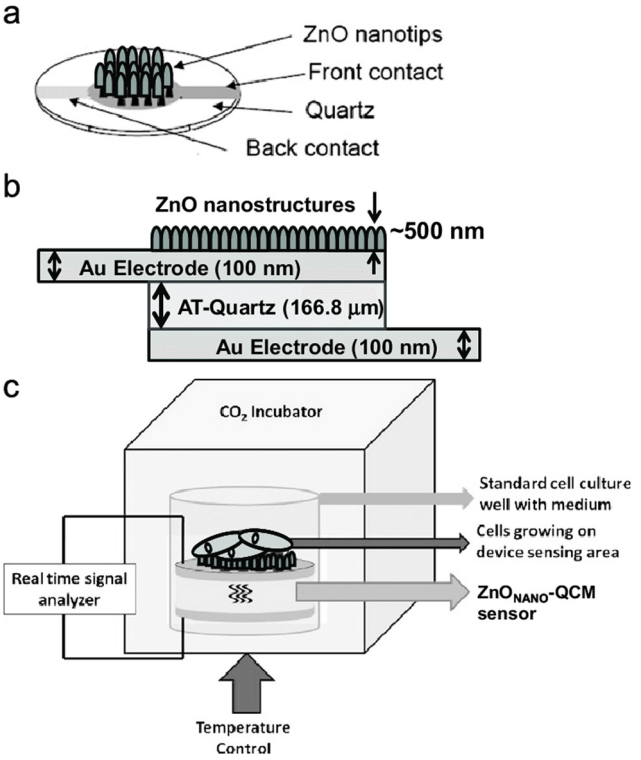

Fig. 11 Nano-QCM based piezoelectric biosensor. Reproduced with permission from ref. 200.

A surface acoustic wave (SAW) is another type of biosensing mechanism under the piezoelectric category. Krishnamoorthy *et al.*[203] reported the detection of interleukin by a ZnO surface acoustic wave (SAW) based biosensor. The ZnO/SiO_2/Si guided shear horizontal surface acoustic wave (SH SAW) based biosensor detected IL-6. The IL-6 attached to ZnO by a direct adsorption process was not efficient compared to immobilization through BSA and MAbs. The larger sensing area was found to have better sensitivity for higher frequency devices. A similar structure was reported by Luo *et al.*[204] for the detection of glucose. The glucose detection was carried out without the use of disposable and expensive glucose test strips, as glucose was detected by mass load change of the sensitive area, which resulted from the change of pH of the testing solution. The sensor was also tested for pH changes due to interferents like ascorbic acid, lactic acid, and uric acid. The change in pH due to these interferents was not significant, indicating the sensor efficiency for application in glucose detection.

Mao *et al.*[205] reported the self-powered piezoelectric biosensing textiles for physiological monitoring and time-motion analysis. Depending on the piezoelectric effect developed due to the interaction between the lactate and lactate oxidase, the moving speed, joint angle, frequency, and sweat lactate concentration of an athlete in real-time can be monitored. The entire process of monitoring and analysis uses no batteries. Using this method, various things (people) in motion can gauge the requirements of their motion and their own physiology. Fig. 12 represents the working mechanism of the self-powered piezoelectric biosensor.

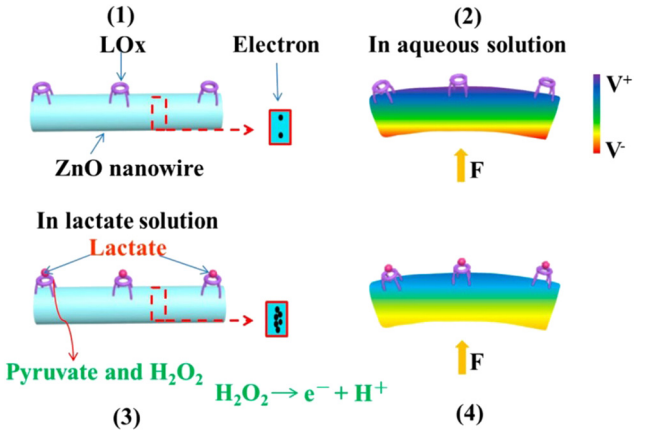

Fig. 12 Working mechanism of self-powered piezoelectric-biosensing textiles for sweat-lactate analysis.[205]

In summary, for piezoelectric biosensors, the detection depends upon the mechanism of mass loading. The change in mass on the surface is recorded as the change in frequency. For piezoelectric sensors, higher mass loading provides higher sensitivity, and low mass loading on the sensor surface could be a limitation. SAW biosensors were observed to function at higher frequencies and provide higher sensitivity as compared to QCMs. Although QCM biosensors present lower sensitivity, they are simpler. The piezoelectric effect harvests mechanical energy from ZnO nanostructures and outputs voltage/current signal. After enzyme or antibody surface modification on ZnO nanowires, the piezoelectric output is a biosensing signal dependent on surface biological processes. Since ZnO nanostructures exhibit excellent piezoelectric properties in addition to other merits they can be considered as a potential candidate for the piezoelectric biosensor design.[205]

4.2.4. ZnO field-effect transistor-based biosensors. Field-effect transistor (FET) based biosensors are attracting increasing interest in recent years. Thus, ZnO-based FET biosensors have been reported. The growth of ZnO nanostructures formed the conductive channel and the channel was of n-type due to the intrinsic n-type nature of the ZnO nanostructure. Ahmad *et al.*[206] reported the solution gated FET based on ZnO nanorods for cholesterol detection. The sensor response was measured by fixing the drain bias and varying the solution concentration on ZnO nanorods. The enzyme solutions were prepared by dissolving ChOx in PBS. The drain current was plotted for solutions with and without cholesterol, and it was found that the current response was higher for the case of the solution containing cholesterol. The sensor showed a LOD of 0.05 μM and a reproducibility of about 5.2%. The sensor showed good selectivity for cholesterol without much selectivity for AA, UA, glucose, and L-Cyst interferents. The sensitivity was reduced by 12% for human blood serum and 35% for whole blood samples due to smaller molecules restricting cholesterol diffusion onto enzymes.

Phosphate detection was reported by Ahmad *et al.*[207] using a ZnO nanorod based FET. The ZnO nanorods were grown on a SiO_2/Si substrate and immobilized with pyruvate oxidase. The as-fabricated FET and ZnO nanorod-based FET were analyzed for phosphate detection. The ZnO nanorod-based FET showed enhanced current response compared to the as-fabricated FET biosensor. The better response is attributed to ZnO nanorods' high specific surface area and better electron transfer ability during electrocatalytic reactions. The sensors showed better reproducibility with a standard deviation of about 4.3%. The FET biosensor showed a linear concentration range from 0.1 μM to 7.0 mM with a sensitivity of 80.57 mA cm^{-2} mM^{-1} and a LOD of 50 nM.

Furthermore, Liu *et al.*[208] reported ZnO nanowire and thin film-based FET biosensors. The sensor showed a change in conductance which was higher in the case of streptavidin due to specific binding between biotin and streptavidin, and a lower change was observed in conductance for common protein IgG non-specific binding. Also, Liu *et al.*[209] reported a ZnO nanowire-based FET biosensor for uric acid detection. The uric acid reaction with uricase produces two hydrogens that change the surface potential, hence the conductance of the biosensor. The sensor showed a linear response for the concentration range from 1 pM to 0.5 mM. The sensor could detect uric acid at a concentration of 1 pM with a 14.7 nS change in conductance. The sensor response time was in the order of a millisecond.

Later, Zong *et al.*[210] reported FET biosensors based on ZnO nanorods immobilized with GOx. A detection scheme of frequency mixing was used for glucose detection with better sensitivity and reduction in the complexity of fabrication and cost. The glucose detection was carried out based on a change in the resulting currents. The sensor showed a good sensitivity of about 1.6 mA μM^{-1} cm^{-2} with a LOD of 1 μM. A non-enzymatic ZnO nanorod-based FET for glucose detection was reported by Ahmad *et al.*[211] NiO quantum dot modified ZnO nanorods were used for sensing purposes. The surface turned to the hydroxide phase upon water adsorption, and in the presence of glucose, it turned to $Ni(OH)_2$, thus producing H_2O_2. The electrooxidation current of H_2O_2 was used for the detection of glucose. The sensor showed two linear current responses for glucose concentrations in the range of 0.001–10 mM and 10–50 mM with respective sensitivity of 13.14 μA cm^{-2} mM^{-1} and 7.31 μA cm^{-2} mM^{-1}. Good selectivity in the presence of interferents was obtained and 97% of the initial response was retained after 8 weeks, indicating its stability. The tests carried out in the whole blood sample and human serum sample indicated that the sensor response was decreased a little in the whole blood sample due to the presence of blood cells and protein fragments.

Ahmad *et al.*[212] also reported vertically aligned ZnO nanorods based on a FET glucose biosensor. The ZnO nanorods were modified by Fe_2O_3, which helped in the catalytic electrooxidation of glucose. The FET biosensor without Fe_2O_3 showed a poor response in the presence of glucose, and with Fe_2O_3, it showed an enhanced response. The current was seen to increase with an increase in glucose concentration with a linear response from 0.05 to 18 mM. The sensor showed a decreased response in the whole blood sample and good selectivity in the presence of interferents and competing sugars. The sensor had a sensitivity of 105.75 μA mM^{-1} cm^{-2}, 12 μM LOD, and 10 s response time, and retained 97.5% of the initial response after

10 weeks. A biosensor based on a ZnO nanorod FET immobilized with GOx for glucose detection was reported by Fathollazadeh *et al.*[213] In this, ZnO nanorods served as the conducting channel for the electrolyte gated FET. The sensor showed good sensitivity towards glucose in positive bias. The change in channel conductivity was due to the hydronium ions produced due to the reaction between GOx and glucose. The LOD of the sensor was 3.8 μM. Recently, a brief review of ZnO nanorod-based FET biosensors was provided by Karim *et al.*[214] In the FET based ZnO biosensor, the sensing mechanism was based on the change in conductance of the channel formed by ZnO nanorods. The nanorod-based FET provides reduced fabrication complexity and costs over conventional three-electrode systems. The FET-based biosensors have high detection potential and higher sensitivity. They have attracted major attention due to their low cost, portability, faster detection, and compatibility for integration on-chip.

4.3. Detection of specific biomolecules

ZnO biosensors have been used for the detection of a variety of biomolecules. Wei *et al.*[215] reported the detection of glucose by hydrothermally synthesized ZnO nanorods. The ZnO nanorods are synthesized hydrothermally, and GOx is immobilized on the surface of ZnO nanorods. A three electrode system is used to perform electrochemical experiments. Cyclic voltammetry measurements show a strong change in the current upon the addition of glucose. Amperometric measurements show that the LOD of the sensor is 0.01 mM with a response time of about 5 s. Cholesterol biosensors with ChOx immobilized ZnO nanoparticles are reported by Umar *et al.*[216] A gold electrode with Nafion-coated ChOx immobilized ZnO nanoparticles is used as the working electrode while Ag/AgCl is used as the reference electrode. The cyclic voltammetry curves showed a peak at 0.355 V in the presence of 0.1 mM cholesterol in 0.1 M PBS buffer solution. When the cholesterol concentration is increased gradually, the currents are found to increase. The sensor had a LOD of 0.37 nM and a sensitivity of 23.7 μA mM^{-1} cm^{-2}. The response time of the sensor was less than 5 s. A ZnO nanorod field-effect transistor (FET) based biosensor for protein detection was reported by Kim *et al.*[217] Biotin-modified ZnO nanorods were used for the study. The ZnO nanorod FET system provides a considerable increase in the current upon exposure to streptavidin, thus indicating its efficiency for streptavidin detection. Later, Sang *et al.*[218] reported the detection of proteins by using ZnO nanowires. The surface was modified by using 3-APTES and biotin-*N*-hydroxysuccinimide ester (NHS-biotin). Streptavidin of varying concentration is injected simultaneously through the microfluidic second channel. Fluorescence intensity indicated the detection of streptavidin. Furthermore, Liu *et al.*[219] reported streptavidin detection using a ZnO nanowire/thin-film biosensor. Recently dengue serotype 2 DNA detection has been reported by Al-Douri *et al.*[220] using sol–gel synthesized aluminum-doped ZnO nanostructures. The nanostructures are dispersed over a p-type Si wafer. An inverse relationship is noticed with current magnitudes decreasing with increasing DNA concentration.

A variety of biosensors for DNA detection have been also reported. Kaur *et al.*[221] reported the detection of *Neisseria meningitidis* DNA by using ZnO thin films. The sputtering method allowed the preparation of ZnO thin films on gold-coated glass prisms and immobilized through a single-stranded DNA probe. The biosensor showed linearity towards DNA over a wide range of concentrations of 10–180 ng μL^{-1} and a good sensitivity of 0.03° ng^{-1} μL^{-1}. Later, Gerbreders *et al.*[222] reported the detection of the *Trichinella* DNA sequence using ZnO nanostructures. DNA primers were developed on the ZnO nanostructures and employed as a working electrode. It is noted that nanotubes lead to higher sensitivity than thin films and nanorods due to their porous structure. Gasparotto *et al.*[223] reported detection of ovarian cancer antigen by using a ZnO nanorod and Au nanoparticle hybrid structure. The structure is synthesized *via* the hydrothermal method. The ZnO nanorod coated with Au nanoparticles efficiently immobilizes ovarian antigen *via* binding with cystamine and glutaraldehyde. Also, Liang *et al.*[224] reported a Au/ZnO thin film to detect breast cancer cells. The surface plasmon resonance (SPR) of the Au/ZnO thin film was compared with the Biocare SPR system. The Biocare SPR system showed good selectivity for higher concentrations of saliva and reduced sensitivity for lower concentrations. The Au/ZnO thin film SPR system displayed linear response for saliva concentrations within 20 U mL^{-1} covering all relevant CA 15-3 concentrations from healthy to affected people. Dopamine detection using APTES capped ZnO quantum dots was reported by Zhao *et al.*[225] The ZnO quantum dots are found to quench fluorescence upon the addition of dopamine. The quantum dots showed quenched fluorescence ability with and without APTES. Better fluorescence quenching without a clear shifting of the peak is observed for APTES capped ZnO quantum dots. The intensity is quenched to 11% for APTES capped and 67% for non-capped quantum dots. The quenching phenomenon is noticed due to the electron transfer mechanism between the quantum dots and dopamine. Rui *et al.*[226] reported the detection of H_2O_2 using cytochrome *c* (Cyt *c*) modified ZnO nanosheets. The nanosheets observed fewer interferences from O_2. The ZnO nanosheets with Cyt *c* showed linear response for H_2O_2 in amperometric calculations compared to bare ZnO nanosheets. The same was used for the detection of extracellular H_2O_2 from living hepatoma cells. The ZnO nanosheets with Cyt *c* showed increased cathodic currents with the addition of phorbol 12-myristate 13-acetate for H_2O_2. Phenolic compound detection was reported by Li *et al.*[227] ZnO nanoparticles immobilized with tyrosinase proved to detect catechol without any mediator. The biosensor showed good sensitivity and stability, and can be used to detect phenolic compounds without any mediator. Salmonella detection based on optical intensity was reported by Viter *et al.*[228] Anti-salmonella antibodies were coated on ZnO nanorods for the detection of salmonella agents. The BSA blocking agent was also coated to avoid unnecessary binding. ZnO nanorods with anti-salmonella antibodies had increased near band edge emission, which further increased with BSA coating. When exposed to salmonella antigens, the PL intensity decreased proportionally to Ag concentration.

In another work, Narang *et al.*[229] reported a CHIT–ZnO nanocomposite film-based biosensor to detect triglyceraldehyde. ZnO–CHIT composites are found to provide a biocompatible environment for enzyme detection. ZnO–CHIT nanocomposites are found to have better currents for triglyceraldehyde with an optimized ZnO : CHIT composite ratio. Too low concentrations of ZnO nanoparticles provide lower enzyme adsorption, thus reducing the sensitivity, and a higher concentration of ZnO nanoparticles increases the obstruction for species diffusion. Devi *et al.*[230] reported xanthine detection using a ZnO nanoparticle and polypyrrole (PPy) composite film. The film was immobilized with xanthine oxidase (XOD) for the detection of xanthine. Cyclic voltammetry results for the XOD/ZnONP/PPy/Pt electrode reported linear currents for the concentration range between 8 μM and 40 μM. ZnO–Au nanocomposites for the detection of rabbit IgG were reported by Wang *et al.*[231] The biosensor based on the ZnO–Au nanocomposite was shown to present better sensitivity than the biosensor based on Au film and Au nanoparticles. The ZnO–Au-based biosensor showed a sensitivity 16 times greater than that of the sensor based on Au films. Recently, a ZnO nanorods–AuNPs electrochemical biosensor was reported by Biasotto *et al.*[232] The sensor was immobilized with an anti-hepatitis C virus antibody to detect the hepatitis virus. AuNPs improved the device's sensitivity, repeatability, and reliability with a LOD of about 0.25 μg μL^{-1}. Also, tellurium doped ZnO nanowires were reported by Khosravi-Nejad *et al.*[233] for label-free detection of hepatitis virus. The sensor had a LOD of 1 pM with a linear detection range from 1 pM to 1 μM. From the above discussion, it can be concluded that ZnO nanostructures can be an effective material for detecting various types of biomolecules because of their high IEP, biocompatibility, chemical activity, and electron mobility. The performance of biosensors depends on their components, especially the matrix material, *i.e.*, the layer between the recognition layer of biomolecule and transducer, as it plays a crucial role in defining the stability, sensitivity, and shelf-life of a biosensor. Table 2 briefly describes various biomolecules that have been sensed by the ZnO nanostructures, the transduction method, and the biosensitive layer used along with the sensor performance.

4.4. Recent works on ZnO nanostructure-based sensors

Haque *et al.*[242] reported ZnO nanoparticles doped with Cu nanoparticles for the detection of myoglobin. The nanocomposite was deposited on a gold plated electrode. The electrochemical sensor was tested with the myoglobin in the concentration range of 3–15 nM. The highest sensitivity recorded was about 10.14 μA nM^{-1} cm^{-2} with a LOD of about 0.46 nM. Naik *et al.*[243] reported the modified carbon paste electrode with Co doped ZnO nanoparticles for the detection of uric acid. The modified electrode under optimal conditions of the influencing parameters exhibited a LOD of about 3.37 μM through a diffusion controlled process. The modified electrode also exhibited two different oxidation peaks for the detection of uric acid and adrenaline separately. Kamaci *et al.*[244] reported the detection of cysteine in tap water and BSA using the ZnO quantum dots fluorescent probe. The LOD value of the biosensor was found to be 0.642 μM, and the linear range was determined to be in the range of 0.1–600 μM. The interference of other analytes such as cations, amino acids, and anions was negligible. Dairy *et al.*[245] reported ZnO nanorods sandwiched between two graphene layers for the detection of glucose based on the piezoelectric effect. The lower graphene layer was fixed at the lower surface and used for the detection of glucose concentration. The number of molecules connected to the upper graphene layer increased as the GOx concentration increased (from 0 to 0.01 M), resulting in an increase in mechanical stress and strain in the ZnO-NRs. Deformation in the crystal structure of ZnO-NRs causes displacement of the negative and positive charge centres, resulting in electric

Table 2 Specifications of representative ZnO-based biosensors along with LOD, linear response, and sensitivity

Target analyte	Biomolecule immobilized on the matrix layer	Matrix layer	Detection method	Sensitivity (S)	LOD	Linear response (L)	Ref.
Glucose	GOx	ZnO nanotubes	Electrochemical	21.7 μA mM^{-1} cm^{-2}	1 μM	50 μM–12 mM	234
Uric acid	Uricase	ZnO nanosheets	Electrochemical	129.81 μA mM^{-1} cm^{-2}	0.019 μM	0.05–2 mM	235
Cholesterol	ChOx	ZnO nanorods	Electrochemical	35.2 mV dec^{-1}	NR	10^{-6}–10^{-2} M	236
CA 19-9	CA 19-9 antibody	ZnO quantum dots	Photoluminescence	0.47 μA U^{-1} mL^{-1}	0.025 U mL^{-1}	1–180 U mL^{-1}	237
Streptavidin	NHS biotin	ZnO nanowires	Fluorescence	NR	417 fM	417 fM–41.7 nM	218
DENV non-structural protein 1	DNA probe	ZnO/Pt–Pd nanocomposite	Electrochemical	NR	4.3 × 10^{-5} M	10^{-6}–10^{-4} M	238
Neisseria meningitidis	ssDNA probe	ZnO thin film	SPR	0.03° ng^{-1} μL^{-1}	5 ng μL^{-1}	10–180 ng μL^{-1}	221
CA 125	Anti-CA 125	ZnO nanorod–AuNP nanohybrid	Electrochemical	NR	2.5 ng μL^{-1}	NR	223
Dopamine	Non-enzymatic	ZnO–CuO composite	Electrochemical	90.9 μA mM^{-1} cm^{-2}	10^{-4} mM	10^{-3}–8 mM	239
H_2O_2	Cytochrome *c*	ZnO nanosheet	Electrochemical	2 ± 0.1 μA mM^{-1} cm^{-2}	0.8 μM	1–1000 μM	226
Salmonella	Anti-salmonella	ZnO nanorods	Photoluminescence	NR	NR	10^{2}–10^{6} cells per mL	228
Goat IgG	Non-enzymatic	ZnO–Au nanocomposite	SPR	NR	0.15 μg mL^{-1}	0.15–2 μg mL^{-1}	231
Xanthine	XOD	ZnO nanoparticles	Electrochemical	NR	0.8 μM	8–40 μM	230
Penicillin	Penicillinase	ZnO nanorods	Electrochemical	121 mV dec^{-1}	NR	100 μM–100 mM	240
H_2O_2	HRP	Flower ZnO–AuNPs	Electrochemical	NR	9 × 10^{-6} M	1.5 × 10^{-5}–1.1 × 10^{-3}	241

potential and piezoelectric polarisation in ZnO-NRs due to the piezoelectric effect. The sensitivity of the designed sensors was in the range of 0.12 to 0.28 mV mM^{-1} for a biosensor with a single ZnO-NR and 0.035 to 0.135 mV mM^{-1} for GR/ZnO-NRs/GR.

Au coated ZnO nanorods immobilized with phenylalanine hydroxylase are reported for the detection of phenylalanine.[246] Enzyme immobilization is achieved by dropping Au–ZnO and phenylalanine hydroxylase onto a paper disc on the graphene screen printed electrodes. Under optimal conditions, the sensor exhibited a linear range of 5.0 nM to 100 μM with a LOD (S/N = 3) and a limit of quantitation of 3.0 nM and 10.0 nM, respectively. A ZnO nanorod-based pH sensor was manufactured by doping magnesium into the sensing membrane, thus leading to an innovative electrolyte insulator semiconductor for pH sensing. The results showed high hydrogen sensitivity, linearity, and drift with 3% magnesium due to enhanced crystalline quality. This sensor can be explored further as a biosensor in the future.[247] Multiple drug sensing was accomplished *via* layers of an acid–base functionalized carbon nanotube and zinc oxide nanocomposite (COOH-CNTs/ZnO/NH_2-CNTs) to detect paracetamol, diclofenac and orphenadrine (PAR, DIC, and ORP) drugs with highly efficient sensitivity and selectivity. Similarly, the FCNTs/ZnO/fCNTs/GCE based sensor detects PAR, DIC, and ORP drugs with femtomolar limits of 46.8, 78, and 60 fM, respectively. This sensor proved six-fold more efficient than bare glassy carbon electrodes due to the increased surface area.[248] This sensor can also be investigated further for detection as a biosensor. Complementary information to the one presented in the present work can be found in literature reports on ZnO based biosensors. ZnO nanowire based FET biosensing was reported by Ditshego *et al.*[249] The review specifically covers the ZnO nanowire based FET biosensors. Other review works based on electrochemical biosensors, SPR biosensors, and metal–oxide modified ZnO nanomaterial based biosensors are reported.[250–253] Further, different mechanisms of biosensing apart from electrochemical sensing and different nanostructure based biosensors are reported.[254] Shetti *et al.*[255] have reported a review of ZnO-based biosensors for electrochemical detection. The other review reported by Xu *et al.*[256] confined the biosensor discussion to quantum dot and 1-D based ZnO biosensors. Thin films for biosensing applications are reported by Arya *et al.*[257] Other reviews are previously reported with discussion specific to cardio biomarker detection,[258] surface plasmon resonance detection,[259] optical biosensors,[260] and enzymatic biosensors.[261] Tripathy *et al.*[262] presented a review of ZnO nanosheet and ZnO based FET biosensors. However, in our manuscript, all the above mentioned topics are discussed in a comprehensive way enabling the readers a wide scope of knowledge. It will give us a bird's eye view of how ZnO based nanostructures can be employed for potential ZNO biosensors.

5. ZnO based POC biosensors

In order to facilitate point-of-care testing, miniature biosensors have been created in recent years that are based on already available handheld devices or microfluidic systems. The measurement of classical physical parameters has seen widespread use of several simple and portable instruments, including thermometers, pressure metres, and pH metres. Efforts have been made to develop novel signalling systems in conjunction with the aforementioned miniaturised devices to provide easy and portable POC testing without the need for cumbersome external instrumentation. As point-of-care (POC) devices, biosensors provide benefits such as quick detection, user friendliness, accuracy, portability, cost-effectiveness, and straightforward on-site detection in the field.[263]

Several groups of researchers have been working on a biosensor based on ZnO nanostructures with the goal of using it for point-of-care diagnostics. Point-of-care testing using a ZnO-based substrate-gate coupled biosensor was described by Fathil *et al.*[264] The device's primary purpose is to analyse cardiac troponin, a biomarker for heart disease. An antibody against cardiac troponin, a biomarker, has been covalently immobilised on a ZnO nanoparticle thin film. Between the two p-type regions, the device incorporates a thin coating of ZnO nanoparticles. I_D in the channel drops when a biomolecule with a strong positive charge, like cardiac troponin, is detected. The detection of cardiac biomarker is done with a LOD of about 3.24 pg mL^{-1}. POC biosensors for pesticide sensing are reviewed by Kalyani *et al.*[265] The review comprises a brief discussion on different types of sensing mechanisms for POC biosensors. Xia *et al.*[266] reported the smartphone based avian influenza biosensor. The virus catching antibodies immobilized on the 3D nanostructures made of polydimethylsiloxane structures with ZnO nanorod templates. The on-chip gold electrodes allow the calorimetric reaction when the virus comes in contact with the sensor. Further, with smartphone imaging and calorimetric reaction a very low LOD of about 8×10^3 EID_{50} per mL is possible.

Zika virus detection using an electrochemical immunosensor is reported by Macedo *et al.*[267] The biosensor is created by manufacturing ZnO nanostructures on a printed circuit board *via* chemical bath deposition, and then immobilising antibodies using cystamine and glutaraldehyde. Evaluation of sensor responses using cyclic voltammetry measured a detection range between 0.1 ng mL^{-1} and 100 ng mL^{-1}, with a very low LOD of 1.0 pg mL^{-1}. In the graphene–ZnO nanorod heterostructure, an electric field enhances the mass transit of the analyte to the sensor surface.[268] For PoC applications, these hybrid nanostructures have been placed on flexible polyethylene terephthalate substrates with screen printed electrodes. ZnO nanorods have been functionalized with aptamers and combined with a smartphone-interfaced low-cost potentiostat. Electrochemical impedance spectroscopy and commercial ELISA kits have confirmed the system's performance with 50 μL analyte. The limit of detection of 1 fg mL^{-1} in human serum with 6.5% coefficient of variation is three orders of magnitude lower than that of PoC devices.

Chaudary *et al.*[269] reported a review on the design of next generation sensor systems based on nanomaterials. The merits of using nanostructure materials in the design of 5th generation sensors include high specific surface area with excellent

porosity, mechanical stability, flexibility, diverse surface chemistries and customizable electrical and optical characteristics; tunable surface terminals, high dispersibility, mechanical and thermal durability, and hydrophilicity which allow machine processing; and degradability, biocompatibility, energy efficiency, and cost-effectiveness.

6. ZnO based systems for COVID-19 detection

The last few decades have been plagued by viral outbreaks that present some of the biggest challenges to public safety. The current coronavirus (COVID-19) disease pandemic has exponentiated society concerns in these issues. Increased research on diagnostic tools is currently being implemented in order to assist with rapid identification of the virus, as mass diagnosis and containment is the best way to prevent the outbreak of the virus.[254] Accurate, rapid, and low-cost molecular diagnostics are essential in managing outbreaks of infectious diseases.[270] The main complication with some repurposed drugs is the delivery process, which can promote secondary effects. In light of the considerations quoted above, the use of ZnO nanoparticles (ZnO-NPs) has been reported in state-of-the-art nano-compounds as a system for drug delivery. In addition, these kinds of systems have been used as a nano-carrier of antibiotics.[271]

Lateral flow assay (LFA)-based qualitative diagnostics of COVID-19 were beneficial for laboratory testing and POCT due to their simple scaling-up capability. Because of their poor technical performance, including detection limit and false-positive and false-negative interferences, such kits could only be used for preliminary screening of large populations. So, LFA-based COVID-19 diagnostic kits have scaling-up capabilities, but the isolation advantage in identifying infectious SARS-CoV-2 should be the main benefit. The detection specificity issue might cause false-positive (other viral interference) and false-negative findings (likely due to mutation).[272]

Due to the lack of effective treatments, simple human-to-human transmission, severe respiratory infections and organ damage, the presence of SARS-CoV-2 throughout the life cycle (water, animals, food, air), unavoidable and frequent viral mutations, *etc.*, COVID-19 monitoring was always the top priority. The finest R&D recommendations thus far have concentrated on re-engineering vaccinations, virus-free indoor air, antimicrobial coating on personal protective equipment, and nanostructure-based biosensors (optical, electrical, and magnetic) for quantitative detection of SARS-CoV-2 at low levels.[272]

In this scope, ZnO based systems are supporting those efforts. Paper based EIS biosensors are designed based on the ZNON NWs for SARS-CoV-2 detection.[270] The ZnO nanowires are directly grown on the working electrodes and are immobilized with the SARS-CoV-2 S-protein receptor-binding domain (RBD) specific to COVID-19. To prepare human serum samples for testing, recombinant IgG antibody (CR3022) to SARS-CoV-2 spike glycoprotein S1 was spiked at different concentrations in human serum to mimic the real patient samples. The employed EIS sensors were able to differentiate the human serum sampled at different concentrations of cr3022 antibody indicating their feasibility for covid diagnosis. For asymptomatic patients, a serological assay with ZnO nanowires is reported for early detection of the virus.[273] A microplate coated with hydrothermally synthesized ZnO nanowires is developed. This plate is coated with SARS-CoV-2 and used for fluorescence immunoassay (FIA) to detect antibodies specific for SARS-CoV-2. The ZnO nanowire microplate is reported to be more sensitive than commercial immunoassay. Cervantes *et al.*[271] reported a theoretical study of nanostructured ZnO as a carrier of drugs. ZnO is coupled with three drugs chloroquine, dipyridamole, and lopinavir. Lopinavir is found to have the highest adsorption energy. From the docking tests, observing the interaction of free medications and composites with the SARS-CoV-2 major protease, it is discovered that the composites have higher coupling energy than free drugs. As a result, ZnO nanoparticles are found to regulate medication dosage on the SARS-CoV-2 target. Later Sportelli *et al.*[274] reported the experimental approach for the ZnO nanoparticles to lower the antigen of SARS-CoV-2 by about 90%. The ZnO nanoparticles are synthesized with the galvanostatic approach in the presence of different stabilizers. Preliminary studies on ZnO nanoparticles and poly ethylene oxide composites showed that ZnO nanoparticles are highly successful as a self-cleaning coating for hard surfaces subjected to SARS-CoV-2 infection. The aforementioned composites could be easily brushed on routinely touched surfaces and let to dry due to their nontoxic and straightforward handy nature. Haghayegh *et al.*[275] reported on carbon screen printed electrodes modified with ZnO nanoparticles in conjugation with reduced graphene oxide nanosheets dispersed in buffer (bbZnO/rGO) for the detection of the nucleocapsid protein antigen (SARS-CoV-2 N-protein antigen). The reported biosensor can yield acceptable sensitivity. For detection of N-protein in spiked samples, the immunobiosensor has a LOD of 21 fg mL^{-1} over a linear range of 1–10 000 pg mL^{-1} and a sensitivity of 32.07 Ω mL pg^{-1} mm^{-2}. The N-protein biosensor can distinguish between positive and negative clinical samples in 15 minutes. In another work, Hamdi *et al.*[276] reported the ZnO nanoparticles with hexagonal wurtzite *P*63*mc* crystal structure. The ZnO nanoparticles are tested for possible interaction with the ACE2 receptor as the possible target for COVID-19 using an *in silico* docking approach. Furthermore, an enhanced dose-dependent cellular uptake was demonstrated.

When rapid and early detection is of interest, strategies based on specific antibody/antigen viral biomarkers have been adopted. The structural proteins of SARS-CoV-2 can be advantageous to employ specific MAb immunoassays. Infected patients' blood, saliva, serum, and nasopharyngeal (NP) swab samples include nucleocapsid protein (N-protein), which has been found to be the most predictive for COVID-19 detection in the early stages of infection, with low vulnerability to mutation. When employed for rapid antigen testing, it has proven to be a dependable disease indicator.[275]

7. Conclusions and future perspectives

The need for biosensors could be understood clearly during this COVID pandemic which requires rapid, effective and delocalized diagnosis. Due to their simplicity, faster detection, and facility to test at the victim's site biosensors can be preferred over conventional testing equipment, which is costly and requires a skilled operator for testing. Research is still progressing for more reliable, accurate, sensitive, and miniaturized biosensor design.

ZnO is a wide bandgap semiconductor with a bandgap of 3.37 eV and a large exciton emission of about 60 meV. ZnO is thus a suitable candidate for biosensors due to its low cost, non-toxicity and ease of fabrication in a variety of morphologies and dimensionalities.

ZnO nanostructure-based biosensors have been reviewed in this document. For biosensors, the bioselective layer plays an important role in the selection of specific targets and sensitivity. The methods of biomolecule adsorption, both direct adsorption and covalent binding, have been presented here. Direct adsorption binds the biomolecule to ZnO by weak van der Waals forces, hydrophobic bonds or ionic bonding. The direct adsorption process is simple, but the biomolecules are not tightly bound to the surface. Covalent binding binds the biomolecules through cross-linking polymers. The molecules are tightly bound to a matrix and retain the bioactivity of the biomolecule. Different ZnO nanostructures for ZnO biosensors have been also discussed. However, there are limitations to using 0-D ZnO nanostructures, despite their improved sensing properties. The main problem is that the nanoparticles have little mobility because of the abundance of grain boundaries. The carrier mobility decreases when the electrons encounter a larger area of space charge as they go from terminal to terminal. One of the main advantages of 1-D ZnO over 0-D ZnO is its superior sensing capabilities. One-dimensional ZnO has a high surface-to-volume ratio and facilitates fast electron transport *via* a direct and stable route. The larger surface-to-volume ratio enables higher enzyme loading capacity improving the biosensor performance. A high aspect ratio is a useful property of 1-D ZnO for biosensors. Enzymes may be loaded onto the vast surface area of 2-D nanostructures. For biochemical sensing applications, 2D materials are advantageous due to their ability to deliver a high density of active surface sites across a vast region. The carrier mobility of 2D materials is also quite high. The electrochemical biosensors produce electrical signals *via* an electrical pathway for monitoring the amount of the target analyte. The amount of the target analyte is monitored by either cyclic voltammetry, potentiometry or amperometry methods. In optical biosensors, the optical transducer produces signals based on absorption, reflectance, and luminescence. Piezoelectric biosensors detect the target biomolecules based on the surface mass loading of the piezoelectric material.

ZnO-based FET biosensors are also reported. In FET-based biosensors, the change in the channel's conductance upon interaction with target analytes is used to determine the detection process. In particular, due to its unique structure and properties, 2D ZnO has been used for the design of a large variety of biosensors. 2D structures offer good conductivity, mechanical stability, and ease of functionalization. Improved amount of binding sites can be observed for the 2D structures due to their higher specific surface area. They can be employed as good flat templates for conjugation with biomolecules and other nanomaterials to improve the sensitivity and selectivity of the designed biosensor. Generally, 2D materials exhibit a large surface area and a high surface to volume ratio while their distinctive electronic structures and atomically thin layers are highly appealing owing to the extraordinary material properties which cannot be achieved using traditional bulk structures. A considerable advantage of nanoscale biosensors is their detecting ability and sensitivity at very small volumes of samples. ZnO-based biosensors feature high IEP, non-toxicity, ease of fabrication, biocompatibility, and low cost. Thus, biosensors for different biomolecules such as glucose, cholesterol, uric acid, DNA, and proteins have been developed based on various transduction mechanisms such as electrochemical, piezoelectric, and optical mechanisms. Also, FET based ZnO nanostructure biosensors are also reported for biosensing applications.

Despite the interesting results obtained, it is still critical to select the specific properties of the nanomaterial for biosensor design. Variation in the properties of ZnO by surface engineering helps in obtaining biosensors with better efficiency. Though there are various methods for synthesizing ZnO nanostructures, obtaining uniform shaped ZnO nanostructures with repeatability is a challenge for biosensing and obtaining high reproducibility is a concern that would help design good point-of-care biosensor devices. As a result, advances in material synthesis, enzyme/protein engineering, and immobilization/conjugation methods will continue to provide innovative nano-engineered segments with enhanced functionality. The ZnO FET biosensors may replace the electrochemical biosensors in the future for miniaturized devices. The medical applications of these devices must be widely researched, as it may represent a huge step in terms of disease diagnosis and control. The practical application of biosensors in the medical diagnosis field is still way ahead, and the research is progressing to combine the electronic and biological systems to design faster, smaller, and cheaper ZnO biosensors.

Abbreviations

ABTS	2,2′-Azino-bis(3-ethylbenzthiazoline-6-sulfonic acid)
AFM	Atomic force microscopy
APTES	Aminopropyl-triethoxysilane
BSA	Bovine serum albumin
CHIT	Chitosan
ChOx	Cholesterol oxidase
CMOS	Complementary metal–oxide–semiconductor
CNTs	Carbon nanotubes
CRP	C-reactive protein
CVD	Chemical vapor deposition
Cyt *c*	Cytochrome *c*

DEZ	Diethyl zinc
DLE	Deep level emission
DMSA	Dimercaptosuccinic acid
DMSO	Dimethyl sulfoxide
DPV	Differential pulse voltammetry
DSP	Dithiobis succinimidyl-propionate
DSS	Disuccinimidyl suberate
EDC	1-Ethyl-3-[3-dimethylaminopropyl]carbodiimide hydrochloride
EF	Enhancement factor
EIS	Electrochemical impedance spectroscopy
ELISA	Enzyme-linked immunosorbent assay
EP	Epinephrine
FET	Field effect transistor
FITC-antiIgG	Fluorescein-conjugated anti-bovine IgG
GOx	Glucose oxidase
H_2O_2	Hydrogen peroxide
HMTA	Hexamethylenetetramine
HRP	Horseradish peroxidase
HRTEM	High-resolution transmission electron microscopy
IEP	Isoelectric point
ITO	Indium tin oxide
LDH	Lactate dehydrogenase
LOD	Limit of detection
MAb	Monoclonal antibody
MBE	Molecular beam epitaxy
MG	Malachite green
MOCVD	Metal–organic CVD
MPTMS	Mercaptopropyl trimethoxysilane
MWCNTs	Multi-walled carbon nanotubes
NAAT	Nucleic acid amplification tests
NBE	Near band edge emission
NHS	*N*-Hydroxysuccinimide
NHS-biotin	Biotin-*N*-hydroxysuccinimide ester
PBS	Phosphate buffer solution
PDA	Phosphonodecanoic acid
PDA	Polydopamine
PECVD	Plasma enhanced CVD
PET	Polyethylene terephthalate
PHDA	Phosphonohexadecanoic acid
PL	Photoluminescence
PLD	Pulsed laser deposition
POC	Point of care
PtNDs	Platinum nanodendrites
PVB	Polyvinyl butyral
PVP	Polyvinyl pyrrolidone
QCM	Quartz crystal microbalance
RBD	Receptor-binding domain
rRT-PCR	Real-time reverse-transcription polymerase chain reaction
SAW	Surface acoustic wave
SCC	Squamous cell carcinoma
SCE	Saturated calomel electrode
SERS	Surface enhanced Raman spectroscopy
SHSAW	Shear horizontal surface acoustic wave
SPE	Screen-printed electrodes
SPR	Surface plasmon resonance
TPSP	Tetragonal pyramid-shaped porous
WHO	World Health Organization
XOD	Xanthine oxidase

Author contributions

M. Sankush Krishna: writing – original draft (lead). Sangeeta Singh: conceptualization (equal), writing – original draft (supporting). Maria Batool: writing – review and editing (equal). Heba Mohamed Fahmy: conceptualization (equal), supervision (equal). Kondaiah Seku: software (lead), formal analysis (equal). Ahmed Esmail Shalan: writing, review, editing (equal). Senentxu Lanceros-Mendez: writing – review, editing (equal), technical support. Muhammad Nadeem Zafar: conceptualization (equal), supervision (lead).

Conflicts of interest

The authors declare no conflict of interest.

Acknowledgements

AES acknowledges the National Research grants from MINECO, Spain, ''Juan de la Cierva'' [FJCI-2018-037717].

References

1 J. D. Whitman, *et al.*, Evaluation of SARS-CoV-2 serology assays reveals a range of test performance, *Nat. Biotechnol.*, 2020, **38**(10), 1174–1183.
2 C. Xie, *et al.*, Comparison of different samples for 2019 novel coronavirus detection by nucleic acid amplification tests, *Int. J. Infect. Dis.*, 2020, **93**, 264–267.
3 L. Guo, *et al.*, Profiling early humoral response to diagnose novel coronavirus disease (COVID-19), *Clin. Infect. Dis.*, 2020, **71**(15), 778–785.
4 M. Srivastava, N. Srivastava, P. K. Mishra and B. D. Malhotra, Prospects of nanomaterials-enabled biosensors for COVID-19 detection, *Sci. Total Environ.*, 2020, **754**, 142363.
5 S. A. Abid, *et al.*, Biosensors as a future diagnostic approach for COVID-19, *Life Sci.*, 2021, **273**, 119117.
6 J.-L. He, *et al.*, Diagnostic performance between CT and initial real-time RT-PCR for clinically suspected 2019 coronavirus disease (COVID-19) patients outside Wuhan, China, *Respir. Med.*, 2020, **168**, 105980.
7 Z. Li, *et al.*, Development and clinical application of a rapid IgM-IgG combined antibody test for SARS-CoV-2 infection diagnosis, *J. Med. Virol.*, 2020, **92**(9), 1518–1524.
8 D. Liu, *et al.*, Trends in miniaturized biosensors for point-of-care testing, *TrAC, Trends Anal. Chem.*, 2020, **122**, 115701.
9 Y. Rasmi, X. Li, J. Khan, T. Ozer and J. R. Choi, Emerging point-of-care biosensors for rapid diagnosis of COVID-19: current progress, challenges, and future prospects, *Anal. Bioanal. Chem.*, 2021, **413**(16), 4137–4159.

10 P. R. Solanki, A. Kaushik, V. V. Agrawal and B. D. Malhotra, Nanostructured metal oxide-based biosensors, *NPG Asia Mater.*, 2011, **3**(1), 17–24.
11 Y. Zhang, Z. Kang, X. Yan and Q. Liao, ZnO nanostructures in enzyme biosensors, *Sci. China Mater.*, 2015, **58**(1), 60–76.
12 M. L. M. Napi, S. M. Sultan, R. Ismail, K. W. How and M. K. Ahmad, Electrochemical-based biosensors on different zinc oxide nanostructures: A review, *Materials*, 2019, **12**(18), 2985.
13 T. Shibata, K. Unno, E. Makino, Y. Ito and S. Shimada, Characterization of sputtered ZnO thin film as sensor and actuator for diamond AFM probe, *Sens. Actuators, A*, 2002, **102**(1–2), 106–113.
14 M. Que, C. Lin, J. Sun, L. Chen, X. Sun and Y. Sun, Progress in ZnO Nanosensors, *Sensors*, 2021, **21**(16), 5502.
15 D. Gedamu, *et al.*, Rapid fabrication technique for interpenetrated ZnO nanotetrapod networks for fast UV sensors, *Adv. Mater.*, 2014, **26**(10), 1541–1550.
16 D. Panda and T.-Y. Tseng, One-dimensional ZnO nanostructures: fabrication, optoelectronic properties, and device applications, *J. Mater. Sci.*, 2013, **48**(20), 6849–6877.
17 K.-F. Lin, H.-M. Cheng, H.-C. Hsu, L.-J. Lin and W.-F. Hsieh, Band gap variation of size-controlled ZnO quantum dots synthesized by sol–gel method, *Chem. Phys. Lett.*, 2005, **409**(4–6), 208–211.
18 G.-C. Yi, C. Wang and W. Il Park, ZnO nanorods: synthesis, characterization and applications, *Semicond. Sci. Technol.*, 2005, **20**(4), S22.
19 P. Yang, *et al.*, Controlled growth of ZnO nanowires and their optical properties, *Adv. Funct. Mater.*, 2002, **12**(5), 323–331.
20 Y. J. Xing, *et al.*, Optical properties of the ZnO nanotubes synthesized *via* vapor phase growth, *Appl. Phys. Lett.*, 2003, **83**(9), 1689–1691.
21 P. K. Samanta and S. Mishra, Wet chemical growth and optical property of ZnO nanodiscs, *Optik*, 2013, **124**(17), 2871–2873.
22 W.-Z. Wang, *et al.*, Aligned ultralong ZnO nanobelts and their enhanced field emission, *Adv. Mater.*, 2006, **18**(24), 3275–3278.
23 S. J. Chen, *et al.*, Structural and optical properties of uniform ZnO nanosheets, *Adv. Mater.*, 2005, **17**(5), 586–590.
24 M. L. M. Napi, S. M. Sultan, R. Ismail, K. W. How and M. K. Ahmad, Electrochemical-based biosensors on different zinc oxide nanostructures: A review, *Materials*, 2019, **12**(18), 2985.
25 B. N. Aini, S. Siddiquee, K. Ampon, K. F. Rodrigues and S. Suryani, Development of glucose biosensor based on ZnO nanoparticles film and glucose oxidase-immobilized eggshell membrane, *Sens. Biosens. Res.*, 2015, **4**, 46–56.
26 R. Ahmad, N. Tripathy, S. H. Kim, A. Umar, A. Al-Hajry and Y.-B. Hahn, High performance cholesterol sensor based on ZnO nanotubes grown on Si/Ag electrodes, *Electrochem. Commun.*, 2014, **38**, 4–7.
27 Z. Dai, G. Shao, J. Hong, J. Bao and J. Shen, Immobilization and direct electrochemistry of glucose oxidase on a tetragonal pyramid-shaped porous ZnO nanostructure for a glucose biosensor, *Biosens. Bioelectron.*, 2009, **24**(5), 1286–1291.
28 S. A. Mozaffari, R. Rahmanian, M. Abedi and H. S. Amoli, Urea impedimetric biosensor based on reactive RF magnetron sputtered zinc oxide nanoporous transducer, *Electrochim. Acta*, 2014, **146**, 538–547.
29 B. Prieto-Simon, M. Campas and J.-L. Marty, Biomolecule immobilization in biosensor development: tailored strategies based on affinity interactions, *Protein Pept. Lett.*, 2008, **15**(8), 757–763.
30 N. R. Shanmugam, S. Muthukumar and S. Prasad, A review on ZnO-based electrical biosensors for cardiac biomarker detection, *Future Sci. OA*, 2017, **3**(4), FSO196.
31 N. Abid, *et al.*, Synthesis of nanomaterials using various top-down and bottom-up approaches, influencing factors, advantages, and disadvantages: A review, *Adv. Colloid Interface Sci.*, 2021, 102597.
32 M. Kawakami, A. B. Hartanto, Y. Nakata and T. Okada, Synthesis of ZnO nanorods by nanoparticle assisted pulsed-laser deposition, *Jpn. J. Appl. Phys.*, 2003, **42**(1A), L33.
33 J. Bae, J.-I. Hong, W. H. Han, Y. J. Choi and R. L. Snyder, Superior field emission properties of ZnO nanocones synthesized by pulsed laser deposition, *Chem. Phys. Lett.*, 2009, **475**(4–6), 260–263.
34 Y. Liu, *et al.*, Synthesis and H2 sensing properties of aligned ZnO nanotubes, *Appl. Surf. Sci.*, 2011, **257**(6), 2264–2268.
35 W.-T. Chiou, W.-Y. Wu and J.-M. Ting, Growth of single crystal ZnO nanowires using sputter deposition, *Diamond Relat. Mater.*, 2003, **12**(10–11), 1841–1844.
36 P. S. Venkatesh, S. Balakumar and K. Jeganathan, Post-annealing effects on the structural and optical properties of vertically aligned undoped ZnO nanorods grown by radio frequency magnetron sputtering, *RSC Adv.*, 2014, **4**(10), 5030–5035.
37 J.-J. Wu and S.-C. Liu, Low-temperature growth of well-aligned ZnO nanorods by chemical vapor deposition, *Adv. Mater.*, 2002, **14**(3), 215–218.
38 S. Y. Bae, H. W. Seo and J. Park, Vertically aligned sulfur-doped ZnO nanowires synthesized *via* chemical vapor deposition, *J. Phys. Chem. B*, 2004, **108**(17), 5206–5210.
39 S.-W. Kim, S. Fujita and S. Fujita, ZnO nanowires with high aspect ratios grown by metalorganic chemical vapor deposition using gold nanoparticles, *Appl. Phys. Lett.*, 2005, **86**(15), 153119.
40 C. C. Wu, D. S. Wuu, P. R. Lin, T. N. Chen and R. H. Horng, Three-step growth of well-aligned ZnO nanotube arrays by self-catalyzed metalorganic chemical vapor deposition method, *Cryst. Growth Des.*, 2009, **9**(10), 4555–4561.
41 X. Liu, X. Wu, H. Cao and R. P. H. Chang, Growth mechanism and properties of ZnO nanorods synthesized by plasma-enhanced chemical vapor deposition, *J. Appl. Phys.*, 2004, **95**(6), 3141–3147.
42 J. R. Creighton and P. Ho, Introduction to chemical vapor deposition (CVD), *Chem. Vap. Deposition*, 2001, **2**, 1–22.
43 M. N. Kamalasanan and S. Chandra, Sol–gel synthesis of ZnO thin films, *Thin Solid Films*, 1996, **288**(1–2), 112–115.

44 S. E. Ahn, *et al.*, Photoresponse of sol–gel-synthesized ZnO nanorods, *Appl. Phys. Lett.*, 2004, **84**(24), 5022–5024.
45 G. S. Wu, *et al.*, Controlled synthesis of ZnO nanowires or nanotubes *via* sol–gel template process, *Solid State Commun.*, 2005, **134**(7), 485–489.
46 M. Guglielmi and G. Carturan, Precursors for sol–gel preparations, *J. Non Cryst. Solids*, 1988, **100**(1–3), 16–30.
47 L. Znaidi, Sol–gel-deposited ZnO thin films: A review, *Mater. Sci. Eng., B*, 2010, **174**(1–3), 18–30.
48 M. T. Htay, Y. Hashimoto, N. Momose and K. Ito, Position-selective growth of ZnO nanowires by ultrasonic spray pyrolysis, *J. Cryst. Growth*, 2009, **311**(20), 4499–4504.
49 E. Kärber, *et al.*, Photoluminescence of spray pyrolysis deposited ZnO nanorods, *Nanoscale Res. Lett.*, 2011, **6**(1), 1–7.
50 L. C. Tien, D. P. Norton, S. J. Pearton, H.-T. Wang and F. Ren, Nucleation control for ZnO nanorods grown by catalyst-driven molecular beam epitaxy, *Appl. Surf. Sci.*, 2007, **253**(10), 4620–4625.
51 Y. W. Heo, *et al.*, Depletion-mode ZnO nanowire field-effect transistor, *Appl. Phys. Lett.*, 2004, **85**(12), 2274–2276.
52 Y. Jian-Feng, *et al.*, Growth and properties of ZnO nanotubes grown on Si (1 1 1) substrate by plasma-assisted molecular beam epitaxy, *J. Cryst. Growth*, 2005, **280**(1–2), 206–211.
53 Y. Hames, Z. Alpaslan, A. Kösemen, S. E. San and Y. Yerli, Electrochemically grown ZnO nanorods for hybrid solar cell applications, *Solar Energy*, 2010, **84**(3), 426–431.
54 J. Elias, R. Tena-Zaera and C. Lévy-Clément, Electrochemical deposition of ZnO nanowire arrays with tailored dimensions, *J. Electroanal. Chem.*, 2008, **621**(2), 171–177.
55 Y. Tang, *et al.*, Electrodeposition of ZnO nanotube arrays on TCO glass substrates, *Electrochem. Commun.*, 2007, **9**(2), 289–292.
56 A. Umar, B. Karunagaran, E. K. Suh and Y. B. Hahn, Structural and optical properties of single-crystalline ZnO nanorods grown on silicon by thermal evaporation, *Nanotechnology*, 2006, **17**(16), 4072.
57 S. Y. Bae, C. W. Na, J. H. Kang and J. Park, Comparative structure and optical properties of Ga-, In-, and Sn-doped ZnO nanowires synthesized *via* thermal evaporation, *J. Phys. Chem. B*, 2005, **109**(7), 2526–2531.
58 X. Zhang, *et al.*, Peculiar ZnO nanopushpins and nanotubes synthesized *via* simple thermal evaporation, *Appl. Phys. Lett.*, 2005, **87**(12), 123111.
59 J. Wang and L. Gao, Hydrothermal synthesis and photoluminescence properties of ZnO nanowires, *Solid State Commun.*, 2004, **132**(3–4), 269–271.
60 K. H. Tam, *et al.*, Defects in ZnO nanorods prepared by a hydrothermal method, *J. Phys. Chem. B*, 2006, **110**(42), 20865–20871.
61 A. Wei, X. W. Sun, C. X. Xu, Z. L. Dong, M. B. Yu and W. Huang, Stable field emission from hydrothermally grown ZnO nanotubes, *Appl. Phys. Lett.*, 2006, **88**(21), 213102.
62 A. B. Djurisic, X. Y. Chen and Y. H. Leung, Recent progress in hydrothermal synthesis of zinc oxide nanomaterials, *Recent Pat. Nanotechnol.*, 2012, **6**(2), 124–134.
63 M. Kawakami, A. B. Hartanto, Y. Nakata and T. Okada, Synthesis of ZnO nanorods by nanoparticle assisted pulsed-laser deposition, *Jpn. J. Appl. Phys.*, 2003, **42**(1A), L33.
64 J. Bae, J.-I. Hong, W. H. Han, Y. J. Choi and R. L. Snyder, Superior field emission properties of ZnO nanocones synthesized by pulsed laser deposition, *Chem. Phys. Lett.*, 2009, **475**(4–6), 260–263.
65 C. Tusche, H. L. Meyerheim and J. Kirschner, Observation of depolarized ZnO (0001) monolayers: formation of unreconstructed planar sheets, *Phys. Rev. Lett.*, 2007, **99**(2), 26102.
66 Y. Liu, *et al.*, Synthesis and H2 sensing properties of aligned ZnO nanotubes, *Appl. Surf. Sci.*, 2011, **257**(6), 2264–2268.
67 W.-T. Chiou, W.-Y. Wu and J.-M. Ting, Growth of single crystal ZnO nanowires using sputter deposition, *Diamond Relat. Mater.*, 2003, **12**(10–11), 1841–1844.
68 M. T. Htay, Y. Hashimoto, N. Momose and K. Ito, Position-selective growth of ZnO nanowires by ultrasonic spray pyrolysis, *J. Cryst. Growth*, 2009, **311**(20), 4499–4504.
69 J. Elias, R. Tena-Zaera and C. Lévy-Clément, Electrochemical deposition of ZnO nanowire arrays with tailored dimensions, *J. Electroanal. Chem.*, 2008, **621**(2), 171–177.
70 S. J. Chen, *et al.*, Structural and optical properties of uniform ZnO nanosheets, *Adv. Mater.*, 2005, **17**(5), 586–590.
71 T. Sahoo, S. K. Nayak, P. Chelliah, M. K. Rath and B. Parida, Observations of two-dimensional monolayer zinc oxide, *Mater. Res. Bull.*, 2016, **75**, 134–138.
72 R. Yakimova, L. Selegard, V. Khranovskyy, R. Pearce, A. L. Spetz and K. Uvdal, ZnO materials and surface tailoring for biosensing, *Front. Biosci.-Elite*, 2012, **4**(1), 254–278.
73 B. Ortiz-Casas, *et al.*, Bio-acceptable 0D and 1D ZnO nanostructures for cancer diagnostics and treatment, *Mater. Today*, 2021, **50**, 533–569.
74 N. Bhalla, *et al.*, A facile approach to fabricate and embed multifunctional nano ZnO into soap matrix and liquid cleansing products for enhanced antibacterial and photostability for health and hygiene applications, *Arabian J. Chem.*, 2022, **15**(6), 103862.
75 H. Hong, *et al.*, Cancer-targeted optical imaging with fluorescent zinc oxide nanowires, *Nano Lett.*, 2011, **11**(9), 3744–3750.
76 Z. Li, R. Yang, M. Yu, F. Bai, C. Li and Z. L. Wang, Cellular level biocompatibility and biosafety of ZnO nanowires, *J. Phys. Chem. C*, 2008, **112**(51), 20114–20117.
77 S. K. Arya, S. Saha, J. E. Ramirez-Vick, V. Gupta, S. Bhansali and S. P. Singh, Recent advances in ZnO nanostructures and thin films for biosensor applications, *Anal. Chim. Acta*, 2012, **737**, 1–21.
78 Y. Zhang, Z. Kang, X. Yan and Q. Liao, ZnO nanostructures in enzyme biosensors, *Sci. China Mater.*, 2015, **58**(1), 60–76.
79 A. Tereshchenko, *et al.*, Optical biosensors based on ZnO nanostructures: advantages and perspectives. A review, *Sens. Actuators, B*, 2016, **229**, 664–677.
80 B. Prieto-Simon, M. Campas and J.-L. Marty, Biomolecule immobilization in biosensor development: tailored strategies based on affinity interactions, *Protein Pept. Lett.*, 2008, **15**(8), 757–763.

81 N. P. Sasidharan, P. Chandran and S. S. Khan, Interaction of colloidal zinc oxide nanoparticles with bovine serum albumin and its adsorption isotherms and kinetics, *Colloids Surf., B*, 2013, **102**, 195–201.
82 E. da Silva, Y. Kembouche, U. Tegner, A. Baun and K. A. Jensen, Interaction of biologically relevant proteins with ZnO nanomaterials: A confounding factor for in vitro toxicity endpoints, *Toxicol. In Vitro*, 2019, **56**, 41–51.
83 T. Xie, *et al.*, Low-index ZnO crystal plane-specific binding behavior of whole Immunoglobulin G proteins, *Langmuir*, 2015, **31**(38), 10493–10499.
84 R. Ahmad, N. Tripathy, N. K. Jang, G. Khang and Y.-B. Hahn, Fabrication of highly sensitive uric acid biosensor based on directly grown ZnO nanosheets on electrode surface, *Sens. Actuators, B*, 2015, **206**, 146–151.
85 M. Klaumünzer, U. Weichsel, M. Mačković, E. Spiecker, W. Peukert and C. Kryschi, Transmission electron microscopy and time resolved optical spectroscopy study of the electronic and structural interactions of ZnO nanorods with bovine serum albumin, *J. Phys. Chem. B*, 2013, **117**(33), 9683–9689.
86 A. Bhogale, *et al.*, Systematic investigation on the interaction of bovine serum albumin with ZnO nanoparticles using fluorescence spectroscopy, *Colloids Surf., B*, 2013, **102**, 257–264.
87 Y. Wang, *et al.*, Research of protein adsorption on the different surface topography of the zinc oxide, *Surf. Interface Anal.*, 2015, **47**(2), 245–252.
88 P. Sanguino, T. Monteiro, S. R. Bhattacharyya, C. J. Dias, R. Igreja and R. Franco, ZnO nanorods as immobilization layers for interdigitated capacitive immunosensors, *Sens. Actuators, B*, 2014, **204**, 211–217.
89 C.-H. Sang, S.-J. Chou, F.-M. Pan and J.-T. Sheu, Fluorescence enhancement and multiple protein detection in ZnO nanostructure microfluidic devices, *Biosens. Bioelectron.*, 2016, **75**, 285–292.
90 R. D. Munje, M. Jacobs, S. Muthukumar, B. Quadri, N. R. Shanmugam and S. Prasad, A novel approach for electrical tuning of nano-textured zinc oxide surfaces for ultra-sensitive troponin-T detection, *Anal. Methods*, 2015, **7**(24), 10136–10144.
91 C. M. Tan, *et al.*, Interdigitated Electrodes integrated with zinc oxide nanoparticles for Cardiac Troponin I biomarker detection, in 2016 IEEE International Conference on Semiconductor Electronics (ICSE), 2016, pp. 220–223.
92 M. F. M. Fathil, *et al.*, Substrate-gate coupling in ZnO-FET biosensor for cardiac troponin I detection, *Sens. Actuators, B*, 2017, **242**, 1142–1154.
93 M. Jacobs, S. Muthukumar, A. P. Selvam, J. E. Craven and S. Prasad, Ultra-sensitive electrical immunoassay biosensors using nanotextured zinc oxide thin films on printed circuit board platforms, *Biosens. Bioelectron.*, 2014, **55**, 7–13.
94 B. Zhang, T. Kong, W. Xu, R. Su, Y. Gao and G. Cheng, Surface functionalization of zinc oxide by carboxyalkylphosphonic acid self-assembled monolayers, *Langmuir*, 2010, **26**(6), 4514–4522.
95 U. Dembereldorj, E.-O. Ganbold, J.-H. Seo, S. Y. Lee, S. I. Yang and S.-W. Joo, Conformational changes of proteins adsorbed onto ZnO nanoparticle surfaces investigated by concentration-dependent infrared spectroscopy, *Vib. Spectrosc.*, 2012, **59**, 23–28.
96 H. Liu, J. Ge, E. Ma and L. Yang, Advanced biomaterials for biosensor and theranostics, *Biomaterials in translational medicine*, Elsevier, 2019, pp. 213–255.
97 S. K. Arya, S. Saha, J. E. Ramirez-Vick, V. Gupta, S. Bhansali and S. P. Singh, Recent advances in ZnO nanostructures and thin films for biosensor applications, *Anal. Chim. Acta*, 2012, **737**, 1–21.
98 M. L. M. Napi, S. M. Sultan, R. Ismail, K. W. How and M. K. Ahmad, Electrochemical-based biosensors on different zinc oxide nanostructures: A review, *Materials*, 2019, **12**(18), 2985.
99 A. Tereshchenko, *et al.*, Optical biosensors based on ZnO nanostructures: advantages and perspectives. A review, *Sens. Actuators, B*, 2016, **229**, 664–677.
100 P. Skládal, Piezoelectric biosensors, *TrAC, Trends Anal. Chem.*, 2016, **79**, 127–133.
101 R. Monosik, M. Stredansky and E. Sturdik, Biosensors—classification, characterization and new trends, *Acta Chim. Slovaca*, 2012, **5**(1), 109–120.
102 B. Rezaei and N. Irannejad, Electrochemical detection techniques in biosensor applications, *Electrochemical Biosensors*, Elsevier, 2019, pp. 11–43.
103 V. Velusamy, K. Arshak, O. Korostynska, K. Oliwa and C. Adley, An overview of foodborne pathogen detection: In the perspective of biosensors, *Biotechnol. Adv.*, 2010, **28**(2), 232–254.
104 S.-J. Choi and I.-D. Kim, Recent developments in 2D nanomaterials for chemiresistive-type gas sensors, *Electron. Mater. Lett.*, 2018, **14**(3), 221–260.
105 F. Alam, A. H. Jalal, S. Forouzanfar, M. Karabiyik, A. R. Baboukani and N. Pala, Flexible and linker-free enzymatic sensors based on zinc oxide nanoflakes for noninvasive L-lactate sensing in sweat, *IEEE Sens. J.*, 2020, **20**(10), 5102–5109.
106 T. Yang, M. Chen, Q. Kong, X. Luo and K. Jiao, Toward DNA electrochemical sensing by free-standing ZnO nanosheets grown on 2D thin-layered MoS2, *Biosens. Bioelectron.*, 2017, **89**, 538–544.
107 D. Zhu, *et al.*, Hierarchical flower-like zinc oxide nanosheets in-situ growth on three-dimensional ferrocene-functionalized graphene framework for sensitive determination of epinephrine and its oxidation derivative, *Appl. Surf. Sci.*, 2020, **526**, 146721.
108 M. Eryiğit, B. K. Urhan, H. Ö. Doğan, T. Ö. Özer and Ü. Demir, ZnO Nanosheets-Decorated ERGO Layers: An Efficient Electrochemical Sensor for Non-Enzymatic Uric Acid Detection, *IEEE Sens. J.*, 2022, **22**(6), 5555–5561.
109 A. Fulati, *et al.*, An intracellular glucose biosensor based on nanoflake ZnO, *Sens. Actuators, B*, 2010, **150**(2), 673–680.
110 S. M. U. Ali, Z. H. Ibupoto, M. Kashif, U. Hashim and M. Willander, A potentiometric indirect uric acid sensor

based on ZnO nanoflakes and immobilized uricase, *Sensors*, 2012, **12**(3), 2787–2797.

111 N. Chauhan, S. Gupta, D. K. Avasthi, R. Adelung, Y. K. Mishra and U. Jain, Zinc oxide tetrapods based biohybrid interface for voltammetric sensing of Helicobacter pylori, *ACS Appl. Mater. Interfaces*, 2018, **10**(36), 30631–30639.

112 U. Chakraborty, *et al.*, A flower-like ZnO–Ag_2O nanocomposite for label and mediator free direct sensing of dinitrotoluene, *RSC Adv.*, 2020, **10**(46), 27764–27774.

113 V. N. Psychoyios, *et al.*, Potentiometric cholesterol biosensor based on ZnO nanowalls and stabilized polymerized lipid film, *Electroanalysis*, 2013, **25**(2), 367–372.

114 N. Akhtar, S. K. Metkar, A. Girigoswami and K. Girigoswami, ZnO nanoflower based sensitive nano-biosensor for amyloid detection, *Mater. Sci. Eng., C*, 2017, **78**, 960–968.

115 S. Saha and V. Gupta, Influence of surface defects in ZnO thin films on its biosensing response characteristic, *J. Appl. Phys.*, 2011, **110**(6), 64904.

116 F. Zhou, *et al.*, Electrodeposition of gold nanoparticles on ZnO nanorods for improved performance of enzymatic glucose sensors, *Mater. Sci. Semicond. Process.*, 2020, **105**, 104708.

117 N. S. Ridhuan, N. Mohamad Nor, K. Abdul Razak, Z. Lockman and N. D. Zakaria, ITO electrode modified with Pt nanodendrites-decorated ZnO nanorods for enzymatic glucose sensor, *J. Solid State Electrochem.*, 2021, **25**(3), 1065–1072.

118 V. Fedorenko, *et al.*, Application of polydopamine functionalized zinc oxide for glucose biosensor design, *Polymers*, 2021, **13**(17), 2918.

119 M. Shukla, T. Dixit, R. Prakash, I. A. Palani and V. Singh, *et al.*, Influence of aspect ratio and surface defect density on hydrothermally grown ZnO nanorods towards amperometric glucose biosensing applications,'', *Appl. Surf. Sci.*, 2017, **422**, 798–808.

120 D. Lee, *et al.*, Enhanced mass sensitivity of ZnO nanorod-grown quartz crystal microbalances, *Sens. Actuators, B*, 2009, **135**(2), 444–448.

121 C.-H. Sang, S.-J. Chou, F.-M. Pan and J.-T. Sheu, Fluorescence enhancement and multiple protein detection in ZnO nanostructure microfluidic devices, *Biosens. Bioelectron.*, 2016, **75**, 285–292.

122 D. Pradhan, F. Niroui and K. T. Leung, High-performance, flexible enzymatic glucose biosensor based on ZnO nanowires supported on a gold-coated polyester substrate, *ACS Appl. Mater. Interfaces*, 2010, **2**(8), 2409–2412.

123 F. Zhang, *et al.*, Immobilization of uricase on ZnO nanorods for a reagentless uric acid biosensor, *Anal. Chim. Acta*, 2004, **519**(2), 155–160.

124 T. Kong, Y. Chen, Y. Ye, K. Zhang, Z. Wang and X. Wang, An amperometric glucose biosensor based on the immobilization of glucose oxidase on the ZnO nanotubes, *Sens. Actuators, B*, 2009, **138**(1), 344–350.

125 K. Brince Paul, S. Kumar, S. Tripathy, S. R. K. Vanjari, V. Singh and S. G. Singh, A highly sensitive self assembled monolayer modified copper doped zinc oxide nanofiber interface for detection of Plasmodium falciparum histidine-rich protein-2: Targeted towards rapid, early diagnosis of malaria,'', *Biosens. Bioelectron.*, 2016, **80**, 39–46, DOI: **10.1016/j.bios.2016.01.036**.

126 F. Zhou, W. Jing, P. Liu, D. Han, Z. Jiang and Z. Wei, Doping Ag in ZnO nanorods to improve the performance of related enzymatic glucose sensors, *Sensors*, 2017, **17**(10), 2214, DOI: **10.3390/s17102214**.

127 M. L. M. Napi, S. M. Sultan, R. Ismail, K. W. How and M. K. Ahmad, Electrochemical-based biosensors on different zinc oxide nanostructures: A review, *Materials*, 2019, **12**(18), 2985.

128 J. Y. Kim, S. Y. Jo, G. J. Sun, A. Katoch, S. W. Choi and S. S. Kim, Tailoring the surface area of ZnO nanorods for improved performance in glucose sensors, *Sens. Actuators, B*, 2014, **192**, 216–220, DOI: **10.1016/j.snb.2013.10.113**.

129 S. Xu and Z. L. Wang, One-dimensional ZnO nanostructures: solution growth and functional properties, *Nano Res.*, 2011, **4**(11), 1013–1098.

130 W.-J. Wu, Q. Zhao, R. Zhou, Y.-C. Liang, W.-B. Zhao and C.-X. Shan, Ratiometric fluorescence sensor based on europium-grafted ZnO quantum dots for visual and colorimetric detection of tetracycline, *Spectrochim. Acta, Part A*, 2021, **259**, 119901.

131 M. Ali, I. Shah, S. W. Kim, M. Sajid, J. H. Lim and K. H. Choi, Quantitative detection of uric acid through ZnO quantum dots based highly sensitive electrochemical biosensor,'', *Sens. Actuators, A*, 2018, **283**, 282–290.

132 X. Ren, *et al.*, Zinc oxide nanoparticles/glucose oxidase photoelectrochemical system for the fabrication of biosensor, *J. Colloid Interface Sci.*, 2009, **334**(2), 183–187.

133 D. Zhao, H. Song, L. Hao, X. Liu, L. Zhang and Y. Lv, Luminescent ZnO quantum dots for sensitive and selective detection of dopamine, *Talanta*, 2013, **107**, 133–139.

134 A. Hayat, W. Haider, Y. Raza and J. L. Marty, Colorimetric cholesterol sensor based on peroxidase like activity of zinc oxide nanoparticles incorporated carbon nanotubes, *Talanta*, 2015, **143**, 157–161.

135 V. Fidal, S. Inguva, S. Krishnamurthy, E. Marsili, J.-P. Mosnier and T. S. Chandra, Mediator-free interaction of glucose oxidase, as model enzyme for immobilization, with Al-doped and undoped ZnO thin films laser-deposited on polycarbonate supports, *Enzyme Microb. Technol.*, 2017, **96**, 67–74.

136 Y.-T. Wang, L. Yu, Z.-Q. Zhu, J. Zhang, J.-Z. Zhu and C. Fan, Improved enzyme immobilization for enhanced bioelectrocatalytic activity of glucose sensor, *Sens. Actuators, B*, 2009, **136**(2), 332–337.

137 B. N. Aini, S. Siddiquee, K. Ampon, K. F. Rodrigues and S. Suryani, Development of glucose biosensor based on ZnO nanoparticles film and glucose oxidase-immobilized eggshell membrane, *Sens. Biosens. Res.*, 2015, **4**, 46–56.

138 T. Dayakar, K. V. Rao, K. Bikshalu, V. Rajendar and S.-H. Park, Novel synthesis and structural analysis of zinc oxide nanoparticles for the non enzymatic glucose biosensor, *Mater. Sci. Eng., C*, 2017, **75**, 1472–1479.

139 A. Mahmoud, M. Echabaane, K. Omri, L. el Mir and R. ben Chaabane, Development of an impedimetric non enzymatic

sensor based on ZnO and Cu doped ZnO nanoparticles for the detection of glucose, *J. Alloys Compd.*, 2019, **786**, 960–968.

140 H. Mirzaei and M. Darroudi, Zinc oxide nanoparticles: Biological synthesis and biomedical applications, *Ceram. Int.*, 2017, **43**(1), 907–914.

141 M. L. M. Napi, S. M. Sultan, R. Ismail, K. W. How and M. K. Ahmad, Electrochemical-based biosensors on different zinc oxide nanostructures: A review, *Materials*, 2019, **12**(18), 2985.

142 S. Zhang, G. Wright and Y. Yang, Materials and techniques for electrochemical biosensor design and construction, *Biosens. Bioelectron.*, 2000, **15**(5–6), 273–282.

143 S. Verma, *et al.*, ZnO-rGO nanocomposite based bioelectrode for sensitive and ultrafast detection of dopamine in human serum, *Biosens. Bioelectron.*, 2020, **165**, 112347.

144 K. B. Babitha, P. S. Soorya, A. P. Mohamed, R. B. Rakhi and S. Ananthakumar, Development of ZnO@ rGO nanocomposites for the enzyme free electrochemical detection of urea and glucose, *Mater. Adv.*, 2020, **1**(6), 1939–1951.

145 J. Yoon, D. Lee, E. Lee, Y. S. Yoon and D.-J. Kim, Ag/ZnO catalysts with different ZnO nanostructures for non-enzymatic detection of urea, *Electroanalysis*, 2019, **31**(1), 17–21.

146 S. Baruah, B. Maibam, C. K. Borah, T. Agarkar, A. Kumar and S. Kumar, A highly receptive ZnO-based enzymatic electrochemical sensor for glucose sensing, *IEEE Sens. J.*, 2021, **21**(13), 14601–14608.

147 M. L. M. Napi, S. M. Sultan, R. Ismail, K. W. How and M. K. Ahmad, Electrochemical-based biosensors on different zinc oxide nanostructures: A review, *Materials*, 2019, **12**(18), 2985.

148 M. Q. Israr, J. R. Sadaf, M. H. Asif, O. Nur, M. Willander and B. Danielsson, Potentiometric cholesterol biosensor based on ZnO nanorods chemically grown on Ag wire, *Thin Solid Films*, 2010, **519**(3), 1106–1109.

149 P. Supraja, V. Singh, S. R. K. Vanjari and S. Govind, Singh, "Electrospun CNT embedded ZnO nanofiber based biosensor for electrochemical detection of Atrazine: a step closure to single molecule detection, *Microsyst. Nanoeng.*, 2020, **6**(1), 1–10.

150 S. M. U. Ali, N. H. Alvi, Z. Ibupoto, O. Nur, M. Willander and B. Danielsson, Selective potentiometric determination of uric acid with uricase immobilized on ZnO nanowires, *Sens. Actuators, B*, 2011, **152**(2), 241–247.

151 M. Q. Israr, J. R. Sadaf, O. Nur, M. Willander, S. Salman and B. Danielsson, Chemically fashioned ZnO nanowalls and their potential application for potentiometric cholesterol biosensor, *Appl. Phys. Lett.*, 2011, **98**(25), 253705.

152 Z. H. Ibupoto, N. Jamal, K. Khun and M. Willander, Development of a disposable potentiometric antibody immobilized ZnO nanotubes based sensor for the detection of C-reactive protein, *Sens. Actuators, B*, 2012, **166**, 809–814.

153 Z. H. Ibupoto, S. M. U. A. Shah, K. Khun and M. Willander, Electrochemical L-lactic acid sensor based on immobilized ZnO nanorods with lactate oxidase, *Sensors*, 2012, **12**(3), 2456–2466.

154 A. Fulati, *et al.*, An intracellular glucose biosensor based on nanoflake ZnO, *Sens. Actuators, B*, 2010, **150**(2), 673–680.

155 Z. Rafiee, A. Mosahebfard and M. H. Sheikhi, High-performance ZnO nanowires-based glucose biosensor modified by graphene nanoplates, *Mater. Sci. Semicond. Process.*, 2020, **115**, 105116.

156 Z. H. Ibupoto, S. M. U. Ali, K. Khun, C. O. Chey, O. Nur and M. Willander, ZnO nanorods based enzymatic biosensor for selective determination of penicillin, *Biosensors*, 2011, **1**(4), 153–163.

157 C. O. Chey, Z. H. Ibupoto, K. Khun, O. Nur and M. Willander, Indirect determination of mercury ion by inhibition of a glucose biosensor based on ZnO nanorods, *Sensors*, 2012, **12**(11), 15063–15077.

158 S. M. U. Ali, M. Kashif, Z. H. Ibupoto, M. Fakhar-e-Alam, U. Hashim and M. Willander, Functionalised zinc oxide nanotube arrays as electrochemical sensors for the selective determination of glucose, *Micro Nano Lett.*, 2011, **6**(8), 609–613.

159 K. Khun, Z. H. Ibupoto, O. Nur and M. Willander, Development of galactose biosensor based on functionalized ZnO nanorods with galactose oxidase, *J. Sens.*, 2012, **2012**, 696247.

160 J. Xia, J. Qing and J. Liu, A sensitive electrochemical impedance DNA biosensor based on ZnO nanorod electrodes for BCR/ABL fusion gene detection, *Int. J. Electrochem. Sci*, 2019, **14**, 4271–4279.

161 S. P. Singh, *et al.*, Cholesterol biosensor based on rf sputtered zinc oxide nanoporous thin film, *Appl. Phys. Lett.*, 2007, **91**(6), 63901.

162 M. Tak, V. Gupta and M. Tomar, Flower-like ZnO nanostructure based electrochemical DNA biosensor for bacterial meningitis detection, *Biosens. Bioelectron.*, 2014, **59**, 200–207.

163 X. Liu, Q. Hu, Q. Wu, W. Zhang, Z. Fang and Q. Xie, Aligned ZnO nanorods: a useful film to fabricate amperometric glucose biosensor, *Colloids Surf., B*, 2009, **74**(1), 154–158.

164 Z. W. Zhao, X. J. Chen, B. K. Tay, J. S. Chen, Z. J. Han and K. A. Khor, A novel amperometric biosensor based on ZnO: Co nanoclusters for biosensing glucose, *Biosens. Bioelectron.*, 2007, **23**(1), 135–139.

165 J. Wang, S. Li and Y. Zhang, A sensitive DNA biosensor fabricated from gold nanoparticles, carbon nanotubes, and zinc oxide nanowires on a glassy carbon electrode, *Electrochim. Acta*, 2010, **55**(15), 4436–4440.

166 Z.-M. Liu, Y.-L. Liu, G.-L. Shen and R.-Q. Yu, Nano-ZnO/chitosan composite film modified electrode for voltammetric detection of DNA hybridization, *Anal. Lett.*, 2008, **41**(6), 1083–1095.

167 R. Khan, A. Kaushik, P. R. Solanki, A. A. Ansari, M. K. Pandey and B. D. Malhotra, Zinc oxide nanoparticles-chitosan composite film for cholesterol biosensor, *Anal. Chim. Acta*, 2008, **616**(2), 207–213.

168 C. Xiang, Y. Zou, L.-X. Sun and F. Xu, Direct electrochemistry and enhanced electrocatalysis of horseradish peroxidase based on flowerlike ZnO–gold nanoparticle–Nafion nanocomposite, *Sens. Actuators, B*, 2009, **136**(1), 158–162.

169 Z. Dai, G. Shao, J. Hong, J. Bao and J. Shen, Immobilization and direct electrochemistry of glucose oxidase on a tetragonal pyramid-shaped porous ZnO nanostructure for a glucose biosensor, *Biosens. Bioelectron.*, 2009, **24**(5), 1286–1291.

170 H. Fatemi, A. A. Khodadadi, A. A. Firooz and Y. Mortazavi, Apple–biomorphic synthesis of porous ZnO nanostructures for glucose direct electrochemical biosensor, *Curr. Appl. Phys.*, 2012, **12**(4), 1033–1038.

171 K. Khun, *et al.*, An electrochemical dopamine sensor based on the ZnO/CuO nanohybrid structures, *J. Nanosci. Nanotechnol.*, 2014, **14**(9), 6646–6652.

172 Y. Zhao, *et al.*, ZnO-nanorods/graphene heterostructure: a direct electron transfer glucose biosensor, *Sci. Rep.*, 2016, **6**, 32327.

173 U. Chakraborty, *et al.*, Microwave-assisted assembly of Ag_2O-ZnO composite nanocones for electrochemical detection of 4-Nitrophenol and assessment of their photocatalytic activity towards degradation of 4-Nitrophenol and Methylene blue dye, *J. Hazard. Mater.*, 2021, **416**, 125771.

174 D. Sharma, M. I. Sabela, S. Kanchi, K. Bisetty, A. A. Skelton and B. Honarparvar, Green synthesis, characterization and electrochemical sensing of silymarin by ZnO nanoparticles: experimental and DFT studies, *J. Electroanal. Chem.*, 2018, **808**, 160–172.

175 N. Tripathy and D.-H. Kim, Metal oxide modified ZnO nanomaterials for biosensor applications, *Nano Convergence*, 2018, **5**(1), 1–10.

176 P. Damborský, J. Švitel and J. Katrlík, Optical biosensors, *Essays Biochem.*, 2016, **60**(1), 91–100.

177 A. Tereshchenko, *et al.*, Optical biosensors based on ZnO nanostructures: advantages and perspectives. A review, *Sens. Actuators, B*, 2016, **229**, 664–677.

178 A. Tereshchenko, *et al.*, Optical biosensors based on ZnO nanostructures: advantages and perspectives. A review, *Sens. Actuators, B*, 2016, **229**, 664–677.

179 A. Galdamez, *et al.*, DNA probe functionalization on different morphologies of ZnO/Au nanowire for bio-sensing applications, *Mater. Lett.*, 2019, **235**, 250–253.

180 A. Tamashevski, Y. Harmaza, E. Slobozhanina, R. Viter and I. Iatsunskyi, Photoluminescent detection of human T-lymphoblastic cells by ZnO nanorods, *Molecules*, 2020, **25**(14), 3168.

181 V. Myndrul, E. Coy, M. Bechelany and I. Iatsunskyi, Photoluminescence label-free immunosensor for the detection of Aflatoxin B1 using polyacrylonitrile/zinc oxide nanofibers, *Mater. Sci. Eng., C*, 2021, **118**, 111401.

182 D. Sodzel, *et al.*, Continuous sensing of hydrogen peroxide and glucose *via* quenching of the UV and visible luminescence of ZnO nanoparticles, *Microchim. Acta*, 2015, **182**(9–10), 1819–1826.

183 D. Sodzel, *et al.*, Continuous sensing of hydrogen peroxide and glucose *via* quenching of the UV and visible luminescence of ZnO nanoparticles, *Microchim. Acta*, 2015, **182**(9–10), 1819–1826.

184 S. N. Sarangi, S. Nozaki and S. N. Sahu, ZnO nanorod-based non-enzymatic optical glucose biosensor, *J. Biomed. Nanotechnol.*, 2015, **11**(6), 988–996.

185 R. Viter, *et al.*, Application of room temperature photoluminescence from ZnO nanorods for salmonella detection, *IEEE Sens. J.*, 2014, **14**(6), 2028–2034.

186 M. A. Iyer, *et al.*, Scanning fluorescence-based ultrasensitive detection of dengue viral DNA on ZnO thin films, *Sens. Actuators, B*, 2014, **202**, 1338–1348.

187 T.-Y. Liu, H.-C. Liao, C.-C. Lin, S.-H. Hu and S.-Y. Chen, Biofunctional ZnO nanorod arrays grown on flexible substrates, *Langmuir*, 2006, **22**(13), 5804–5809.

188 C.-C. Chang, N.-F. Chiu, D. S. Lin, Y. Chu-Su, Y.-H. Liang and C.-W. Lin, High-sensitivity detection of carbohydrate antigen 15-3 using a gold/zinc oxide thin film surface plasmon resonance-based biosensor, *Anal. Chem.*, 2010, **82**(4), 1207–1212.

189 K.-E. Kim, T. G. Kim and Y.-M. Sung, Enzyme-conjugated ZnO nanocrystals for collisional quenching-based glucose sensing, *CrystEngComm*, 2012, **14**(8), 2859–2865.

190 G. Kaur, M. Tomar and V. Gupta, Nanostructured zinc oxide thin film for application to surface plasmon resonance based cholesterol biosensor, *International Workshop on Thin Films for Electronics, Electro-Optics, Energy, and Sensors*, 2015, vol. 9667, p. 966706.

191 L. Sun, *et al.*, A white-emitting ZnO–Au nanocomposite and its SERS applications, *Appl. Surf. Sci.*, 2012, **258**(20), 7813–7819.

192 K. Sivashanmugan, J.-D. Liao, B. H. Liu, C.-K. Yao and S.-C. Luo, Ag nanoclusters on ZnO nanodome array as hybrid SERS-active substrate for trace detection of malachite green, *Sens. Actuators, B*, 2015, **207**, 430–436.

193 N. K. Singh, B. Jain and S. Annapoorni, ZnO modified gold disc: A new route to efficient glucose sensing, *Sens. Actuators, B*, 2011, **156**(1), 383–387.

194 Q. Tao, *et al.*, ''Controlled growth of ZnO nanorods on textured silicon wafer and the application for highly effective and recyclable SERS substrate by decorating Ag nanoparticles, *Mater. Res. Bull.*, 2014, **54**, 6–12.

195 S.-C. Yang, Y.-C. Shen, T.-C. Lu, T.-L. Yang and J.-J. Huang, Tumor detection strategy using ZnO light-emitting nanoprobes, *Nanotechnology*, 2012, **23**(5), 55202.

196 A. Dorfman, N. Kumar and J. Hahm, Nanoscale ZnO-enhanced fluorescence detection of protein interactions, *Adv. Mater.*, 2006, **18**(20), 2685–2690.

197 A. Dorfman, N. Kumar and J. Hahm, Highly sensitive biomolecular fluorescence detection using nanoscale ZnO platforms, *Langmuir*, 2006, **22**(11), 4890–4895.

198 P. Tetyana, P. M. Shumbula and Z. Njengele-Tetyana, Biosensors: Design, Development and Applications, *Nanopores*, IntechOpen, 2021.

199 M. Wang, *et al.*, Self-Powered Biosensor for Specifically Detecting Creatinine in Real Time Based on the Piezo-Enzymatic-Reaction Effect of Enzyme-Modified ZnO Nanowires, *Biosensors*, 2021, **11**(9), 342.

200 P. I. Reyes, Z. Duan, Y. Lu, D. Khavulya and N. Boustany, ZnO nanostructure-modified QCM for dynamic monitoring of cell adhesion and proliferation, *Biosens. Bioelectron.*, 2013, **41**, 84–89.
201 D. Lee, *et al.*, Enhanced mass sensitivity of ZnO nanorod-grown quartz crystal microbalances, *Sens. Actuators, B*, 2009, **135**(2), 444–448.
202 X. Wang, H. Yu, D. Lu, J. Zhang and W. Deng, Label free detection of the breast cancer biomarker CA15. 3 using ZnO nanorods coated quartz crystal microbalance, *Sens. Actuators, B*, 2014, **195**, 630–634.
203 S. Krishnamoorthy, A. A. Iliadis, T. Bei and G. P. Chrousos, An interleukin-6 ZnO/SiO2/Si surface acoustic wave biosensor, *Biosens. Bioelectron.*, 2008, **24**(2), 313–318.
204 J. Luo, M. Xie, P. Luo, B. Zhao, K. Du and P. Fan, A sensitive glucose biosensor without using glucose test strips based on ZnO/SiO2/Si surface acoustic wave device, *Mater. Lett.*, 2014, **130**, 14–16.
205 Y. Mao, M. Shen, B. Liu, L. Xing, S. Chen and X. Xue, Self-powered piezoelectric-biosensing textiles for the physiological monitoring and time-motion analysis of individual sports, *Sensors*, 2019, **19**(15), 3310.
206 R. Ahmad, N. Tripathy and Y.-B. Hahn, High-performance cholesterol sensor based on the solution-gated field effect transistor fabricated with ZnO nanorods, *Biosens. Bioelectron.*, 2013, **45**, 281–286.
207 R. Ahmad, M.-S. Ahn and Y.-B. Hahn, ZnO nanorods array based field-effect transistor biosensor for phosphate detection, *J. Colloid Interface Sci.*, 2017, **498**, 292–297.
208 J. Liu, J. Goud, P. M. Raj, M. Iyer, Z. L. Wang and R. R. Tummala, Real-time protein detection using ZnO nanowire/thin film bio-sensor integrated with microfluidic system, in 2008 58th Electronic Components and Technology Conference, 2008, pp. 1317–1322.
209 X. Liu, *et al.*, Enzyme-coated single ZnO nanowire FET biosensor for detection of uric acid, *Sens. Actuators, B*, 2013, **176**, 22–27.
210 X. Zong and R. Zhu, ZnO nanorod-based FET biosensor for continuous glucose monitoring, *Sens. Actuators, B*, 2018, **255**, 2448–2453.
211 R. Ahmad and Y.-B. Hahn, *et al.*, Nonenzymatic flexible field-effect transistor based glucose sensor fabricated using NiO quantum dots modified ZnO nanorods, *J. Colloid Interface Sci.*, 2018, **512**, 21–28.
212 R. Ahmad, M.-S. Ahn and Y.-B. Hahn, Fabrication of a non-enzymatic glucose sensor field-effect transistor based on vertically-oriented ZnO nanorods modified with Fe2O3, *Electrochem. Commun.*, 2017, **77**, 107–111.
213 M. Fathollahzadeh, *et al.*, Immobilization of glucose oxidase on ZnO nanorods decorated electrolyte-gated field effect transistor for glucose detection, *J. Solid State Electrochem.*, 2018, **22**(1), 61–67.
214 S. S. A. Karim, C.-F. Dee, B. Y. Majlis and M. A. Mohamed, Recent progress on fabrication of zinc oxide nanorod-based field effect transistor biosensors, *Sains Malays.*, 2019, **48**(6), 1301–1310.
215 A. Wei, *et al.*, Enzymatic glucose biosensor based on ZnO nanorod array grown by hydrothermal decomposition, *Appl. Phys. Lett.*, 2006, **89**(12), 123902.
216 A. Umar, M. M. Rahman, M. Vaseem and Y.-B. Hahn, Ultra-sensitive cholesterol biosensor based on low-temperature grown ZnO nanoparticles, *Electrochem. Commun.*, 2009, **11**(1), 118–121.
217 J. S. Kim, W. Il Park, C.-H. Lee and G.-C. Yi, ZnO nanorod biosensor for highly sensitive detection of specific protein binding, *J. Korean Phys. Soc.*, 2006, **49**, 1635–1639.
218 C.-H. Sang, S.-J. Chou, F.-M. Pan and J.-T. Sheu, Fluorescence enhancement and multiple protein detection in ZnO nanostructure microfluidic devices, *Biosens. Bioelectron.*, 2016, **75**, 285–292.
219 J. Liu, J. Goud, P. M. Raj, M. Iyer, Z. L. Wang and R. R. Tummala, Real-time protein detection using ZnO nanowire/thin film bio-sensor integrated with microfluidic system, in 2008 58th Electronic Components and Technology Conference, 2008, pp. 1317–1322.
220 Y. Al-Douri, K. Gherab, K. M. Batoo and E. H. Raslan, Detecting the DNA of dengue serotype 2 using aluminium nanoparticle doped zinc oxide nanostructure: synthesis, analysis and characterization, *J. Mater. Res. Technol.*, 2020, **9**(3), 5515–5523.
221 G. Kaur, A. Paliwal, M. Tomar and V. Gupta, Detection of *Neisseria meningitidis* using surface plasmon resonance based DNA biosensor, *Biosens. Bioelectron.*, 2016, **78**, 106–110.
222 V. Gerbreders, *et al.*, ZnO nanostructure-based electrochemical biosensor for Trichinella DNA detection, *Sens. Biosens. Res.*, 2019, **23**, 100276.
223 G. Gasparotto, J. P. C. Costa, P. I. Costa, M. A. Zaghete and T. Mazon, Electrochemical immunosensor based on ZnO nanorods-Au nanoparticles nanohybrids for ovarian cancer antigen CA-125 detection, *Mater. Sci. Eng., C*, 2017, **76**, 1240–1247.
224 Y.-H. Liang, C.-C. Chang, C.-C. Chen, Y. Chu-Su and C.-W. Lin, Development of an Au/ZnO thin film surface plasmon resonance-based biosensor immunoassay for the detection of carbohydrate antigen 15-3 in human saliva, *Clin. Biochem.*, 2012, **45**(18), 1689–1693.
225 D. Zhao, H. Song, L. Hao, X. Liu, L. Zhang and Y. Lv, Luminescent ZnO quantum dots for sensitive and selective detection of dopamine, *Talanta*, 2013, **107**, 133–139.
226 Q. Rui, K. Komori, Y. Tian, H. Liu, Y. Luo and Y. Sakai, Electrochemical biosensor for the detection of H2O2 from living cancer cells based on ZnO nanosheets, *Anal. Chim. Acta*, 2010, **670**(1–2), 57–62.
227 Y.-F. Li, Z.-M. Liu, Y.-L. Liu, Y.-H. Yang, G.-L. Shen and R.-Q. Yu, A mediator-free phenol biosensor based on immobilizing tyrosinase to ZnO nanoparticles, *Anal. Biochem.*, 2006, **349**(1), 33–40.
228 R. Viter, *et al.*, Application of room temperature photoluminescence from ZnO nanorods for salmonella detection, *IEEE Sens. J.*, 2014, **14**(6), 2028–2034.
229 J. Narang and C. S. Pundir, Construction of a triglyceride amperometric biosensor based on chitosan–ZnO

nanocomposite film, *Int. J. Biol. Macromol.*, 2011, **49**(4), 707–715.

230 R. Devi, M. Thakur and C. S. Pundir, Construction and application of an amperometric xanthine biosensor based on zinc oxide nanoparticles–polypyrrole composite film, *Biosens. Bioelectron.*, 2011, **26**(8), 3420–3426.

231 L. Wang, *et al.*, Water-soluble ZnO–Au nanocomposite-based probe for enhanced protein detection in a SPR biosensor system, *J. Colloid Interface Sci.*, 2010, **351**(2), 392–397.

232 G. Biasotto, J. P. C. Costa, P. I. Costa and M. A. Zaghete, ZnO nanorods-gold nanoparticle-based biosensor for detecting hepatitis C, *Appl. Phys. A: Mater. Sci. Process.*, 2019, **125**(12), 1–7.

233 F. Khosravi-Nejad, M. Teimouri, S. Jafari Marandi and M. Shariati, The highly sensitive impedimetric biosensor in label free approach for hepatitis B virus DNA detection based on tellurium doped ZnO nanowires, *Appl. Phys. A: Mater. Sci. Process.*, 2019, **125**(9), 1–8.

234 T. Kong, Y. Chen, Y. Ye, K. Zhang, Z. Wang and X. Wang, An amperometric glucose biosensor based on the immobilization of glucose oxidase on the ZnO nanotubes, *Sens. Actuators, B*, 2009, **138**(1), 344–350.

235 R. Ahmad, N. Tripathy, N. K. Jang, G. Khang and Y.-B. Hahn, Fabrication of highly sensitive uric acid biosensor based on directly grown ZnO nanosheets on electrode surface, *Sens. Actuators, B*, 2015, **206**, 146–151.

236 M. Q. Israr, J. R. Sadaf, M. H. Asif, O. Nur, M. Willander and B. Danielsson, Potentiometric cholesterol biosensor based on ZnO nanorods chemically grown on Ag wire, *Thin Solid Films*, 2010, **519**(3), 1106–1109.

237 B. Gu, C. Xu, C. Yang, S. Liu and M. Wang, ZnO quantum dot labeled immunosensor for carbohydrate antigen 19-9, *Biosens. Bioelectron.*, 2011, **26**(5), 2720–2723.

238 C. Singhal, C. S. Pundir and J. Narang, A genosensor for detection of consensus DNA sequence of Dengue virus using ZnO/Pt-Pd nanocomposites, *Biosens. Bioelectron.*, 2017, **97**, 75–82.

239 K. Khun, *et al.*, An electrochemical dopamine sensor based on the ZnO/CuO nanohybrid structures, *J. Nanosci. Nanotechnol.*, 2014, **14**(9), 6646–6652.

240 Z. H. Ibupoto, S. M. U. Ali, K. Khun, C. O. Chey, O. Nur and M. Willander, ZnO nanorods based enzymatic biosensor for selective determination of penicillin, *Biosensors*, 2011, **1**(4), 153–163.

241 C. Xiang, Y. Zou, L.-X. Sun and F. Xu, Direct electrochemistry and enhanced electrocatalysis of horseradish peroxidase based on flowerlike ZnO–gold nanoparticle–Nafion nanocomposite, *Sens. Actuators, B*, 2009, **136**(1), 158–162.

242 M. Haque, H. Fouad, H.-K. Seo, O. Y. Alothman and Z. A. Ansari, Cu-doped ZnO nanoparticles as an electrochemical sensing electrode for cardiac biomarker myoglobin detection, *IEEE Sens. J.*, 2020, **20**(15), 8820–8832.

243 E. I. Naik, H. S. B. Naik, M. S. Sarvajith and E. Pradeepa, Co-precipitation synthesis of cobalt doped ZnO nanoparticles: Characterization and their applications for biosensing and antibacterial studies, *Inorg. Chem. Commun.*, 2021, **130**, 108678.

244 U. D. Kamaci and M. Kamaci, Selective and sensitive zno quantum dots based fluorescent biosensor for detection of cysteine, *J. Fluoresc.*, 2021, **31**(2), 401–414.

245 A. R. Al-Dairy, B. Albiss and A. A. Jaradat, Computational Modeling of ZnO-NRs and Graphene Nanostructure as a Glucose Biosensor, *Sens. Imaging*, 2021, **22**(1), 1–13.

246 M. Rahimi-Mohseni, J. B. Raoof, T. A. Aghajanzadeh and R. Ojani, Phenylketonuria monitoring in human blood serum by mosses extract/ZnO@ Au nanoarrays-loaded filter paper as a novel electrochemical biosensor, *Microchem. J.*, 2021, **160**, 105739.

247 E. M. Al-Khalqi, M. A. Abdul Hamid, N. H. Al-Hardan and L. K. Keng, Highly sensitive magnesium-doped ZnO nanorod pH sensors based on electrolyte–insulator–semiconductor (EIS) Sensors, *Sensors*, 2021, **21**(6), 2110.

248 T. Kokab, *et al.*, Simultaneous femtomolar detection of paracetamol, diclofenac, and orphenadrine using a carbon nanotube/zinc oxide nanoparticle-based electrochemical sensor, *ACS Appl. Nano. Mater.*, 2021, **4**(5), 4699–4712.

249 N. M. J. Ditshego, ZnO nanowire field effect transistor for biosensing: A review, *J. Nano Res.*, 2019, **60**, 94–112.

250 N. Tripathy and D.-H. Kim, Metal oxide modified ZnO nanomaterials for biosensor applications, *Nano Convergence*, 2018, **5**(1), 1–10.

251 G. S. Mei, P. S. Menon and G. Hegde, ZnO for performance enhancement of surface plasmon resonance biosensor: a review, *Mater. Res. Express*, 2020, **7**(1), 12003.

252 N. P. Shetti, S. D. Bukkitgar, K. R. Reddy, C. V. Reddy and T. M. Aminabhavi, ZnO-based nanostructured electrodes for electrochemical sensors and biosensors in biomedical applications, *Biosens. Bioelectron.*, 2019, **141**, 111417.

253 H. Beitollahi, S. Tajik, F. G. Nejad and M. Safaei, Recent advances in ZnO nanostructure-based electrochemical sensors and biosensors, *J. Mater. Chem. B*, 2020, **8**(27), 5826–5844.

254 S. Imran, S. Ahmadi and K. Kerman, Electrochemical biosensors for the detection of SARS-CoV-2 and other viruses, *Micromachines*, 2021, **12**(2), 174.

255 N. P. Shetti, S. D. Bukkitgar, K. R. Reddy, C. V. Reddy and T. M. Aminabhavi, ZnO-based nanostructured electrodes for electrochemical sensors and biosensors in biomedical applications, *Biosens. Bioelectron.*, 2019, **141**, 111417.

256 C. Xu, C. Yang, B. Gu and S. Fang, Nanostructured ZnO for biosensing applications, *Chin. Sci. Bull.*, 2013, **58**(21), 2563–2566.

257 S. K. Arya, S. Saha, J. E. Ramirez-Vick, V. Gupta, S. Bhansali and S. P. Singh, Recent advances in ZnO nanostructures and thin films for biosensor applications, *Anal. Chim. Acta*, 2012, **737**, 1–21.

258 N. R. Shanmugam, S. Muthukumar and S. Prasad, Ultrasensitive and low-volume point-of-care diagnostics on flexible strips–a study with cardiac troponin biomarkers, *Sci. Rep.*, 2016, **6**(1), 1–10.

259 G. S. Mei, P. S. Menon and G. Hegde, ZnO for performance enhancement of surface plasmon resonance biosensor: a review, *Mater. Res. Express*, 2020, **7**(1), 12003.

260 A. Tereshchenko, *et al.*, Optical biosensors based on ZnO nanostructures: advantages and perspectives. A review, *Sens. Actuators, B*, 2016, **229**, 664–677.
261 Y. Zhang, Z. Kang, X. Yan and Q. Liao, ZnO nanostructures in enzyme biosensors, *Sci. China Mater.*, 2015, **58**(1), 60–76.
262 N. Tripathy and D.-H. Kim, Metal oxide modified ZnO nanomaterials for biosensor applications, *Nano Convergence*, 2018, **5**(1), 1–10.
263 D. Liu, *et al.*, Trends in miniaturized biosensors for point-of-care testing, *TrAC, Trends Anal. Chem.*, 2020, **122**, 115701.
264 M. F. M. Fathil, *et al.*, Substrate-gate coupling in ZnO-FET biosensor for cardiac troponin I detection, *Sens. Actuators, B*, 2017, **242**, 1142–1154.
265 N. Kalyani, S. Goel and S. Jaiswal, On-site sensing of pesticides using point-of-care biosensors: a review, *Environ. Chem. Lett.*, 2021, **19**(1), 345–354.
266 Y. Xia, *et al.*, Smartphone-based point-of-care microfluidic platform fabricated with a ZnO nanorod template for colorimetric virus detection, *ACS Sens.*, 2019, **4**(12), 3298–3307.
267 A. M. Faria and T. Mazon, Early diagnosis of Zika infection using a ZnO nanostructures-based rapid electrochemical biosensor, *Talanta*, 2019, **203**, 153–160.
268 B. Chakraborty, A. Das, N. Mandal, N. Samanta, N. Das and C. R. Chaudhuri, Label free, electric field mediated ultrasensitive electrochemical point-of-care device for CEA detection, *Sci. Rep.*, 2021, **11**(1), 1–12.
269 V. Chaudhary, A. K. Kaushik, H. Furukawa and A. Khosla, Review—Towards 5th generation AI and IoT driven sustainable intelligent sensors based on 2D mxenes and borophene, *ECS Sens. Plus*, 2022, **1**, 013601.
270 X. Li, *et al.*, Enhancing the performance of paper-based electrochemical impedance spectroscopy nanobiosensors: An experimental approach, *Biosens. Bioelectron.*, 2021, **177**, 112672.
271 E. Díaz-Cervantes, C. Zenteno-Zúñiga, V. Rodríguez-González and F. Aguilera-Granja, Design of ZnO-Drug Nanocarriers against the Main Protease of SARS-CoV-2 (COVID-19): An In Silico Assay, *Appl. Nano*, 2021, **2**(3), 257–266.
272 A. Kaushik and E. Mostafavi, To manage long COVID by selective SARS-CoV-2 infection biosensing, *The Innovation*, 2022, **3**(5), 100303.
273 J. Kim, *et al.*, ZnO Nanowire-Based Early Detection of SARS-CoV-2 Antibody Responses in Asymptomatic Patients with COVID-19, *Adv. Mater. Interfaces*, 2022, 2102046.
274 M. C. Sportelli, *et al.*, On the Efficacy of ZnO Nanostructures against SARS-CoV-2, *Int. J. Mol. Sci.*, 2022, **23**(6), 3040.
275 F. Haghayegh, R. Salahandish, M. Hassani and A. Sanati-Nezhad, Highly Stable Buffer-Based Zinc Oxide/Reduced Graphene Oxide Nanosurface Chemistry for Rapid Immunosensing of SARS-CoV-2 Antigens, *ACS Appl. Mater. Interfaces*, 2022, **14**(8), 10844–10855.
276 M. Hamdi, H. M. Abdel-Bar, E. Elmowafy, A. El-Khouly, M. Mansour and G. A. S. Awad, Investigating the internalization and COVID-19 antiviral computational analysis of optimized nanoscale zinc oxide, *ACS Omega*, 2021, **6**(10), 6848–6860.